
**Exploration of the Mechanisms Underlying
Cell Fate Transitions and Intercellular
Communications in Mammary Tissue**

Yueqing Xu



**A thesis submitted in conformity with the requirements
for the degree of Doctor of Philosophy**

The University of Edinburgh

2025

Abstract

Background:

The mammary tissue undergoes morphological remodelling during puberty and pregnancy, forming mature alveolar structures during lactation. This process involves proliferation and differentiation of mammary epithelial cells and dynamic adaptations in stromal cells and adipocytes within the surrounding fat pad. During pregnancy and lactation, luminal progenitors specialise into alveolar cells responsible for the synthesis of milk proteins and lipids. However, the molecular dynamics during this process is not elucidated yet. Mammary epithelial cells originate not only from mammary stem cells but also from stromal cells that undergo stromal-epithelial transition in response to hormonal stimulations, though the transcriptional mechanisms driving this process are unknown. Adipocytes, which constitute a major cellular population within the mammary fat pad, undergo dedifferentiation during lactation. This process is potentially attributed to expanding epithelial structures. In addition, adipocytes facilitate mammary gland development, as their absence impairs morphogenesis and functions of the mammary gland during puberty, pregnancy, and lactation. Additionally, high-fat diet (HFD) suppresses pubertal mammary gland development, likely via adipocyte metabolic reprogramming. However, the molecular basis of adipocyte-epithelial crosstalk remains poorly defined. This study investigates transcription factors regulating epithelial cell fate during mammary gland development, bi-directional epithelial-adipocyte interactions, and the underlying mechanisms of HFD induced impaired mammary gland development.

Methods:

Single-nucleus RNA sequencing (snRNA-seq) was performed on mammary

tissues from virgin, mid-pregnant, and lactating mice to map the dynamics of cell composition and cell-type-specific transcription profiles. Stromal subpopulations with epithelial characteristics were identified and transcription factors enriched in these cells were analysed. Similarly, luminal subpopulations were further delineated to identify lipid-synthesizing alveolar cells, followed by screening of transcription factors. Cell-cell communication networks were constructed based on ligand-receptor pairs to identify candidate signalling molecules between epithelial cells and adipocytes. Based on the analytic results in the snRNA-seq data, a series of experiments were performed for functional validation, including 1) FOXP1 overexpression in primary stromal cells; 2) STAT5 phosphorylation inhibition in mammary organoids; 3) IL15 treatment during *in vitro* adipogenesis of primary preadipocytes; 4) phenotypic characterization of NRG4-knockout mice. Moreover, a HFD mouse model was established by feeding mice an HFD from 3 to 10 weeks of age. snRNA-seq was performed on mammary tissues from HFD-fed mice to assess diet-induced changes in cell composition and cell-type-specific transcription profiles, followed by comparative analysis of mammary development in HFD-fed wild-type and NRG4-knockout mice.

Results:

The results uncovered the cellular and molecular mechanisms underlying cell fate transitions and intercellular communications of both epithelial and stromal cells during mammary gland development in five different aspects. First, FOXP1 overexpression in stromal cells suppressed adipogenic differentiation but failed to induce expression of epithelial genes, suggesting stromal-epithelial transition requires additional regulators. Second, inhibiting STAT5 phosphorylation in mammary organoids impaired lipid droplet formation, which indicated the indispensable roles of STAT5A in alveolar lipogenesis. Third, IL15 treatment did not alter adipogenesis of preadipocytes or lipid accumulation during this process, contradicting its hypothesized role in adipocyte dedifferentiation. Forth, NRG4-

knockout mice showed no significant defects in pubertal mammary development or lactation, though subtle trends suggested a potential regulatory role in facilitating pubertal mammary gland development. Fifth, HFD suppressed mammary gland development, but NRG4 deletion did not exacerbate this phenotype, suggesting either functional compensation or limited involvement of NRG4 in HFD-mediated defects.

Conclusions:

This thesis investigates transcriptional and signalling networks governing cell fate transitions of mammary epithelial cells and stromal cells. First, stromal-epithelial transition is likely driven by combinatorial transcriptional regulation rather than single transcription factors FOXP1. Second, STAT5 was identified as a critical regulator promoting lipid synthesis in alveolar cells. Third, contrary to the previous study, functional validation revealed no direct effect of IL15 on adipogenesis or lipid metabolism. Fourth, despite the conserved NRG4-ERBB4 interaction across developmental stages, *Nrg4* knockout mice exhibited no overt defects in mammary gland development during puberty or lactation, suggesting compensatory mechanisms. Fifth, NRG4 might not be the major mediator of HFD-induced defects in mammary gland development, though compensatory mechanisms cannot be excluded. In summary, this work advances the understanding of transcriptional and signalling networks within cells in the mammary tissue during postnatal mammary gland development.

Keywords: mammary gland, cell differentiation, transcription factors, intercellular communications

Lay Summary

The mammary gland changes significantly during different life stages such as puberty, pregnancy, and lactation to prepare for milk production. These changes involve not only the growth and transformation of milk-producing cells, but also shifts in the surrounding supportive tissue and fat cells. Additionally, eating a high-fat diet has been linked to delayed breast development during puberty. However, many details about how these processes work at the molecular level are still unclear. This study tried to find out how cells in the mammary gland change during development, especially focusing on how milk-producing cells and fat cells influence each other.

This study found that mammary gland development involves a complex network of signals. Milk-producing cells were formed under the control of a variety of regulators. For example, a molecule, STAT5, was found to be essential for the cells to make milk fat. In turn, loss of another molecule, NRG4, did not lead to dominant problems on mammary gland development, whether under normal conditions or in cases of obesity. Overall, this research helps us better understand how different types of cells work together in the mammary gland and how diet can influence these processes. These insights may one day help improve maternal health.

Acknowledgements

First and foremost, I would like to express my heartfelt gratitude to my supervisor, Prof. Chaochen Wang, for his invaluable guidance and support throughout my doctoral research project. His expertise, critical feedback, encouragement, and patience were essential to shape the direction and execution of my work. Thank you for fostering a stimulating research environment and placing your trust in my abilities.

I am also deeply grateful to my colleagues for their generous assistance and collaboration in various aspects of the experimental work. Their technical help, thoughtful discussions, and moral support have been greatly appreciated and made this journey much more enriching. I would particularly like to thank Teng Wang for contributing experimental data to the section of this study involving STAT5, as acknowledged in the relevant chapter. In addition, I am grateful to Weijian Wang, Yihui Cen and Zezhen Lu for their assistance with the decontamination step of the single-nuclei sequencing analysis. I would also like to specifically acknowledge Yimin and Qian Tang for their valuable assistance with completing parts of the experimental work.

Lastly, I wish to extend my sincerest thanks to my parents and friends for their unwavering emotional support and care throughout my academic journey. Their understanding, encouragement, and companionship outside the lab have been a constant source of strength and comfort.

This work would not have been possible without the support of each and every one of you.

Declaration

I declare that this thesis represents my original research and has been composed solely by me. The experimental work presented in this thesis is almost entirely my own work, except where collaborative contributions have been acknowledged and clearly indicated in the text. All supporting literature, resources, and data from external sources have been properly referenced. This thesis has not been submitted for any previous degree or qualification.

Yueqing Xu

Table of Contents

Abstract.....	i
Lay Summary.....	iv
Acknowledgements	v
Declaration.....	vi
List of Figures	xii
List of Tables	xiv
Abbreviations	xvi
Chapter 1 Introduction.....	1
1.1 Overview of Mammary Tissue Development.....	1
1.1.1 Anatomical Structure and Function	1
1.1.2 Postnatal Development of The Mammary Gland	6
1.2 Cell Fate Transitions in Mammary Tissue	7
1.2.1 Importance of Cell Fate Transitions During Mammary Gland Development.....	7
1.2.2 Alveolar Cell Specification	9
1.2.3 PDGFR α^+ Stromal Cell Differentiation Potential	13
1.2.4 Loss of Lipid Droplets in Adipocytes	17
1.2.5 Mammary Epithelial Differentiation Regulated by Intercellular Signals..	20
1.3 Influences of Abnormal Lipid Metabolisms on Mammary Gland Development	21
1.3.1 Influences of Adipocyte Dysfunction on Mammary Gland Development	21
1.3.2 Diet-Induced Obesity and Mammary Gland Developmental Defects ...	23
1.4 Single-Cell Technologies Applied in Mammary Development Studies	26
1.5 Research Objectives	28

Chapter 2 Materials and Methods31
2.1 Materials.....	.31
2.1.1 Reagents31
2.1.2 Reagent Setup.....	.34
2.1.3 Antibodies42
2.1.4 Kits42
2.1.5 Primers44
2.2 Mice.....	.46
2.2.1 Mouse Strains and Maintenance46
2.2.2 Mouse Mating and Pregnancy Examination46
2.2.3 <i>Nrg4</i> Knockout Mice Maintenance47
2.2.4 High-Fat Diet Treatment48
2.3 Genotyping48
2.3.1 DNA Extraction48
2.3.2 PCR For <i>Nrg4</i> Allele.....	.48
2.4 Reverse Transcription and Quantitative PCR (qPCR)49
2.4.1 RNA Extraction49
2.4.2 Reverse Transcription50
2.4.3 qPCR50
2.5 Plasmids.....	.51
2.5.1 Foxp1 Plasmid Construction51
2.5.2 Gel Extraction53
2.6 Transformation54
2.6.1 Plasmid Extraction54
2.7 Cells56
2.7.1 Cell Lines and Maintenance56
2.7.2 Thawing and Freezing Cells56
2.7.3 Transfection and Lentivirus Concentration56

Deleted: 55

Deleted: 55

2.7.4 Transduction and Antibiotic Selection57
2.8 Histology	<u>58</u>
2.8.1 Whole Mount Staining.....	<u>58</u>
2.8.2 Paraffin Embedding and Sectioning.....	58
2.8.3 Haematoxylin and Eosin (H&E) Staining	<u>59</u>
2.8.4 Immunohistochemistry (IHC) Staining	59
2.9 Primary Stromal Cells Adipogenesis <i>In Vitro</i>	60
2.9.1 Primary Stromal Cells Isolation.....	60
2.9.2 FOXP1 Overexpression	61
2.9.3 Adipogenesis	61
2.9.4 Oil Red O Staining and Imaging	61
2.10 Primary Mammary Organoid Lipogenesis <i>In Vitro</i>	62
2.10.1 Primary Mammary Organoid Isolation	62
2.10.2 Lipogenesis Induction	63
2.10.3 Staining and Imaging	63
2.11 Primary Preadipocytes Adipogenesis <i>In Vitro</i>	64
2.11.1 Primary Preadipocyte Isolation	64
2.11.2 Adipogenesis.....	65
2.11.3 Staining and Imaging	<u>66</u>
2.12 Single-Nuclei RNA Sequencing Analysis	66
2.12.1 Mammary Tissue Harvest for Sequencing.....	66
2.12.2 Pre-processing and Clustering	66
2.12.3 Visualisation.....	<u>69</u>
2.12.4 Cell Type Identification.....	69
2.12.5 Deconvolution	70
2.12.6 Correlation Analysis	71
2.12.7 Identification of Differentiation Trajectory.....	71
2.12.8 Comparison of Top Transcriptional Regulators among Clusters.....	72

2.12.9 Identification of Intercellular Communications	73
2.13 Quantification and Statistical Analysis.....	74

Chapter 3 Single-Nucleus Sequencing Profiles Cell Map in Mammary

Tissue	<u>77</u>	Deleted: 76
3.1 Introduction	<u>77</u>	Deleted: 76
3.2 Single-Nucleus Sequencing Experimental Design.....	<u>78</u>	Deleted: 77
3.3 Clustering and Cell Type Identification.....	<u>79</u>	Deleted: 78
3.4 Identification of Differential Expressed Genes	<u>82</u>	Deleted: 81
3.5 Estimating Cell Fraction of Bulk RNA Sequencing Data	<u>85</u>	Deleted: 84
3.6 Discussion	<u>87</u>	Deleted: 86

Chapter 4 Identification of Potential Transcription Factors in Mammary

Epithelial Cell Fate Determination	<u>90</u>	Deleted: 89
4.1 Introduction	<u>90</u>	Deleted: 89
4.2 Bi-Directional Differentiation of Stromal Cells	<u>91</u>	Deleted: 90
4.2.1 A Stromal Cell Population with Mammary Epithelial Characteristics	<u>91</u>	Deleted: 90
4.2.2 Potential Transcription Factors Controlling Stromal Cell Differentiation	<u>93</u>	Deleted: 92
4.2.3 Effects of FOXP1 Overexpression on Stromal Cell Specification	<u>95</u>	Deleted: 94
4.3 STAT5 Phosphorylation Regulates Alveolar Cells Lipogenesis.....	<u>97</u>	Deleted: 96
4.3.1 Identification of Alveolar Cell in Single-Nucleus Sequencing Data	<u>97</u>	Deleted: 96
4.3.2 Potential Transcription Factors Directing Lipid Production in Alveolar Cells	<u>100</u>	Deleted: 99
4.3.3 Effects of Inhibiting STAT5 Phosphorylation on <i>In Vitro</i> Mammary Organoid Lipogenesis.....	<u>103</u>	Deleted: 102
4.4 Discussion	<u>105</u>	Deleted: 104

Chapter 5 Identification of Potential Cell-Cell Communication Signals in Mammary Tissue

5.1 Introduction	<u>107</u>	Deleted: 106
------------------------	------------	---------------------

5.2 Effects of Alveolar Cell-Produced Interleukin-15 on Adipocyte Dedifferentiation During Lactation 108

Deleted: 107

 5.2.1 Crosstalk Between Mammary Epithelial Cells and Adipocytes at Lactation 108

Deleted: 107

 5.2.2 Effects of IL15 on Adipogenesis of Preadipocytes 110

Deleted: 109

5.3 Effects of Adipocyte-Derived Neuregulin-4 on Mammary Gland Development 112

Deleted: 111

 5.3.1 Potential Regulatory Role of Adipocyte-Derived NRG4-ERBB4 Signalling in Alveolar Specification 112

Deleted: 111

 5.3.2 Effects of NRG4 on Alveologenesis and Breastfeeding 113

Deleted: 112

 5.3.3 Effects of NRG4 on Mammary Gland Development During Puberty 115

Deleted: 114

5.4 Discussion 116

Deleted: 115

Chapter 6 Single-Nucleus Sequencing Reveals the Mechanisms of HFD-Induced Mammary Gland Development Defects 118

Deleted: 117

6.1 Introduction 118

Deleted: 117

6.2 High-Fat Diet Affects Mammary Gland Development During Puberty 119

Deleted: 118

6.3 Effects of NRG4 Deletion on Mammary Gland Development of High-Fat Diet Fed Mice 122

Deleted: 121

6.4 Discussion 124

Deleted: 123

Chapter 7 Discussion and Future Perspectives 126

Deleted: 125

References 138

Deleted: 137

List of Figures

Figure 1.1 Schematic diagram of mammary gland development after birth.....	2
Figure 1.2 Diagram illustrating the mechanism of stromal-epithelial transition.	15
Figure 1.3 Diagram illustrating differentiation dynamics of mammary adipocytes during pregnancy, lactation and involution.	18
Figure 2.1 Timeline of time mating.	47
Figure 3.1 Schematic diagram highlighting the experimental design for snRNA-seq and downstream analyses.	<u>79</u> Deleted: 78
Figure 3.2 snRNA-seq identifies 6 cell types in the mammary tissue.	<u>80</u> Deleted: 79
Figure 3.3 Proportion of each cell type at different stages.	<u>82</u> Deleted: 81
Figure 3.4 Expression of cell type-specific markers identified through snRNA-seq.	<u>83</u> Deleted: 82
Figure 3.5 Cell fraction imputation of bulk RNA-sequencing data.....	<u>86</u> Deleted: 85
Figure 3.6 The number of detected genes per cell in snRNA-seq versus scRNA-seq data.	<u>89</u> Deleted: 88
Figure 4.1 Identification of a stromal subpopulation with epithelial features.	<u>92</u> Deleted: 91
Figure 4.2 Potential transcription factors involved in stromal-epithelial transition.	<u>94</u> Deleted: 93
Figure 4.3 Overexpression of FOXP1 suppressed adipogenesis of stromal cells.	<u>96</u> Deleted: 95
Figure 4.4 Identification of lipid-containing alveolar cells in luminal clusters.	<u>98</u> Deleted: 97
Figure 4.5 Identification of alveolar-specific lipogenesis genes.	<u>100</u> Deleted: 99
Figure 4.6 Potential transcription factors promoting differentiation and lipid production of alveolar cells.....	<u>101</u> Deleted: 100
Figure 4.7 Efficiency of STAT5 phosphorylation inhibitor STAT5-IN-1.	<u>103</u> Deleted: 102
Figure 4.8 Inhibiting STAT5 phosphorylation suppressed lipid production in	

mammary organoids.	104	Deleted: 103
Figure 5.1 Potential epithelial-derived signals inducing dedifferentiation of adipocytes during lactation.....	109	Deleted: 108
Figure 5.2 Effects of IL15 on lipid synthesis of preadipocytes.	111	Deleted: 110
Figure 5.3 Potential adipocyte-derived signals promoting luminal growth and differentiation.....	113	Deleted: 112
Figure 5.4 Effects of global NRG4 knockout on lactating functions of the mammary gland.	114	Deleted: 113
Figure 5.5 Effects of global Nrg4 KO on mammary gland development during puberty.....	116	Deleted: 115
Figure 6.1 HFD induces weight gain and abnormal mammary gland development.	120	Deleted: 119
Figure 6.2 snRNA-seq of cells in mammary tissues from mice fed by HFD and ND.	121	Deleted: 120
Figure 6.3 Effects of global Nrg4 knockout on ductal morphogenesis of the mammary gland under HFD.....	123	Deleted: 122

List of Tables

Table 2.1 Composition of Tail Lysis Buffer.....	34
Table 2.2 Composition of LB media	35
Table 2.3 Composition of LB agar plate	35
Table 2.4 Composition of 293T/preadipocyte culture medium	36
Table 2.5 Composition of 293T freezing medium	36
Table 2.6 Composition of Carnoy's solution	36
Table 2.7 Composition of carmine stain	36
Table 2.8 Composition of primary SVF digestion stock buffer.....	37
Table 2.9 Composition of primary SVF digestion buffer	38
Table 2.10 Composition of SVF culture medium	38
Table 2.11 Composition of adipogenesis induction medium.....	39
Table 2.12 Composition of adipogenesis differentiation medium	39
Table 2.13 Composition of primary mammary organoid digestion buffer	39
Table 2.14 Composition of basal organoid medium	40
Table 2.15 Composition of lactation medium	40
Table 2.16 Composition of OWB	40
Table 2.17 Composition of fructose-glycerol clearing solution	41
Table 2.18 Composition of Krebs Ringers (KR) Buffer, 25 × Stock	41
Table 2.19 Composition of primary preadipocyte digestion buffer.....	41
Table 2.20 Composition of <i>TransZol Up</i> Kit.....	42
Table 2.21 Composition of <i>TransScript® All-in-One First-Strand cDNA Synthesis SuperMix</i> for qPCR (One-Step gDNA Removal) Kit.....	42
Table 2.22 Composition of 2 × <i>PerfectStart® Green qPCR SuperMix</i> Kit.....	42
Table 2.23 Composition of FastPure Gel DNA Extraction Mini Kit	43
Table 2.24 Composition of BM Seamless Cloning Kit	43

Table 2.25 Composition of FastPure Plasmid Mini Kit	43
Table 2.26 Composition of NucleoBond Xtra Midi kit for transfection-grade plasmid DNA.....	43
Table 2.27 Composition of DAB Substrate Kit.....	44
Table 2.28 Primer list for genotyping.....	44
Table 2.29 Primer list for plasmid construction.....	44
Table 2.30 Primer list for qPCR	45
Table 2.31 PCR reaction mixture for genotyping.....	48
Table 2.32 PCR programme for genotyping	49
Table 2.33 Reaction mixture for reverse transcription	50
Table 2.34 qPCR reaction mixture.	50
Table 2.35 qPCR programme.....	50
Table 2.36 PCR mixture for DNA fragment amplification	51
Table 2.37 PCR programme for DNA fragment amplification	51
Table 2.38 Mixture for pCDH-IRES-neo plasmid restriction digestion.....	52
Table 2.39 Mixture for seamless cloning	52
Table 2.40 Mixture for pCDH-EF1 α -HA-Foxp1-IRES-neo plasmid restriction digestion.....	<u>53</u>
Table 2.41 Mixture for 293T transfection	56
Table 2.42 Canonical markers used for cell type identification	69
Table 3.1 Cell type-specific markers identified by snRNA-seq data.....	<u>84</u>

Deleted: 52

Deleted: 83

Abbreviations

ANOVA	Analysis of variance
BOM	Basal organoid medium
BSA	Bovine serum albumin
C/EBP	CCAAT/enhancer-binding protein
ddH ₂ O	Double-distilled water
DEG	Differential expressed genes
ECM	Extracellular matrix
EGFR	Epidermal growth factor receptor
ELF5	E74-like factor 5
ER	Oestrogen receptor
GO	Gene ontology
HFD	High-fat diet
H&E	Haematoxylin and Eosin
IBMX	3-isobutyl-1-methylxanthine
IGF1	Insulin-growth factor-1
IHC	Immunohistochemistry
IL15	Interleukin 15
JAK	Janus kinase
KO	Knockout
L1	Lactation day 1
L5	Lactation day 5
LB medium	Luria-Bertani medium
MaSC	Mammary stem cell
MG	Mammary gland
ND	Normal diet

NRG	Neuregulin
OWB	Organoid washing buffer
OXTR	Oxytocin receptor
P13.5	Pregnancy day 13.5
PBS	Phosphate-buffered saline
PCA	Principal components analysis
PCR	Polymerase chain reaction
PDGFC	Platelet derived growth factor C
PDGFR α	Platelet derived growth factor receptor alpha
PKA	Protein kinase A
Plin2	Perilipin 2
PPAR γ	Peroxisome proliferator-activated receptor gamma
PR	Progesterone receptor
PRL	Prolactin
PRLR	Prolactin receptor
P/S	Penicillin-Streptavidin
RBPJ	Recombination signal binding protein for immunoglobulin kappa J region
RT	Room temperature
scRNA-seq	Single-cell RNA sequencing
SD	Standard deviation
snRNA-seq	Single-nucleus RNA sequencing
STAT	Signal transducer and activator of transcription
SVF	Stromal-vascular fraction
TEB	Terminal end bud
UMAP	Uniform manifold approximation and projection
WAP	Whey acidic protein
WT	Wild-type

Chapter 1

Introduction

1.1 Overview of Mammary Tissue Development

1.1.1 Anatomical Structure and Function

The mammary gland is a specialized organ in mammals responsible for synthesis and delivery of breast milk. Breast milk plays an irreplaceable role in supporting growth and development of neonates, not only by providing essential nutrients but also delivering biological active components to help establishing their early immune environment (K. E. Lyons et al., 2020). Breastfeeding protects infants from a range of diseases, effectively reducing the incidence of gastrointestinal tract infections, asthma, and obesity while enhancing neonatal survival rates (Dogaru et al., 2014; Horta et al., 2015; Klopp et al., 2017; L. Wang et al., 2017; D. Xu et al., 2024; L. Xu et al., 2017). The quality of breastfeeding is closely related to the functional coordination of various cell types within the mammary tissue.

The mammary tissue is composed of the mammary epithelium surrounded by the stromal fat pad. The mammary epithelium, which are responsible for milk production in the mature mammary gland, consists of ducts and alveoli formed by mammary epithelial cells. Surrounding the mammary epithelium, the stromal fat pad includes stromal cells that provide structural support and adipocytes that contribute to energy storage and cellular signalling.

Mammary Epithelial Cells

The mammary epithelium is organized as a bilayered structure composed of mammary stem cells (MaSCs), basal cells and luminal cells ([Figure 1.1C](#)). Basal cells form the outer layer of the mammary epithelium while luminal cells constitute

Deleted: Figure 1.1

Formatted: Default Paragraph Font

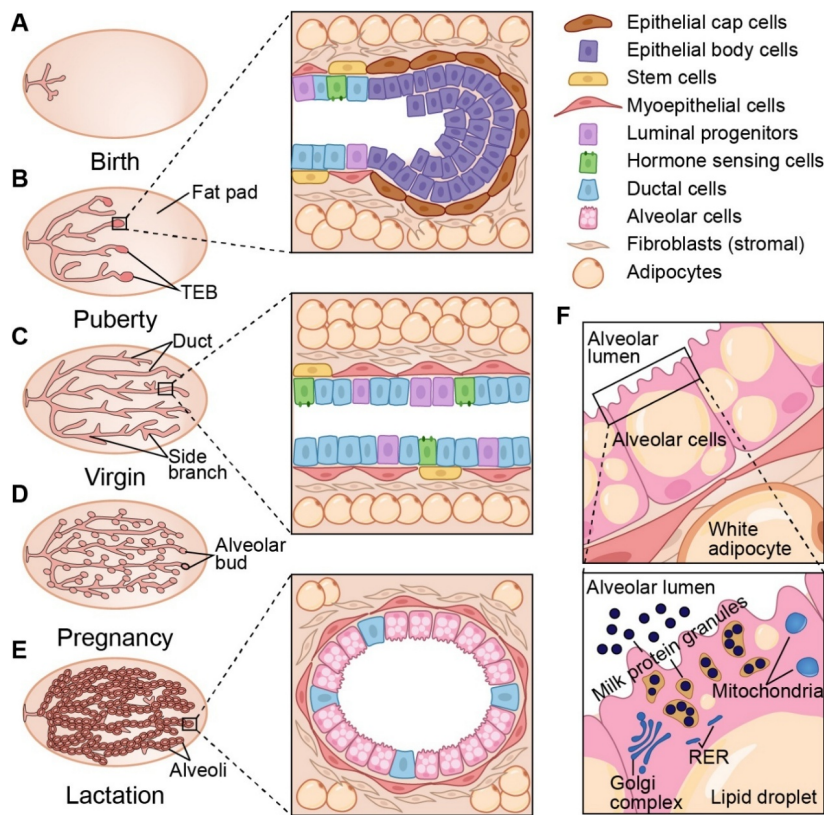


Figure 1.1 Schematic diagram of mammary gland development after birth.

A. The rudimentary mammary glands formed at birth. B. During puberty, mammary epithelial cells proliferate and the mammary ducts invade into the stromal fat pad. The ductal elongation is driven by terminal end buds (TEBs), which are composed of highly proliferative epithelial cap cells and body cells. C. In mature virgin, the mammary gland fills the fat pad with its ducts and side branches. The ductal epithelium is composed of the outer basal layer and the inner luminal layer. The basal layer contains myoepithelial cells and stem cells while the luminal layer contains luminal progenitors, hormone sensing cells and ductal cells. D. During pregnancy, epithelial cells expand and differentiate to form alveolar buds. E. The alveoli are mature and produce breast milk during lactation. The alveoli are composed of myoepithelial cells in the outer layer and alveolar cells and ductal cells in the inner layer. F. The alveolar cells synthesize and secrete milk protein and milk fats. They contain Golgi complex, rough endoplasmic reticulum (RER) and mitochondria. Modified from Cinti, 2018; Inman et al., 2015.

the inner layer. MaSCs are primarily located in the basal layer of the mammary epithelium.

MaSCs, identified by cell surface markers CD24 (heat stable antigen) and either CD29 (β 1-integrin) or CD49f (α 6-integrin), are multipotent stem cells that can give rise to lineage-specific unipotent progenitors, which further differentiate into basal cells and luminal cells (Shackleton et al., 2006; Stingl et al., 2006). In addition, MaSCs possess self-renewal capacity to sustain the stem cell reservoir (Y. A. Zeng & Nusse, 2010). Multipotency and the self-renewal capacity enable MaSCs to reconstitute a mammary gland after transplantation into a cleared mammary fat pad (Kordon & Smith, 1998; Stingl et al., 2006). In addition to MaSCs, a subset of basal cells exhibits multipotency and self-renewal capacity, serving as a reservoir for regenerating epithelial cells (H. Han et al., 2002; Prater et al., 2014).

The basal lineage population includes both stem-like basal cells and myoepithelial cells (Prater et al., 2014). Basal cells express specific markers cytokeratin 5 (KRT5) and cytokeratin 14 (KRT14), which distinguish them from other epithelial cells (Inman et al., 2015; Van Keymeulen et al., 2011). Stem-like basal cells are known for their high proliferative capacity and multipotency, which enable them to self-renew and differentiate into various types of epithelial cells to repopulate a mammary gland (Prater et al., 2014). Myoepithelial cells are differentiated basal cells with contractile properties, characterised by the enriched expressions of genes encoding actin and myosin filaments, such as *Acta2* and *Myh11*. During lactation, oxytocin binds to oxytocin receptor (OXTR) on myoepithelial cells to induce contraction, which enables myoepithelial cells to facilitate milk ejection. In addition to the contractile functions, a proportion of myoepithelial cells obtain lineage-restricted repopulating potential, allowing them to contribute to the regeneration and maintenance of the basal layer of mammary epithelium (Prater et al., 2014). Moreover, basal cells secrete growth factors that modulate the

maturity of luminal cells (Forster et al., 2014).

Luminal cells, characterised by the specific expression of cytokeratin 8 (KRT8) and cytokeratin 18 (KRT18), are the key components of the mammary gland epithelium and play essential roles in its development and function (Inman et al., 2015; Van Keymeulen et al., 2011). Based on their functions, luminal cells can be classified into luminal progenitors, hormone sensing cells, ductal cells and alveolar cells. Luminal progenitors are unipotent and serve as a reservoir for generating mature luminal cells, which contributes to the maintenance and expansion of the mammary epithelium during postnatal development of the mammary gland (Rios et al., 2014; Van Keymeulen et al., 2011; Wuidart et al., 2016). Hormone-sensing cells express oestrogen receptors (ER) and progesterone receptors (PR), which allow them to detect the hormonal changes and regulate the differentiation of neighbouring luminal cells and basal cells through paracrine signalling (Brisken et al., 1998; Mallepell et al., 2006; Tarulli et al., 2013). Ductal cells are hormone receptor-negative (ER^+PR^-) luminal cells, which form the epithelial lining of the mammary ducts (C. Wang et al., 2017). Ductal cells respond to paracrine signals from hormone-sensing cells, which regulate their proliferation and differentiation for ductal elongation of the mammary gland during puberty (Beleut et al., 2010). Characterised by expression of milk proteins such as whey acidic protein (WAP) and β -casein, alveolar cells are essential for milk production and secretion during lactation.

Alveolar cells obtain distinct morphological characteristics as they contain milk protein granules and lipid droplets (Figure 1.1F), making their morphology more similar to adipocytes rather than epithelial cells (Morroni et al., 2004; Prokesch et al., 2014). Although alveolar cells undergo lipid accumulation, they are distinct from conventional adipocytes. Alveolar cells not only contain several large lipid droplets separated by cytoplasmic membranes but also exhibit larger mitochondria and an

Deleted: Figure 1.1

Formatted: Default Paragraph Font

abundance of rough endoplasmic reticulum ([Figure 1.1F](#)), which ensure the ability of synthesizing proteins and lipids in breast milk (Morroni et al., 2004). More importantly, lipid-containing alveolar cells express distinct lipogenesis genes compared to other adipocytes. For instance, lipid droplets in alveolar epithelial cells are coated with the lipid-binding protein perilipin 2 (PLIN2) while lipid droplets in conventional white adipocytes are coated with perilipin 1 (PLIN1) (Prokesch et al., 2014). These differences indicate that though alveolar cells undergo lipid accumulation, they obtain characteristics distinct from conventional adipocytes.

Deleted: Figure 1.1

Formatted: Default Paragraph Font

Stromal Cells

The mammary stromal cells consist of diverse types of cells, including mesenchymal cells such as adipocyte progenitors and fibroblasts. Fibroblasts are embedded within the mammary fat pad and play crucial roles in the survival and morphogenesis of the mammary epithelial cells (Liu et al., 2012; Makarem et al., 2013; Simian et al., 2001). Fibroblasts are not only responsible for synthesizing extracellular matrix (ECM) components, such as collagen and fibronectin, but also remodelling the ECM through degradation by enzymes, which provides structural support for the morphogenesis and homeostasis of the mammary gland (Simian et al., 2001; Wiseman & Werb, 2002). Sharing the similar genetic characteristics with fibroblasts, adipocyte progenitors support the mammary gland development through differentiation into mature adipocytes. Maturation of adipocyte progenitors contributes to the expansion of the mammary fat pad, which provides the structural framework for ductal elongation during puberty. Moreover, adipocyte progenitors can generate luminal and basal cells under the stimulation of oestrogen and progesterone (Joshi et al., 2019).

Mammary Adipocytes

White adipocytes which contain a large unilocular lipid droplet in their cytoplasm

are the main components of the fat pad in the non-lactating mammary tissue. Adipocytes are indispensable for mammary gland development during puberty, supported by the evidence that lipodystrophic mice have impaired mammary gland development (Brenot et al., 2020). During lactation, lipid contents in adipocytes reduce or even disappear, indicating a possibility that lipids in adipocytes serve as a reservoir for the high metabolic demands of milk production (Elias et al., 1973; Gregor et al., 2013; Russell et al., 2007). Mammary adipocytes regulate the growth of mammary epithelium through various signalling pathways, which will be discussed in later sections (Jin et al., 2015; Lin & Li, 2007).

1.1.2 Postnatal Development of The Mammary Gland

The mammary gland undergoes significant development and remodelling during key physiological stages such as puberty, pregnancy, and lactation, driven by hormonal and intercellular interactions. The mammary gland originates from the ectoderm of the embryo and forms a rudimentary ductal tree at birth ([Figure 1.1A](#)) (Inman et al., 2015). The rudimentary ducts remain quiescent after birth until hormonal stimulation at the onset of puberty. During puberty, the mammary ducts invade into the fat pad, elongate and branch under the control of hormones such as oestrogen and progesterone (W. R. Lyons, 1958). During ductal expansion, terminal end buds (TEBs) are formed at the invading tips of the elongating mammary ducts. TEB is a highly proliferative structure consisting of an outer layer of cap cells enclosing multilayered body cells ([Figure 1.1B](#)) (Silberstein & Daniel, 1982; Williams & Daniel, 1983). Cap cells are considered to give rise to myoepithelial cells while body cells differentiate into luminal cells (L. Hennighausen & Robinson, 2005; Silberstein & Daniel, 1982; Williams & Daniel, 1983). The mammary gland finally fills the fat pad in the mature virgin, with the bilayered ductal structure consisting of luminal cells with apical orientation and basal cells possessing at the basal side ([Figure 1.1C](#)). After sexual maturity, mammary

Deleted: Figure 1.1

Formatted: Default Paragraph Font

Deleted: Figure 1.1

Formatted: Default Paragraph Font

Deleted: Figure 1.1

Formatted: Default Paragraph Font

epithelial cells still undergo proliferation and apoptosis in each oestrous cycle (Fata et al., 2001).

At the onset of pregnancy, under the stimulations of hormones such as progesterone and prolactin, mammary epithelial cells proliferate and differentiate rapidly to form alveolar buds, which later develop into secretory alveoli that synthesize and eject breast milk ([Figure 1.1D, E](#)). Synchronized with lobuloalveolar development, adipocytes in the fat pad regress to generate space for the expansion of the mammary epithelium. During pregnancy, the luminal progenitors specialize into alveolar cells that are capable of synthesising milk proteins and fats (Morroni et al., 2004; Prokesch et al., 2014). In addition, lineage tracing revealed that part of luminal cells was derived from adipocyte progenitors at mid-pregnancy, suggesting that luminal progenitors are not the only source of mature luminal cells (Joshi et al., 2019). After tissue remodelling and epithelial specialization during pregnancy, the alveoli are mature and almost fill the whole mammary fat pad at the beginning of lactation ([Figure 1.1D, E](#)). During lactation, the alveolar cells synthesize and secrete milk into the alveolar lumen ([Figure 1.1F](#)). Breast milk in the lumen is squeezed out through the contraction of myoepithelial cells under the stimulation of oxytocin. Meanwhile, as the fat pad filled with the mammary epithelium, some adipocytes lose their lipid droplets and undergo dedifferentiation (Q. A. Wang et al., 2018; Zwick et al., 2018). Upon weaning, mammary epithelial cells undergo apoptosis and the mammary gland is remodelled back to its adult state.

Deleted: Figure 1.1

Formatted: Default Paragraph Font

Deleted: Figure 1.1

Formatted: Default Paragraph Font

Deleted: Figure 1.1

Formatted: Default Paragraph Font

1.2 Cell Fate Transitions in Mammary Tissue

1.2.1 Importance of Cell Fate Transitions During Mammary Gland Development

Cell fate specification is a critical process in mammary gland development, as it ensures the proper formation and function of diverse cell types that constitute this

complex organ. In postnatal mammary gland development, MaSCs generate committed progenitors for the basal and luminal epithelial lineages, which subsequently differentiate into distinct subtypes of functional basal and luminal cells.

This process occurs during puberty, pregnancy and lactation. Specification of stem cells and progenitor cells is regulated by hormone signalling and molecular pathways, which trigger intracellular signalling cascades to modulate the activity of transcription factors. Errors in cell fate specification can lead to defects in establishing and maintaining functional ductal and alveolar structures of the mammary gland. For example, deletion of ER in mammary epithelial cells disrupts postnatal development, resulting in the absence of TEB formation and ductal elongation (Feng et al., 2007; Mallepell et al., 2006). Similarly, loss of ER in milk-secreting alveolar cells leads to defects in lobuloalveolar development and nursing (Feng et al., 2007; Mallepell et al., 2006). Moreover, in molecular aspect, silencing the Notch effector Cbf-1 in MaSCs promotes excessive proliferation of MaSCs and progenitor cells while impairing their proper differentiation into luminal cells (Bouras et al., 2008). In addition to mammary epithelial cells, regulating the differentiation and function of stromal cells and adipocytes is important for maintaining tissue homeostasis and supporting adaptive remodelling during different physiological stages. For instance, promoting lipogenesis in adipocytes by deletion of adipocyte-XBP1 reduces the milk production and litter growth (Gregor et al., 2013).

In summary, cell fate specification in the mammary gland is a highly coordinated process relies on the interplay of hormonal signalling and cell-cell interactions to ensure the proper development and function of the mammary gland. Essential processes determining fate of epithelial cells, stromal cells and adipocytes in the mammary tissue occur during pregnancy and lactation. During these stages, luminal epithelial cells specialize into milk-producing alveolar cells, which

synthesize necessary proteins and fats in breast milk. In addition, some stromal cells also serve as a source of luminal cells during pregnancy. Furthermore, morphology and genetic characteristics of adipocytes change during lactation, indicating that adipocytes are dedifferentiated at this stage. In the following sections, these aspects will be explored in greater depth, examining the mechanisms of alveolar cell specification, the differentiation potential of stromal cells, and the fascinating phenomenon of adipocyte dedifferentiation during lactation.

1.2.2 Alveolar Cell Specification

To fulfil the vital function of lactation, luminal cells differentiate into alveolar cells which are dedicated to synthesizing and secreting essential nutrients such as milk proteins and milk fat. The specification of alveolar cells is tightly regulated by multiple hormones and signalling molecules, which orchestrate the activity of downstream transcription factors to modulate cell type-specific gene expressions. Extensive research has identified a variety of transcription factors and signalling pathways that play crucial roles in alveogenesis, including STAT5, GATA3 and ELF5 (Asselin-Labat et al., 2007; Chakrabarti et al., 2012; Choi et al., 2009; Cui et al., 2004; Gallego et al., 2001; Jones et al., 1999, p. 199; Kouros-Mehr et al., 2006; Oakes et al., 2008).

STAT5 is a transcription factor from the signal transducer and activator of transcription (STAT) family that primarily mediates cellular responses to diverse extracellular cytokines and growth factors. Composed of STAT5A and STAT5B, STAT5 is the key transcription factor promoting the proliferation and differentiation of luminal cells in the mammary gland. Although loss of STAT5A and STAT5B in mammary epithelial cells has no effect on basal stem cell populations and primary ductal outgrowth, it significantly reduces the abundance of luminal progenitors, which suppresses side branching during puberty and alveolar formation during

pregnancy (Cui et al., 2004; Vafaizadeh et al., 2010; Yamaji et al., 2009). Moreover, even deletion of STAT5 in differentiated alveolar cells results in premature apoptosis and a sparser alveolar structure, underscoring its necessity for alveolar cell survival (Cui et al., 2004). Interestingly, defects in alveolar formation caused by conditional knockout of STAT5A and STAT5B in mammary epithelial cells can be rescued by merely reintroducing STAT5A into *Stat5a/Stat5b*-deficient cells, indicating that STAT5A and STAT5B demonstrate distinct functions in regulating luminal differentiation (Yamaji et al., 2009). STAT5A is essential for both establishing the luminal progenitor population during puberty and promoting lobuloalveolar development during pregnancy. Compared to wild-type and STAT5B knockout mice, the STAT5A knockout mice exhibited significantly reduced side branching in mammary ducts during pubertal development (Teglund et al., 1998). On the contrary, overexpressing STAT5A by introducing the expression of a constitutively activated mouse Stat5a mutant (cS5-F) in mammary epithelial cells triggered hyperproliferation of mammary epithelium and premature alveolar formation in virgin mice (Vafaizadeh et al., 2010). Furthermore, STAT5A deletion disrupts alveolar formation and impairs the lactation function of the murine mammary gland (Liu et al., 1997). Depletion of STAT5A in mammary epithelial cells specifically suppresses the development of alveolar cells as early as pregnancy day 6, indicating that STAT5A is indispensable for the specialization from luminal progenitors to alveolar progenitors during early pregnancy (Yamaji et al., 2013). Consistently, compared to mid-pregnancy, STAT5A expression in mammary epithelial cells significantly increases at the onset of lactation, which further emphasizes its sustained roles in alveolar cell function and maintenance (L. Hennighausen & Robinson, 2005). On the other hand, although STAT5B-null mice exhibit reduced side branching, their alveolar expansion during pregnancy remains relatively normal (Teglund et al., 1998). In summary, STAT5, especially STAT5A, is essential for the proliferation, differentiation, and survival of the luminal cells.

STAT5 deletion in mammary epithelial cells leads to opposing changes in GATA3 and ELF5 expression, both of which are indispensable for normal development of the mammary gland (Asselin-Labat et al., 2007; Oakes et al., 2008; Reichenstein et al., 2011; Yamaji et al., 2009). Expression of GATA3 in the mammary tissue increases when abrogating STAT5 expression during lactation, suggesting that GATA3 compensates part of STAT5 function to preserve the differentiation of luminal cells (Reichenstein et al., 2011). On the contrary, ELF5 expression significantly decreases in luminal progenitors after STAT5 deletion, indicating ELF5 might be a downstream target of STAT5 (Yamaji et al., 2009).

GATA3 belongs to the GATA family of zinc-finger transcription factors which play essential roles in cell fate specification. GATA3 is restricted to the luminal lineage and necessary for ductal elongation and alveolar maturation (Asselin-Labat et al., 2007; Kouros-Mehr et al., 2006). Different from the effects of STAT5 deletion, loss of GATA3 results in an expansion of the luminal progenitor population (Asselin-Labat et al., 2007; Kouros-Mehr et al., 2006). This finding indicates that GATA3 mainly drives the differentiation of luminal progenitors rather than contributing to their generation or maintenance. Subsequently, luminal differentiation disrupted by GATA3 deletion leads to failure of TEBs formation, which consequently impairs ductal elongation and branching morphogenesis (Asselin-Labat et al., 2007; Kouros-Mehr et al., 2006). On the other hand, similar to STAT5, GATA3 knockout in alveolar cells reduces both the number and size of alveoli during late pregnancy and lactation, highlighting its integral roles in maintaining survival of alveolar cells (Asselin-Labat et al., 2007; Kouros-Mehr et al., 2006). Therefore, GATA3 is critical for differentiation of luminal cells and maintenance of lactation.

ELF5 (E74-like factor 5) is a ETS transcription factor that restricts the luminal lineage and facilitates the alveolar specification (Oakes et al., 2008). Although ELF5 deletion in mammary epithelial cells does not affect ductal morphogenesis, it

disrupts lobuloalveolar development by preventing the differentiation of luminal progenitors (Chakrabarti et al., 2012; Choi et al., 2009; Oakes et al., 2008). Conversely, induced ELF5 expression in virgin mice triggers alveolar specification and milk secretion, while simultaneously interfering with ductal morphogenesis (Oakes et al., 2008). Although ELF5 expression in luminal progenitors is influenced by STAT5 through a STAT5-binding motif in the distal region of the *Eif5* gene promoter, it can be modulated independently by hormone-stimulated signalling pathways (Harris et al., 2006; H. J. Lee et al., 2013; Yamaji et al., 2009). Furthermore, another study suggests that ELF5 binds to the proximal *Stat5* promoter to regulate the expression of *Stat5* gene, supported by the evidence that ELF5 depletion leads to reduced STAT5A expression in mature mammary glands (Choi et al., 2009). In addition to directly regulating STAT5 expression, ELF5 sustains STAT5 activity by inhibiting negative mediators of STAT5 phosphorylation (Choi et al., 2009).

STAT5 phosphorylation is a key step in JAK/STAT5 signalling pathway, which plays a vital role in mammary gland development during pregnancy and lactation (L. Hennighausen & Robinson, 2005). Binding of prolactin (PRL) and its receptor (PRLR) or ERBB4 and its ligands can activate this pathway (Gallego et al., 2001; Jones et al., 1999). Upon binding of prolactin to the transmembrane receptor PRLR, a conformational change occurs in the PRLR dimer, which leads to the phosphorylation of specific tyrosine residues by Janus kinase-2 (JAK2) (Y. Han et al., 1997; Pezet et al., 1997). During this process, STAT5 is recruited and activated through phosphorylation (DaSilva et al., 1996). Activated STAT5 translocates into the nucleus, where it binds to specific sites on the chromatin DNA to regulate the expression of downstream genes (Wakao et al., 1995). Similar to PRLR, the binding of ERBB4 ligands to ERBB4 activates STAT5, thereby transmitting growth and differentiation signals in alveolar cells. ERBB4 belongs to the epidermal growth factor receptor (EGFR) family, and its activation is regulated by neuregulins (NRG)

or other EGF-related polypeptides (Carraway III et al., 1997; Holmes et al., 1992; Plowman et al., 1993). These ligands are secreted by mammary epithelial cells or surrounding cells and exert their effects on luminal cells through paracrine signalling. For instance, neuregulin-1 (NRG1) secreted by basal cells activates ERBB4/STAT5A signalling in luminal cells in a paracrine manner, which promotes the maturation of luminal progenitors (Forster et al., 2014). Signalling pathways mediated by ERBB4 are indispensable for luminal differentiation and alveolar formation. Even in the presence of prolactin, ERBB4 deletion in mammary epithelial cells results in incomplete alveolar specification and reduced alveolar formation (Long et al., 2003). Additionally, activated STAT5 cannot be detected in alveolar cells lacking ERBB4, suggesting that ERBB4 plays a more prominent role in activating STAT5 in alveolar cells than PRLR (Long et al., 2003; Tidcombe et al., 2003).

In order to support lactation, luminal progenitors differentiate into alveolar cells that are responsible for milk production. This process is regulated by hormone-induced signalling pathways and their downstream transcription factors such as STAT5, GATA3, and ELF5. Activated by prolactin or ERBB4 ligands, JAK/STAT5 is the core downstream signalling pathway of hormonal regulation. Particularly, ERBB4 plays a vital role in activating STAT5 for alveolar differentiation. Although the mechanisms of alveolar specification are well-studied, whether these transcription factors and signalling pathways are involved in regulating lipid synthesis in alveolar cells remains unknown.

1.2.3 PDGFR α ⁺ Stromal Cell Differentiation Potential

Platelet derived growth factor receptor alpha (PDGFR α) is a marker of adipocyte progenitors in white adipose tissue. PDGFR α ⁺ stromal cells can differentiate into mature white adipocytes both in vitro and in vivo (Y.-H. Lee et al., 2012). In addition, PDGFR α ⁺ stromal cells serve as a reservoir for mammary epithelial cells.

PDGFR α ⁺ stromal cells migrate into the mammary epithelium and differentiate into mammary epithelial cells in response to oestrogen and progesterone stimulation

(Figure 1.2) (Joshi et al., 2019). A progeny of PDGFR α ⁺ cells that expresses mammary epithelial markers across various developmental stages of the mammary gland has been identified within the mammary epithelium (Joshi et al., 2019). As PDGFR α ⁺ stromal cells are previously regarded as precursors of some stromal cells such as fibroblasts and adipocytes, this finding provides an insight into the differentiation potential of PDGFR α ⁺ stromal cells in the mammary gland.

PDGFR α ⁺ stromal cell-derived mammary epithelial cells are observed in the mammary gland as early as the embryonic stage without exogenous oestrogen and progesterone stimulation and persist through prepubertal and pubertal development. Lineage tracing proves that PDGFR α ⁺ stromal cells give rise to both basal cells and hormone receptor-negative luminal cells during puberty. After sexual maturation, the stromal-epithelial transition diminishes and is only prominently detected after exogenous oestrogen and progesterone treatment. During pregnancy, the stromal-epithelial transition is reactivated and luminal cells derived from PDGFR α ⁺ stromal cell are observed at mid-gestation. Further investigations demonstrate that hormonal signals inducing the stromal-epithelial transition are responded by the mammary epithelial cells, which subsequently promote the expression of platelet derived growth factor C (PDGFC) in mammary epithelial cells. PDGFC secreted by mammary epithelial cells induces migration of PDGFR α ⁺ stromal cells to mammary epithelium, where PDGFR α ⁺ stromal cells undergo transition into epithelial cells (Joshi et al., 2019). Although this study provides a possible signalling pathway directing the stromal-epithelial transition, the downstream mechanisms underlying this process remain unclear.

Activation of PDGFR α might initiates downstream signalling pathways, which regulate cell proliferation, survival, and differentiation. STAT5 phosphorylation was

Deleted: Figure 1.2

Formatted: Default Paragraph Font

Formatted: Highlight

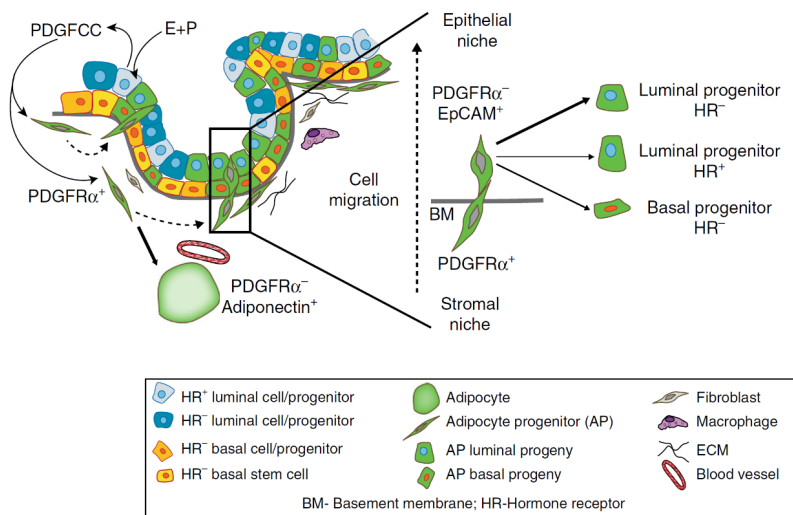


Figure 1.2 Diagram illustrating the mechanism of stromal-epithelial transition.

PDGFR α^+ stromal cells are found in the mammary stromal niche and have the potential to differentiate into Adiponectin $^+$ adipocytes within the mammary fat pad or transition into EpCAM $^+$ epithelial cells. In response to oestrogen and progesterone (E+P) stimulation, mammary epithelial cells secrete PDGFCC, which is a PDGFR α ligand. Under the induction of PDGFCC, PDGFR α^+ stromal cells migrate toward the epithelial niche and primarily generate hormone receptor-negative (HR $^-$) epithelial progeny (Joshi et al., 2019).

detected in human CD34 $^+$ hematopoietic progenitor cells expressing FIP1L1-PDGFR α , suggesting that STAT5 may serve as a downstream mediator of signalling pathways activated by PDGFR α binding (Buitenhuis et al., 2007). As STAT5 is an essential transcription factor governing the proliferation and differentiation of luminal cells, it is likely that activation of PDGFR α triggers STAT5 phosphorylation, thereby facilitating the stromal-epithelial transition. However, it does not account for the transition into basal cells, implying the involvement of a more complex downstream signalling network in this process.

Another well-studied function of PDGFR α^+ stromal cells is adipogenesis, a process whereby PDGFR α^+ stromal cells differentiate into adipocytes. Adipocyte

differentiation is regulated by a complex network of signalling pathways and transcription factors. Peroxisome proliferator-activated receptor gamma (PPAR γ) and CCAAT/enhancer-binding proteins (C/EBPs) are the master regulators of adipogenesis, which orchestrate the expression of genes involved in lipid metabolism and adipocyte functions. Early in adipogenesis, C/EBP β and C/EBP δ are induced in response to hormonal and environmental cues. Subsequently, PPAR γ and C/EBP α are activated and drive the maturation of adipocytes by promoting lipid accumulation and insulin sensitivity (Farmer, 2006). In addition to transcription factors, insulin and insulin-growth factor-1 (IGF1) signalling through the PI3K/AKT pathway enhances adipocyte differentiation by promoting lipid accumulation and activating PPAR γ and C/EBP α (Rosen & MacDougald, 2006). A balanced interplay between these regulatory factors ensures proper adipose tissue development and function.

Adipogenesis can be effectively induced *in vitro* under the control of chemical inducers, including 3-isobutyl-1-methylxanthine (IBMX), dexamethasone, and insulin (Student et al., 1980). IBMX is a phosphodiesterase inhibitor that increases intracellular cyclic AMP levels, leading to the activation of protein kinase A (PKA) and the induction of early adipogenic transcription factors such as PPAR γ (Gurriarán-Rodríguez et al., 2011). Similarly, dexamethasone is a synthetic glucocorticoid which further promotes C/EBP β expression through activating the glucocorticoid receptor (Z. Wu et al., 1996). By activating the key transcription factors involved in adipogenesis, these inducers initiate a well-orchestrated gene expression program that drives the differentiation of adipocyte progenitors into functionally mature adipocytes filled with lipid droplets.

PDGFR α^+ stromal cells play pivotal roles in both adipogenesis and mammary gland development, serving as progenitors for mature white adipocytes while also contributing to the mammary epithelial lineage. The mechanisms underlying

adipogenesis from PDGFR α^+ stromal cells are well-studied and can be effectively replicated *in vitro*. In contrast, the mechanisms governing the stromal-epithelial transition remain incompletely understood.

1.2.4 Loss of Lipid Droplets in Adipocytes

Adipocytes make up the major part of the stromal fat pad in the non-lactating mammary tissue. Concomitant with lactogenesis, mammary adipocytes regress to generate space for the expanding mammary epithelium. A recent study demonstrates that mammary adipocytes disappear through dedifferentiation into preadipocytes rather than apoptosis during lactation ([Figure 1.3](#)) (Q. A. Wang et al., 2018). Lineage tracing of mammary adipocytes during pregnancy and lactation reveals that adipocytes that are tightly surrounded by epithelium structure obtain a smaller size and lose their lipid droplets at lactation day 10. In addition, PDGFR α^+ cells in the stromal-vascular fractions (SVFs) from lactating mammary tissues contain a significant proportion of cells that have formerly expressed *Adipoq*, a marker for adipocytes. Furthermore, transcriptome profiles of these cells are similar to the PDGFR α^+ adipocyte progenitor cells which have never expressed *Adipoq*. These results support the statement that part of adipocytes in the mammary tissue undergo dedifferentiation during lactation. However, another study argued that most adipocytes still expressed the markers of mature adipocytes such as *Perilipin* and *Adipoq* at the same stage, though they obtained a morphology with smaller and unambiguous lipid droplets (Zwick et al., 2018). Taken together, these two studies highlight the same phenomenon that the size of adipocytes reduces in regions where mammary alveoli are more densely packed. Therefore, it comes up with a possibility that mammary adipocytes undergo a process that they gradually reduce their lipid synthesis and finally dedifferentiate in response to environmental cues from mammary epithelium.

Deleted: Figure 1.3

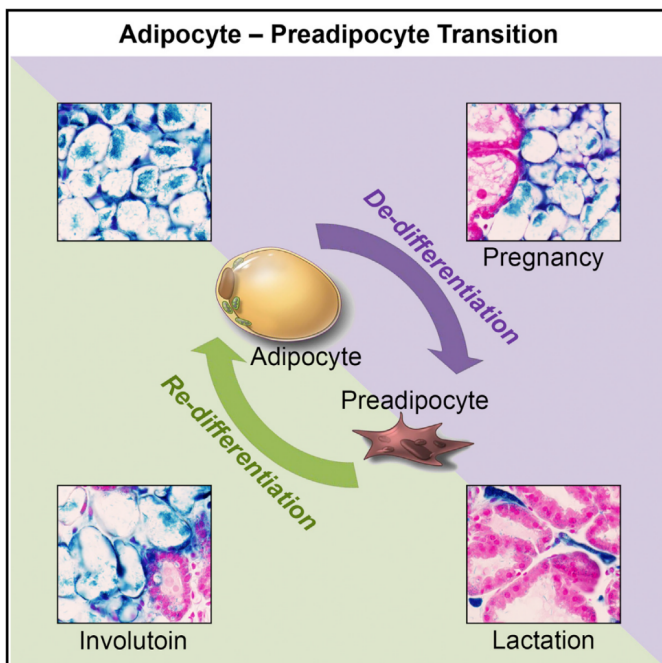


Figure 1.3 Diagram illustrating differentiation dynamics of mammary adipocytes during pregnancy, lactation and involution.

Mammary adipocytes dedifferentiate into preadipocytes during lactation and redifferentiate into mature adipocytes during involution (Q. A. Wang et al., 2018).

Adipocyte dedifferentiation occurs in various circumstances, induced by signalling pathways as well as mechanical pressure. Previous studies find that adipocyte dedifferentiation is influenced by several key signalling pathways, including the Wnt/ β -catenin, TGF- β and Notch signalling pathways. Wnt3a is shown to promote adipocyte dedifferentiation by suppressing the expression of adipogenic markers while increasing fibroblast-like characteristics (Gustafson & Smith, 2010). Similarly, TGF- β 1 is observed to reduce adipogenic gene expression and promote the transformation of adipocytes into fibroblast-like cells (Côté et al., 2017). Furthermore, mice with NOTCH1 overexpression demonstrate a reduction in adipogenic markers, loss of lipid droplets, and a shift towards an undifferentiated

phenotype (Bi et al., 2016). In addition to signalling pathways, mechanical pressure such as osmotic pressure is also implicated in adipocyte dedifferentiation. Elevated osmotic pressure induces dedifferentiation of adipocytes via activating the Wnt/β-catenin signalling (Y. Li et al., 2020). Moreover, the compression-induced dedifferentiated adipocytes have adipogenic potential to redifferentiate into mature adipocytes after induction (Y. Li et al., 2020).

During lactation, mammary adipocytes undergo significant remodelling so as to create space for expanding mammary epithelium. Previous findings suggest that part of the mammary adipocytes lose their lipid droplets through dedifferentiation (Q. A. Wang et al., 2018). These dedifferentiated adipocytes may serve as a transient cell population that facilitates glandular expansion during lactation while retaining the potential to redifferentiate into mature adipocytes upon weaning (Q. A. Wang et al., 2018). However, the underlying mechanisms inducing adipocyte dedifferentiation during lactation remain unexplored. Adipocyte dedifferentiation has been observed in response to multiple factors, including activation of signalling pathways such as Wnt/β-catenin, TGF-β and Notch, as well as osmotic pressure. It is plausible that similar mechanisms drive the remodelling of adipocytes in the lactating mammary gland. The close interactions between adipocytes and the expanding alveoli suggest that mechanical compression from the epithelium structure could trigger lipid droplet loss and initiate dedifferentiation. A similar dedifferentiation phenomenon is observed in the stromal fat pad infiltrated by mammary tumours which generate physical stress and affect surrounding adipocytes (Zhu et al., 2022). In addition to mechanical pressure, the expanding and differentiating mammary epithelium might also secrete signalling molecules and regulate adipocyte remodelling through paracrine signalling. Interactions between luminal cells and adipocytes found previously suggest that luminal cells transduce signalling molecules to suppress excessive thermogenesis in mammary adipocytes under cold exposure (Patel et al., 2023). However, the key ligands

activating signalling pathways, such as Wnt/β-catenin, TGF-β and Notch, implicated in adipocyte dedifferentiation have not been found predominantly expressed in mammary epithelial cells during lactation. Nevertheless, other epithelial-derived signals that promote adipocyte dedifferentiation may exist and require to be identified for better understanding of whether the cell-cell communications driving this process.

1.2.5 Mammary Epithelial Differentiation Regulated by Intercellular Signals

Cell-cell communications through signalling molecules within the mammary tissue are essential for the postnatal development of the mammary gland. Previous studies found that coordinating the complex interactions among different types of epithelial cells enables the normal development of the mammary gland. Progesterone promotes alveolar formation during pregnancy through inducing RankL secretion by hormone sensing cells, which subsequently activates ELF5 expression in luminal progenitors (H. J. Lee et al., 2013). In addition to paracrine signals from hormone sensing cells, neuregulin 1 (NRG1) secreted by basal cells induces STAT5 phosphorylation through binding to ERBB4, and therefore facilitates lactogenesis (Forster et al., 2014). Disruptions in these signalling pathways can impair mammary gland development, leading to developmental defects and dysfunction of the mammary gland. Therefore, understanding the cell-cell communications within the mammary tissue is crucial for addressing conditions where aberrant signalling can impair normal mammary gland development.

As one of the major components of the mammary tissue, adipocytes are indispensable for mammary gland development. Mammary adipocytes produce adipokines such as leptin and adiponectin that directly affect growth and functions of mammary epithelial cells. Lipodystrophic mice exhibit loss of adipose tissue and impaired ductal elongation of the mammary gland (Brenot et al., 2020). However,

alveolar formation in lipodystrophic mice was retained after leptin treatment, indicating that adipocytes might facilitate the lobuloalveolar development through leptin-mediated intercellular interactions (Brenot et al., 2020). This assumption is supported by research that leptin induced STAT5 phosphorylation in lactating mammary gland cultured *in vitro* stimulates the synthesis of a milk protein, β -casein (Lin & Li, 2007). Apart from leptin, mice with altered adiponectin expression exhibit disrupted alveolar structure and impaired lactation, suggesting that precise regulation of adiponectin levels is crucial for maintaining mammary gland homeostasis throughout lactation (Jin et al., 2015).

Although the effects of adipocyte-derived signals on mammary gland development have been proved, adipocytes may regulate mammary gland development through other factors, as leptin treatment alone in lipodystrophic mice failed to fully restore normal mammary gland development (Brenot et al., 2020). Mature adipocytes secrete an adipokine neuregulin 4 (NRG4), which can activate ERBB4 signalling in hepatocytes (G.-X. Wang et al., 2014). As ERBB4 is an indispensable mediator for alveogenesis during pregnancy and lactation, it is possible that mammary adipocytes regulate luminal differentiation and alveolar specification through NRG4. However, whether NRG4 contributes to luminal differentiation and alveolar specification through the ERBB4/STAT5 signalling pathway remains to be further clarified.

1.3 Influences of Abnormal Lipid Metabolisms on Mammary Gland Development

1.3.1 Influences of Adipocyte Dysfunction on Mammary Gland Development

Adipocytes regulate both ductal morphogenesis and lactating function of the mammary gland and adipocyte dysfunction impairs the development of the mammary gland. Adipocyte ablation results in severe defects in the mammary gland development characterized by the significant decrease in both the number

of TEBs and the extent of secondary branching (Brenot et al., 2020; Landskroner-Eiger et al., 2010). However, the mammary gland development is restored by transplanting the mammary epithelium into wild-type recipient mammary fat pads where endogenous epithelium has been cleared, indicating that adipocytes are necessary for ductal morphogenesis of the mammary gland (Brenot et al., 2020). In contrast, leptin-deficient ob/ob mice retain adipose tissues but still exhibit defective mammary gland development (Brenot et al., 2020). Ectopic fat pad transplantation successfully rescues mammary gland development in ob/ob mice but not in lipodystrophic mice without adipose tissue, emphasizing the necessity for both direct adipocyte-epithelial interactions and adipocyte-derived signals in ensuring proper ductal morphogenesis of the mammary gland (Brenot et al., 2020). In addition to the absence of adipocytes and leptin, loss of *Pxmp2* in adipocytes also impairs ductal elongation and branching during puberty (Vapola et al., 2014). *Pxmp2* deletion in adipocytes disrupts peroxisomal lipid metabolism in the mammary fat pad, indicating that lipid homeostasis maintained by adipocytes is required for mammary epithelial growth (Vapola et al., 2014). These findings highlight the importance of adipocytes in directing pubertal ductal elongation of the mammary gland.

Adipocyte dysfunction disrupts pubertal mammary gland development, which subsequently affects lobuloalveolar development and lactation. Additionally, the influence of adipocytes on post-pubertal mammary gland development requires further exploration. Adipocyte depletion after sexual maturation leads to excessive tertiary branching and premature lobuloalveolar differentiation, indicating adipocytes are essential for preventing precocious alveolar formation and maintaining proper ductal architecture of the mammary gland in adulthood (Landskroner-Eiger et al., 2010). During pregnancy and lactation, lobuloalveolar development and milk composition in lipodystrophic mice or *Pxmp2*^{-/-} mice remain comparable to those of wild-type mice despite the reduced milk production caused

by limited ductal outgrowth during puberty (Brenot et al., 2020; Vapola et al., 2014). However, as insufficient milk production in these mice results in poor pup growth and survival, the specific impacts of adipocyte dysfunction on lactation are illustrated by another study. Deletion of XBP1 in adipocytes, a mediator of prolactin-induced lipogenesis suppression, impairs lipid mobilization during lactation, leading to excessive maternal adiposity and lactation defects (Gregor et al., 2013). These findings underscore the crucial role of adipocytes as metabolic regulators in lobuloalveolar differentiation and lactation.

In summary, the presence and functional integrity of mammary adipocytes are vital for proper mammary gland development. Adipocytes contribute to mammary gland development by facilitating ductal elongation during puberty and mobilising lipids to support milk production during lactation. Adipocyte dysfunction induced by genetic manipulation leads to defects in epithelial proliferation and specialisation. Similarly, metabolic dysregulation such as diet-induced obesity leads to alterations of lipid metabolism in adipocytes and consequently results in abnormal ductal morphogenesis and lactogenesis of the mammary gland (Flint et al., 2005; Kamikawa et al., 2009). Diet-induced obesity involves complicated metabolic changes and the specific mechanisms by which HFD impairs mammary gland development require further exploration.

1.3.2 Diet-Induced Obesity and Mammary Gland Developmental Defects

Obesity driven by the long-term consumption of HFD adversely affects various body functions by disrupting normal metabolic and endocrine signalling. HFD leads to an excessive accumulation of white adipose tissue, where adipocytes undergo hypertrophy and inflammation, and exhibit altered synthesis of hormonal signals such as leptin and adiponectin. These alterations not only compromise the capacity of adipocytes to maintain metabolic homeostasis but also affect the developmental processes dependent on hormonal signalling, including mammary gland

development. Diet-induced obesity may impair breastfeeding as the breastfeeding period reduces in women with body mass index (BMI) over 30 (Kugyelka et al., 2004; Ramji et al., 2017).

To further understand the impacts of obesity on mammary gland development, how diet-induced obesity affects the morphology and functions of the mammary gland is investigated in mouse models. Diet-induced obesity leads to reduced branching frequency and incomplete myoepithelial cell lining, indicating impaired pubertal development of the mammary gland (Kamikawa et al., 2009). Moreover, the microenvironment of the mammary gland is altered in obese mice, characterized by increased adipocyte size, collagen deposition and macrophage infiltration (Kamikawa et al., 2009). The obesity-induced developmental defects in the mammary might be attributed to metabolic changes in adipocytes as obese mice demonstrate increased expression of leptin which is secreted by adipocytes and suppresses proliferation of mammary epithelial cells *in vitro* (Kamikawa et al., 2009). Therefore, diet-induced obesity disrupts mammary gland ductal morphogenesis by altering the local microenvironment in non-pregnant mice. These structural and functional impairments of the mammary gland might further affect the remodelling of the mammary gland during pregnancy and lactation, reflecting in abnormal milk production with reduced expression of milk proteins and alterations in lipid synthesis (Flint et al., 2005; Saben et al., 2014). Obesity lowered the expression of key milk proteins such as WAP, casein, and lactalbumin (Flint et al., 2005). In addition, de novo lipid synthesis and production of medium-chain fatty acids decrease due to reduced acetyl-CoA carboxylase levels (Saben et al., 2014). Furthermore, reduction of Plin2 levels might impair lipid storage and mobilization within the milk-producing alveolar cells (Saben et al., 2014). Although expression levels of WAP and casein recover at day 10 of lactation, the milk lipid quality remains suboptimal throughout the lactation period (Flint et al., 2005; Saben et al., 2014). More importantly, the expression level of lactalbumin, which is essential for

lactose synthesis and milk excretion, is still significantly suppressed in obese dams at lactation day 10, possibly resulting in inadequate milk supply to pups (Flint et al., 2005). Similar to the non-pregnant mice, diet-induced obese mice also exhibit an increase in adipocyte size within the lactating mammary gland (Flint et al., 2005; Saben et al., 2014). Although it is proved that obesity induced by high-fat diet leads to abnormal development of adipocytes and mammary epithelial cells, whether diet-induced obesity affects mammary gland development through its impacts on adipocyte function remains unclear.

HFD induces changes in the microenvironment of the mammary tissue which modulate the expression of various regulatory factors. For instance, leptin level is upregulated in mice fed by HFD, indicating its role in obesity-induced defects of the mammary gland development. However, other adipocyte-derived hormonal signals might also govern this process. Emerging research suggested that NRG4 demonstrates protective roles against HFD-induced obesity and metabolic disorders (Z. Chen et al., 2017; Zhang, Zhu, et al., 2023). Diet-induced obesity significantly reduces the NRG4 levels in epididymal white fat and liver and overexpressing NRG4 suppresses diet-induced weight gain and fatty liver (Y. Ma et al., 2016). On the contrary, NRG4-deficient mice exhibit slight weight gain and elevated triglyceride levels in both plasma and liver under HFD conditions (G.-X. Wang et al., 2014). Mechanistically, NRG4 binds to ERBB3/ERBB4 and activates downstream signalling in hepatocytes, thereby reducing lipogenesis and protecting hepatocytes from insulin resistance and hepatic steatosis (G.-X. Wang et al., 2014). Therefore, it can be inferred that diet-induced obesity reduces NRG4 levels in the mammary tissue, resulting in insufficient ERBB4 activation in mammary epithelial cells and ultimately impairing mammary gland development and functions. Nevertheless, the impacts of NRG4 on mammary gland development are still unknown in both healthy and obese conditions.

1.4 Single-Cell Technologies Applied in Mammary Development Studies

Single-cell RNA sequencing (scRNA-seq) is a high-resolution technique for transcriptomic profiling of individual cells, providing insights into cellular heterogeneity and gene expression dynamics. Single-cell transcriptome profiles are accessed by isolating single cells, capturing and reverse-transcribing their mRNA into complementary DNA, amplifying the complementary DNA, and sequencing it using next-generation sequencing platforms. This process enables the analysis of gene expression at single-cell resolution, which provides critical information about cellular states and transitions. Compared to bulk RNA sequencing which generates an averaged gene expression profile, scRNA-seq identifies distinct subpopulations within a tissue, revealing differences between individual cells. With the advancement of scRNA-seq technology, an increasing number of studies utilize this technique to investigate fundamental questions, including the identification of novel cell subpopulations within mammary tissue and the characterization of key transcription factors and signalling pathways that regulate cell differentiation during mammary gland development.

The mammary gland is a highly heterogeneous organ composed of multiple cell types. scRNA-seq reveals distinct subsets of basal and luminal cells at different developmental stages, which provides insights into their dynamic changes during development (Bach et al., 2017; H. Sun et al., 2018; Wuidart et al., 2016). For instance, a rare subpopulation of CDH5⁺ cells in the basal lineage is identified as quiescent MaSCs (H. Sun et al., 2018). Moreover, two functionally distinct subpopulations in the luminal lineage, the Rspol⁺/Aldhla3⁺ luminal progenitor and the Lipa⁺/Csn2⁺/Lalba⁺ lactation progenitor are revealed by scRNA-seq (Pervolarakis et al., 2020). After identifying subpopulations of stem cells, progenitors and differentiated cells in the basal and luminal lineages, cell differentiation trajectories and developmental dynamics can be reconstructed by pseudotime analysis of the scRNA-seq data. For example, pseudotime analysis

delineates the differentiation pathways of MaSCs into luminal lineage and basal lineage (García Solá et al., 2021; Giraddi et al., 2018). scRNA-seq of mammary epithelial cells from embryonic, postnatal and adult stages reveals that most fetal MaSCs give rise to both unipotent basal and luminal progenitors, which further differentiate during puberty (Giraddi et al., 2018). Furthermore, scRNA-seq of mammary epithelial cells from adult, gestation and lactation mice demonstrated that luminal progenitors can further specify into hormone sensing lineage and alveolar secretory lineage (Bach et al., 2017; García Solá et al., 2021). Subsequently, scRNA-seq facilitates the identification of key transcription factors and signalling pathways that govern cell specification during mammary gland development. For instance, transcription factor FOXA1 is specifically expressed in hormone-responsive luminal cells, whereas ELF1 was specifically expressed in secretory luminal cells, further elucidating the regulatory landscape of mammary cell fate determination (Giraddi et al., 2018). In addition, scRNA-seq helps identify cell type-specific ligands which are potentially involved in intercellular signalling during mammary gland development (Song et al., 2023). Amphiregulin is identified as a key ligand in hormone sensing cells, which regulates the proliferation and differentiation of mammary epithelial cells through the EGFR signalling pathway (Ciarloni et al., 2007; Song et al., 2023). In summary, the application of scRNA-seq in mammary gland research provides an essential molecular framework for mammary gland biology through capturing developmental dynamics, identifying key transcription factors and mapping intercellular interactions of the mammary epithelial cells.

Although scRNA-seq has significantly advanced the understanding of mammary gland development at the cellular level, most studies primarily focus on mammary epithelial cells, paying little attention to the changes in other cell populations within the mammary tissue which also contribute to its development. In addition, cell-cell communications between mammary epithelial cells and stromal cells such as

adipocytes and their progenitors have been proved crucial for mammary gland development (Brenot et al., 2020; Joshi et al., 2019; Lin & Li, 2007). Therefore, incorporating these cells in single-cell sequencing is necessary for a comprehensive analysis of intercellular signalling that facilitates mammary gland development and functions. However, the application of scRNA-seq on other cell populations within the mammary tissue is restricted by the enzymatic dissociation required for single-cell isolation, as this process can introduce stress artefacts and preferentially lose fragile cells such as adipocytes. To mitigate the selective underrepresentation of certain cell populations resulting from the isolation process, single-nucleus RNA sequencing (snRNA-seq) offers an alternative approach by analysing nuclei extracted from frozen tissues, which preserves native transcriptomic signatures while circumventing the need for dissociation protocols. Consequently, snRNA-seq can provide a more accurate composition of the cellular diversity within the mammary gland, enabling deeper investigation of cell lineage specification, regulatory network dynamics and intercellular communications during mammary gland development, which are critical for understanding both normal physiology and disease progression in the mammary tissue.

1.5 Research Objectives

Despite substantial progress in understanding the cellular and molecular mechanisms of mammary gland development, several critical issues remain unsolved. Notably, while the stromal-epithelial transition, where PDGFR α^+ stromal cells contribute to the mammary epithelial lineage, has been described, transcription factors driving this transition remain unclear. Similarly, although key transcription factors directing alveolar cell specification have been identified, the transcription factors specifically governing alveolar lipogenesis are not fully elucidated.

Another unresolved question centres on the bidirectional communications between

adipocytes and luminal cells. During lactation, the expanding mammary epithelium appears to induce adipocyte dedifferentiation, characterized by a marked reduction of lipid droplets in mammary adipocytes. However, the specific intercellular signals mediating this process remain undefined. On the other hand, the underlying mechanisms of how adipocytes regulate the growth and differentiation of mammary epithelial cells through intercellular communications require further investigation.

The impacts of diet-induced obesity on mammary gland development adds another layer of complexity. It is known that HFD induces obesity and alters adipocyte function, leading to changes in the secretion of adipokines. However, how high-fat diet-induced modifications in adipocyte-derived signals contribute to developmental and lactation defects in the mammary gland remains a critical gap in our current knowledge.

In summary, this thesis tries to address the following aims:

1. Identify key transcription factors that drive the differentiation of PDGFR α^+ stromal cells into mammary epithelial cells.
2. Identify key transcription factors that regulate lipid synthesis and storage in alveolar cells.
3. Elucidate the intercellular communications between adipocytes and luminal epithelial cells, with a particular focus on how the expanding mammary epithelium induces adipocyte dedifferentiation during lactation and how adipocytes, in turn, influence the growth and differentiation of mammary epithelial cells.
4. Explore how diet-induced obesity alters adipocyte-derived signals and consequently impairs mammary gland development and function.

To achieve these goals, this project first employed snRNA-seq to obtain high-resolution transcriptomic profiles of diverse cell populations within the mammary gland. Subsequent experimental validations, including both *in vitro* assays and *in*

vivo models, were conducted to validate the roles of identified factors. This research is expected to enhance our understanding of mammary gland biology by uncovering novel regulatory networks that govern cell fate determination and intercellular communications while also shedding light on the impacts of metabolic disorders on tissue development.

Chapter 2

Materials and Methods

2.1 Materials

2.1.1 Reagents

60%fat Kcal% high fat diet (Medicience, #MD12033)
10%fat Kcal% normal diet (Medicience, #MD12031)
1M Tris-HCl (pH 8.0) (Solarbio, #T1150)
0.5M EDTA pH 8.0 (Biosharp, #BL518A)
Sodium Dodecyl Sulfate (SDS) (Solarbio, #S8010-500g)
Sodium chloride (Sinopharm, #7647-14-5)
Proteinase K (TransGen, #GE201-01)
TE Buffer (pH = 8.0) (Solarbio, #T1120)
Ethanol (Sinopharm, #64-17-5)
Isopropanol (Sinopharm, #67-63-0)
Chloroform (Sinopharm, #67-66-3)
Glacial acetic acid (Sinopharm, #64-19-7)
Xylene (Sinopharm, #1330-20-7)
2 × Rapid Taq Master Mix (Vazyme, #P222-01)
REGULAR AGAROSE (BIOWEST, #BY-R0100)
50 × TAE Buffer (Biomed, #EL102)
GelGreen Nucleic Acid Gel Stain (10,000x) (EL110-02)
DNase/RNase free water (Biomed, #RA114-01)
2 × Phanta Max Master Mix (Vazyme, #P515-02)
rCutSmartTM Buffer (NEB, #B6004S)
BamHI-HF (NEB, #R3136S)

EcoRI-HF (NEB, #R3101S)
TOP10 Competent Cells (Biomed, #BC101-01)
Tryptone (Thermo, #LP0042B)
Yeast Extract (Thermo, #LP0021B)
LB Broth Agar (Sangon, #A507003-0250)
Ampicillin (Macklin, #A800429-25g)
DMEM high glucose (GENOM, #GNM12800-5)
Fetal Bovine Serum (Prime) (ExcellBio, #FSP500)
Penicillin-Streptomycin (100x) (TranGen, #FG101-01)
PBS buffer PH7.2 (GENOM, #GNM20012-5)
Trypsin (0.25%, EDTA⁺ and Phenol Red (TransGen, #FG301-01)
DMSO (Dimethyl sulfoxide) (Cell culture grade) (Solarbio, #D8371)
GeneTwin™ Transfection Reagent (Biomed, #TG101-02)
GML-PC™ Lentivirus Concentration Kit (Genomeditech, GM-040801)
Polybrene (hexadimethrine bromide) (YEASEN, #40804ES76)
Aluminum potassium sulfate dodecahydrate (Sigma-Aldrich, #C1022-25G)
Carmine (Sigma-Aldrich, #237086-100G)
Methyl salicylate (D&B, #K898001-500MI)
Formalin Solution (10%) (Biosharp, #BL401A)
Haematoxylin (Servicebio, #G1004)
Haematoxylin Differentiate Solution (Servicebio, #G1039)
Haematoxylin Bluing Solution (Servicebio, #G1040)
Eosin (Servicebio, #G1001)
Neutral balsam (Sinopharm, #96949-21-2)
Improved Citrate Antigen Retrieval Solution (50 ×) (Beyotime, #P0083)
Phosphate Buffered Saline, Powder (Biosharp, #BL601A)
Tween-20 (Solarbio, #T8220-500ml)
Enhanced Endogenous Peroxidase Blocking Buffer (Beyotime, #P0100B)

10% Normal Donkey Serum (Servicebio, #G1217)
Hydrochloric acid (Sinopharm, #7647-01-0)
Haematoxylin (Biosharp, #BL700B-1)
Neutral balsam (Solarbio, #G8590)
Hepes Buffer (Macklin, #H917699-500ml)
D-(+)-Glucose (Macklin, #D810588-500g)
Potassium chloride (Macklin, #P816348)
Calcium chloride (Sigma-Aldrich, #V900266-500G)
KH₂PO₄ (Sinopharm, #7778-77-0)
MgSO₄·7H₂O (Sinopharm, #10034-99-8)
Roche Collagenase A from Clostridium histolyticum (Roche, #10103586001)
Albumin Bovine (BSA) (BioFroxx, #4240GR100)
ACK Lysing Buffer (Gibco, #A1049201)
Advanced DMEM/F12 (Gibco, #12634010)
GlutaMAX™ Supplement (Gibco, #35050061)
Geneticin™ Selective Antibiotic (G418 Sulfate) (50 mg/mL) (Gibco, #10131)
Recombinant Human Insulin (Solarbio, #I8830)
IBMX (3-Isobutyl-1-methylxanthine) (MCE, #HY-12318)
1 mg/mL dexamethasone (Yuanye, #R22035)
Rosiglitazone (Macklin, #R832516-1g)
Triiodothyronine (Macklin, #T819947-5mg)
4% Paraformaldehyde Fixative (Biosharp, #BL539A)
Oil Red O staining solution (Sigma-Aldrich, #O1391)
D-PBS (Beyotime, #C0221D)
DNase I Solution (1 mg/mL) (Stem cell, #07900)
Corning® Matrigel® Basement Membrane Matrix (Corning, #356234)
Insulin-Transferrin-Selenium-Ethanolamine (ITS-X) (100 ×) (Gibco, #51500056)
Recombinant Mouse PRL (C-6His) (Novoprotein, #C17X)

Hydrocortisone (MCE, #HY-N0583)
STAT5 phosphorylation inhibitor (MCE, #HY-101853)
Corning® Cell Recovery Solution (Corning, #354253)
BODIPY 493/503 (GLPBIO, #GC42959)
DAPI (US EVERBRIGHT, #D4054)
Triton X-100 (Solarbio, #T8200-500ml)
D-(-)-Fructose (Sangon, #A600213-0500)
Glycerol (Macklin, #G810575-500ml)
ImmEdge Hydrophobic Barrier Pen (ACD, #30018)
Streptavidin magnetic beads (NEB, #S1420S)
Recombinant Human IL-15 Protein (R&D System, #247-ILB-005/CF)

2.1.2 Reagent Setup

Tail lysis buffer for Genomic DNA Extraction

Table 2.1 Composition of Tail Lysis Buffer

Components	Final concentrations
1 M Tris-HCl (pH = 8.0)	100 mM
0.5 M EDTA	5 mM
SDS	0.2% (wt/vol)
NaCl	200 mM
double-distilled water (ddH ₂ O)	

The lysis buffer was autoclaved at 121°C for 20 minutes.

1 × TAE buffer

50 × TAE Buffer was diluted in ddH₂O.

Agarose gel

The proper weight of agarose was dissolved in 1 × TAE buffer. The mixture was boiled until the solution became clear without visible particles and cooled to

approximately 50-60°C. The cooled gel solution was supplemented with GelGreen Nucleic Acid Gel Stain at a 1:10,000 dilution and solidified in a gel tray with the combs. The gel was placed into 1 × TAE buffer for DNA loading and electrophoresis.

70% (vol/vol) ethanol

100% ethanol was diluted with DNase/RNase-free water.

100 mg/mL ampicillin solution

Ampicillin powder was dissolved in ddH₂O.

Luria-Bertani (LB) medium

Table 2.2 Composition of LB media

Components	Final concentration
Tryptone	10 g/L
Yeast Extract	5 g/L
NaCl	10 g/L
ddH ₂ O	

The LB medium was autoclaved at 121°C for 20 minutes. To prepare LB medium with ampicillin, the ampicillin solution was added to the LB medium to reach a final concentration of 50 µg/mL.

LB agar plate with ampicillin

Table 2.3 Composition of LB agar plate

Components	Final concentrations
Tryptone	10 g/L
Yeast Extract	5 g/L
NaCl	10 g/L
Agar	15 g/L
ddH ₂ O	

The medium was autoclaved at 121°C for 20 minutes and ampicillin solution was added to the cooled medium to reach a final concentration of 100 µg/mL. The medium was solidified in sterile 10 cm Petri dishes at room temperature (RT).

293T/preadipocyte culture medium

Table 2.4 Composition of 293T/preadipocyte culture medium

Components	Final concentrations
DMEM high glucose	
Fetal Bovine Serum (prime)	5% (vol/vol)
Penicillin-Streptavidin (100 ×)	1% (vol/vol)

The fetal bovine serum (FBS) and the Penicillin-Streptavidin (P/S) solution were added to the DMEM high glucose medium ([Table 2.4](#)). The final concentration of penicillin and streptavidin was 100 U/mL and 100 mg/mL, respectively.

Deleted: Table 2.4

Formatted: Font: Not Bold

293T freezing medium

Table 2.5 Composition of 293T freezing medium

Components	Final concentrations
293T culture medium	90% (vol/vol)
DMSO	10% (vol/vol)

Carnoy's solution

Table 2.6 Composition of Carnoy's solution

Components	Final concentrations
100% Ethanol	60% (vol/vol)
Chloroform	30% (vol/vol)
Glacial acetic acid	10% (vol/vol)

Carmine stain

Table 2.7 Composition of carmine stain

Components	Final concentrations

Aluminum potassium sulfate dodecahydrate	5 g/L
Carmine	2 g/L
ddH ₂ O	

The solution was boiled for at least 40 minutes and filtered to remove undissolved stain.

1 × citrate antigen retrieval solution

50 × improved Citrate Antigen Retrieval Solution was diluted in ddH₂O.

PBST

PBST was composed of 0.1% Tween-20 in the PBS solution.

1% (vol/vol) acid alcohol

Hydrochloric acid was diluted in 100 % ethanol.

100 mg/mL Collagenase A

Collagenase A (Roche) was dissolved in Advance DMEM/F12.

Primary SVF digestion stock buffers

Table 2.8 Composition of primary SVF digestion stock buffer

Components	Final concentrations
1 M Hepes Buffer	100 mM
Glucose	5 mM
KCl	50 mM
CaCl ₂	1 mM
NaCl	120 mM
ddH ₂ O	

The pH of the stock buffers was adjusted to 7.4 with NaOH or HCl.

Primary SVF digestion buffer

Table 2.9 Composition of primary SVF digestion buffer

Components	Final concentrations
BSA	1.5% (wt/vol)
100 mg/mL Collagenase A	1 mg/mL
Primary SVFs digestion stock buffer	

The digestion buffer was sterilized by filtration through a 0.22 µm membrane.

SVF culture medium

Table 2.10 Composition of SVF culture medium

Components	Final concentrations
Fetal Bovine Serum (prime)	5% (vol/vol)
GlutaMAX™ Supplement	1% (vol/vol)
Penicillin-Streptavidin (100 ×)	1% (vol/vol)
Advance DMEM/F12	

G418 selection medium

G418 sulfate was added to SVF culture medium and the final concentration of G418 was 1 mg/mL.

10 mM HCl

Hydrochloric acid was diluted with ddH₂O.

5 mg/mL insulin

Human recombinant insulin was dissolved in 10 mM HCl.

200 Mm IBMX

IBMX was dissolved in DMSO.

1 µM Triiodothyronine

Triiodothyronine was dissolved and diluted in DMSO.

1 mM Rosiglitazone

Rosiglitazone was dissolved and diluted in DMSO.

Adipogenesis induction medium

Table 2.11 Composition of adipogenesis induction medium

Components	Final concentrations
5 mg/mL insulin	5 µg/mL
200 mM IBMX	0.5 mM
1 µM Triiodothyronine	200 pM
1 mM Rosiglitazone	1 µM
1 mg/mL dexamethasone	1 µM
Culture medium	

Adipogenesis differentiation medium

Table 2.12 Composition of adipogenesis differentiation medium

Components	Final concentrations
1 µM Triiodothyronine	200 pM
1 mM Rosiglitazone	1 µM
5 mg/mL insulin	5 µg/mL
Culture medium	

2.5% (wt/vol) BSA

BSA was dissolved in D-PBS.

Primary mammary organoid digestion buffer

Table 2.13 Composition of primary mammary organoid digestion buffer

Components	Final concentrations
100 mg/mL Collagenase A	2 mg/mL
Trypsin	2 mg/mL
5 mg/mL insulin	5 µg/mL

Fetal Bovine Serum (prime)	5% (vol/vol)
Penicillin-Streptavidin (100 ×)	1% (vol/vol)
Advanced DMEM/F12	

The digestion buffer was sterilized by filtration through a 0.22 µm membrane.

Basal organoid medium

Table 2.14 Composition of basal organoid medium

Components	Final concentrations
Insulin-Transferrin-Selenium-Ethanolamine (ITS-X) (100 ×)	1% (vol/vol)
Penicillin-Streptavidin (100 ×)	1% (vol/vol)
GlutaMAX™ Supplement	1% (vol/vol)
Advanced DMEM/F12	

1 mg/mL hydrocortisone

Hydrocortisone was dissolved and diluted in DMSO to prepare 1 mg/mL hydrocortisone.

200 µg/mL prolactin

To prepare 200 µg/mL prolactin, prolactin was dissolved in ddH₂O.

Lactation medium

Table 2.15 Composition of lactation medium

Components	Final concentrations
1 mg/mL hydrocortisone	1 µg/mL
200 µg/mL prolactin	1 µg/mL
Basal organoid medium	

Organoid washing buffer (OWB)

Table 2.16 Composition of OWB

Components	Final concentrations
Triton X-100	0.1% (vol/vol)
BSA	0.2% (wt/vol)
PBS	

Fructose-glycerol clearing solution

Table 2.17 Composition of fructose-glycerol clearing solution

Components	Final concentrations
Fructose	2.5 M
Glycerol	60% (vol/vol)
ddH ₂ O	

Krebs Ringers (KR) Buffer, 25 × Stock

Table 2.18 Composition of Krebs Ringers (KR) Buffer, 25 × Stock

Components	Final concentrations
NaCl	3 M
KCl	120 mM
KH ₂ PO ₄	30 mM
MgSO ₄	30 mM
CaCl ₂	65 mM
ddH ₂ O	

Primary preadipocyte digestion buffer

Table 2.19 Composition of primary preadipocyte digestion buffer

Components	Final concentrations
BSA	3.5%
100 mg/mL Collagenase A	1 mg/mL
1 M Hepes Buffer	25 mM
Glucose	2 mM
25 × KR Buffer	1 ×
ddH ₂ O	

2.1.3 Antibodies

ActivAbTMAnti-NRG4 Polyclonal Antibody (Solarbio, #K003447P)
Anti-STAT5 (phospho Y694) antibody [E208] (abcam, # ab32364)
HRP-conjugated Goat Anti-Rabbit/mouse IgG (Sangon, #D110073)
Anti-EpCAM-biotin antibody, 0.5 mg/mL (Invitrogen, #13-5791-82)

2.1.4 Kits

TransZol Up (TransGen, #ET111-01)

Table 2.20 Composition of *TransZol Up* Kit

Components
<i>TransZol Up</i>
RNA Extraction Agent
RNA Dissolving Solution

TransScript[®] All-in-One First-Strand cDNA Synthesis SuperMix for qPCR (One-Step gDNA Removal) (TransGen, #AT341-02)

Table 2.21 Composition of *TransScript[®] All-in-One First-Strand cDNA Synthesis SuperMix for qPCR (One-Step gDNA Removal)* Kit

Components
5× <i>TransScript[®] All-in-One SuperMix for qPCR</i>
gDNA Remover
RNase-free Water

2 × PerfectStart[®] Green qPCR SuperMix (TansGen, #AQ601-02)

Table 2.22 Composition of *2 × PerfectStart[®] Green qPCR SuperMix* Kit

Components
2 × <i>PerfectStart[®] Green qPCR SuperMix</i>
Nuclease-free Water

FastPure Gel DNA Extraction Mini Kit (Vazyme, #DC301-01)

Table 2.23 Composition of FastPure Gel DNA Extraction Mini Kit

Components
Buffer GDP
Buffer GW
Elution Buffer
FastPure DNA Mini Columns-G

BM Seamless Cloning Kit (Biomed, #CL116-02)

Table 2.24 Composition of BM Seamless Cloning Kit

Components
2 × Seamless Cloning Mix

FastPure Plasmid Mini Kit (Vazyme, #DC201-01)

Table 2.25 Composition of FastPure Plasmid Mini Kit

Components
RNase A (Added to Buffer P1 before the first use)
Buffer P1
Buffer P2
Buffer P3
Buffer PW1
Buffer PW2
Elution Buffer
FastPure DNA Mini Columns

NucleoBond Xtra Midi kit for transfection-grade plasmid DNA (MACHEREY-NAGEL, #740410.50)

Table 2.26 Composition of NucleoBond Xtra Midi kit for transfection-grade plasmid DNA

Components
RNase A (Added to Buffer RES before the first use)
Buffer RES
Buffer LYS
Buffer NEU

Buffer EQU
Buffer WASH
Elution ELU
NucleoBond® Xtra Midi Columns
NucleoBond® Xtra Midi Column Filters

DAB Substrate Kit (ZSGB-BIO, #ZLI-9018)

Table 2.27 Composition of DAB Substrate Kit

Components
DAB Substrate Buffer
DAB Substrate (20 x)

50 µL of DAB Substrate was diluted in 950 µL of DAB Substrate Buffer.

2.1.5 Primers

Primers for genotyping

Table 2.28 Primer list for genotyping

Primers	Sequence (5'-3')
Nrg4-KO-F	TTTGCTAATGGAACATTGGCGC
Nrg4-KO-R	AGTTTATCAAGAGTGATTGTTGCTTCAG
Nrg4-WT-F	AGGCTCAGTAGGAGACCCTATTCA
Nrg4-WT-R	TTGAAACAGGGTTCATTAGAGCCC

Primers for plasmid construction

Table 2.29 Primer list for plasmid construction

Primers	Sequence (5'-3')
HA-	ATGATGTTCCGGATTATGCAATGCAAGAACATCTGGG
Foxp1_fwd	TCTG
IRES-	AGGGGCGCGGCCGCAGATCCTCACTCCATGTCCT
Foxp1_rev	CATTTAC
pCDH-EF1α-	ACTCTAGAGCTAGCGAATTGCCACCATGTATCCG
HA_fwd	TATGATGTTCCGGATTATGC

Primers for qPCR

Table 2.30 Primer list for qPCR

Primers	Sequence (5'-3')
18Sreg3-qPCR-F	CTCAACACGGGAAACCTCAC
18Sreg3-qPCR-R	CGCTCCACCAACTAAGAACG
Foxp1-qPCR-F	GGATCAGGCCATCCAGAACCG
Foxp1-qPCR-R	GGACCGAGTGTACCGAAGTG
Epcam-qPCR-F	CCTGAGAGTGAACGGAGAGC
Epcam-qPCR-R	CCCGCGATGACTGCTAATGA
Acta2-qPCR-F	GTCCCAGACATCAGGGAGTAA
Acta2-qPCR-R	TCGGATACTTCAGCGTCAGGA
Myh11-qPCR-F	GAGCAAACTCAGGAGAGGAAAC
Myh11-qPCR-R	GTCCCGAGCGTCCATTCTTC
Nrg1-qPCR-F	ATGGAGATTATCCCCCAGACA
Nrg1-qPCR-R	GTTGAGGCACCCCTCTGAGAC
Adipoq-qPCR-F	TGTT CCTCTTAATCCTGCCA
Adipoq-qPCR-R	CCAACCTGCACAAGTCCCTT
Pparg-qPCR-F	TCGCTGATGCACTGCCTATG
Pparg-qPCR-R	GAGAGGTCCACAGAGCTGATT
Plin1-qPCR-F	CAGCAGAATATGCCGCCAAC
Plin1-qPCR-R	GAAGGGGCTGACTCCTTGT
Fabp4-qPCR-F	GGATTGGTCACCATCCGGT
Fabp4-qPCR-R	CCAGCTTGTACCATCTCGT
Acaca-qPCR-F	ATGGGCGGAATGGTCTTTTC
Acaca-qPCR-R	TGGGGACCTTGTCTTCATCAT
Fasn-qPCR-F	GGAGGTGGTGATAGCCGGTAT
Fasn-qPCR-R	TGGGTAAATCCATAGAGCCAG
Gpat3-qPCR-F	TCCCTATCTGGCACCATCCA
Gpat3-qPCR-R	GCTCAAACCAAGACGTGAGGA
Wap-qPCR-F	CGCTCAGAACCTAGAGGAACA
Wap-qPCR-R	CGGGTCCTACCACAGGAAAC
Olah-qPCR-F	GTTTGTGTCAAAAGCCGGATG
Olah-qPCR-R	GTTTCTCTCCAGCCAGTCTTA
Ppard-qPCR-F	TCCATCGTCAACAAAGACGGG
Ppard-qPCR-R	ACTTGGGCTCAATGATGTCAC
Fabp3-qPCR-F	ACCTGGAAGCTAGTGGACAG

Fabp3-qPCR-R	TGATGGTAGTAGGCTTGGTCAT
Gpat4-qPCR-F	AGCTTGATTGTCAACCTCCTG
Gpat4-qPCR-R	CCGTTGGTGTAGGGCTTGT
Plin2-qPCR-F	GACCTTGTGTCTCCGCTTAT
Plin2-qPCR-R	CAACCGCAATTGTGGCTC
Nrg4-qPCR-F	CACGCTGCGAAGAGGTTTC
Nrg4-qPCR-R	CGCGATGGTAAGAGTGAGGA

2.2 Mice

2.2.1 Mouse Strains and Maintenance

C57BL/6J: females, 6-10 weeks

C57BL/6N: females, 6-12 weeks

Nrg4: females, 6-10 weeks

Animals were maintained in Laboratory Animal Centre affiliated with Zhejiang University-University of Edinburgh Institute. The animal study was conducted under ethical approval (No. ZJU20240026) granted by the Institutional Animal Ethics Committee of Zhejiang University. Mice were housed in cages under 12-hour light/dark cycles.

2.2.2 Mouse Mating and Pregnancy Examination

Two adult female mice were mated with individually housed males from 17:00 to 08:30 the following morning. C57BL/6N mice were used for both snRNA-seq sample collection and mammary organoid isolation. The presence of vaginal plugs in mated females was checked at approximately 08:30. After examination, the females were separated from the males for the remainder of the day. Females with vaginal plugs were defined as pregnancy day 0.5 ([Figure 2.1](#)). However, the presence of a vaginal plug does not confirm pregnancy. To accurately determine pregnancy corresponding to the plug date, females identified with plugs were not reintroduced for timed mating for at least 14 days or until pregnancy failure was

Deleted: Figure 2.1

confirmed. To obtain mammary tissue at pregnancy day 13.5 (P13.5), pregnant females were euthanized on pregnancy day 13.5 ([Figure 2.1](#)). To collect mammary tissue at lactation day 5 (L5), pregnant females were allowed to give birth and nurse their pups until 5 days postpartum ([Figure 2.1](#)).

Deleted: Figure 2.1

Deleted: Figure 2.1

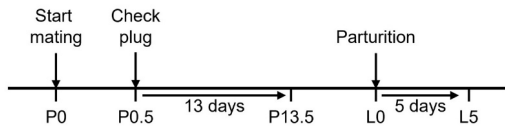


Figure 2.1 Timeline of time mating.

P0/P0.5/P13.5, pregnancy day 0/0.5/13.5; L0/L5, lactation day 0/5.

2.2.3 *Nrg4* Knockout Mice Maintenance

The *Nrg4^{-/-}* mice were purchased from GemPhamatech Co., Ltd. To disrupt the protein function of NRG4, CRISPR/Cas9 technology was applied to knock out exon3-exon5 of *Nrg4*-213 (ENSMUST00000164721.7) transcript, which contains most of the coding sequence. The *Nrg4^{-/-}* mice were crossed with C57BL/6J mice to generate *Nrg4^{+/-}* mice, which were bred to generate *Nrg4^{+/+}* and *Nrg4^{-/-}* mice for the experiment. New-born mice with the desired genotype were screened by polymerase chain reaction (PCR).

To explore the function of NRG4 on lactogenesis, *Nrg4^{-/-}* and *Nrg4^{+/+}* female mice were mated with *Nrg4^{+/-}* male and allowed to litter. Pups were nursed by *Nrg4^{-/-}* or *Nrg4^{+/+}* dams and weighed at postnatal day 5, day 10 and day 15.

To explore the function of NRG4 on mammary gland development during puberty, mammary tissues from *Nrg4^{-/-}* and *Nrg4^{+/+}* female mice were harvested at 6 weeks old. In addition, mammary tissues from *Nrg4^{-/-}* and *Nrg4^{+/+}* female mice fed by 60%fat Kcal% high-fat diet (Medicience) were harvested at 10-week-old.

Left-side thoracic mammary tissues were collected for RNA extraction. Right-side

abdominal mammary tissues were collected for carmine whole mount staining. Left-side abdominal mammary tissues were collected for paraffin embedding and sections.

2.2.4 High-Fat Diet Treatment

Wild-type C57BL/6N female mice were fed by 60%fat Kcal% high-fat diet (Medicience) or 10%fat Kcal% normal diet (Medicience) from 3-week-old. Mammary tissues were harvested at 10 weeks old. Tissue harvest was performed the same as *Nrg4* knockout mice.

2.3 Genotyping

2.3.1 DNA Extraction

Tails were lysed in 500 μ L of tail lysis buffer freshly supplemented with 200 μ g/mL proteinase K (Solarbio) at 56°C overnight. Dissolved tissues were vortexed and centrifuged for 10 minutes at 13,000 rpm. For DNA precipitation, supernatant was mixed with 500 μ L isopropanol by inverting several times. Precipitated DNA was dissolved in 100 μ L TE buffer (Solarbio) at 65°C for 30 minutes.

2.3.2 PCR For *Nrg4* Allele

PCR mix was prepared as follow:

Table 2.31 PCR reaction mixture for genotyping

Components	Volume in μ L
2 \times Rapid Taq Master Mix (Vazyme)	7.5 μ L
10 μ M <i>Nrg4</i> -KO-F/ <i>Nrg4</i> -WT-F	0.5 μ L
10 μ M <i>Nrg4</i> -KO-R/ <i>Nrg4</i> -WT-R	0.5 μ L
Genomic DNA	2 μ L
ddH ₂ O	4.5 μ L
Total	15 μ L

PCR was performed under the following conditions:

Table 2.32 PCR programme for genotyping

Step	Temperature	Time	Cycle
Denaturation	95°C	5 minutes	1
Denaturation	95°C	30 seconds	36
Annealing	58°C	30 seconds	36
Extension	72°C	45 seconds	36
Extension	72°C	5 minutes	1
Hold	12°C	∞	-

PCR products were subjected to electrophoresis with 1.5-2% agarose gel in 1 × TAE buffer, running at 120 volts for 40 minutes. The expected band for *Nrg4* is 640 bp, and for wild-type is 412 bp.

2.4 Reverse Transcription and Quantitative PCR (qPCR)

2.4.1 RNA Extraction

For RNA extraction from tissues, mammary tissues were homogenized in 1 mL *TransZol* Up (TransGen) by homogenizer at 60 Hertz for 45 seconds twice. For RNA extraction from cells, cells grown in monolayer in culture dishes or cell pellets collected from suspension were lysed by 1 mL *TransZol* Up. The homogenized samples were incubated at RT for 5 minutes and mixed 200 µL of RNA Extraction Agent (TransGen) by gently vertexing for 15 seconds. The mixture was incubated at room temperature for 3 minutes and centrifuged at 12,000 × g for 15 minutes at 4°C. The aqueous phase containing RNA was mixed with 500 µL of isopropanol by gently inversion. The samples were incubated at RT for 10 minutes followed by a 10-minute centrifugation at 12,000 × g and 4°C to precipitate RNA. The RNA pellets were washed with 70% ethanol twice. After washing, the RNA pellets were air-dried at RT for 5-10 minutes and dissolved in 20-50 µL RNA Dissolving Solution (TransGen) by incubating at 56°C for 10 minutes.

2.4.2 Reverse Transcription

Reverse transcription was performed using *TransScript® All-in-One First-Strand cDNA Synthesis SuperMix for qPCR (One-Step gDNA Removal) Kit* (TransGen). RNA and reagents were mixed as follow:

Table 2.33 Reaction mixture for reverse transcription

Components	Volume in μL
RNA	1 μg
5 x SuperMix	4 μL
gDNA Remover	1 μL
Nuclease-free water	Up to 20 μL
Total	20 μL

Samples were incubated at 42°C for 15 minutes followed by 85°C for 5 seconds to inactivate enzymes.

2.4.3 qPCR

qPCR mix was prepared as follow:

Table 2.34 qPCR reaction mixture.

Components	Volume in μL
2 × <i>PerfectStart® Green qPCR SuperMix</i> (TransGen)	7.5 μL
10 μM primer-forward	0.5 μL
10 μM primer-reverse	0.5 μL
cDNA (diluted 10-fold with Nuclease-free Water)	5 μL
Nuclease-free Water (TransGen)	1.5 μL
Total	15 μL

qPCR was performed under following conditions:

Table 2.35 qPCR programme

Step	Temperature	Time	Cycle
Denaturation	94°C	30 seconds	1
Denaturation	94°C	5 seconds	45
Annealing	60°C	30 seconds	45

2.5 Plasmids

2.5.1 Foxp1 Plasmid Construction

HA-tagged Foxp1 was obtained from cDNA of primary preadipocytes. HA-tagged Foxp1 was amplified by two-round PCR (

Table 2.36.

Table 2.37).

Table 2.36 PCR mixture for DNA fragment amplification

Components	Volume in μ L
2 × Phanta Master Max Mix (Vazyme)	25 μ L
10 μ M HA-Foxp1_fwd (first round)/	0.5 μ L
10 μ M pCDH-EF1 α -HA_fwd (second round)	
10 μ M IRES-Foxp1_rev	0.5 μ L
cDNA (first round)/	1 μ L
DNA fragment from the first round (second round)	
ddH ₂ O	Up to 50 μ L
Total	50 μ L

PCR programme

Table 2.37 PCR programme for DNA fragment amplification

Step	Temperature	Time	Cycle
Denaturation	95°C	3 minutes	1
Denaturation	95°C	15 seconds	29 (first round) 11 (second round)
Annealing	56°C	15 seconds	29 (first round) 11 (second round)
Extension	72°C	90 seconds	29 (first round) 11 (second round)
Extension	72°C 12°C	5 minutes	1 Hold

The PCR product was separated by electrophoresis with 1% agarose gel in 1 × TAE buffer, running at 100 volts for 40 minutes and the target band was about

Deleted: Table 2.36

Formatted: Font: Not Bold

Formatted: Space Before: 0 pt

Deleted: Table 2.37

Formatted: Font: Not Bold

2000bp. The single stripe of DNA fragment was excised from agarose gel and purified by FastPure Gel DNA Extraction Mini Kit (Vazyme).

To prepare vector for cloning, the plasmid pCDH-IRES-neo was linearized using linearized using enzyme BamHI and EcoRI (

Table 2.38).

Table 2.38 Mixture for pCDH-IRES-neo plasmid restriction digestion

Components	Volume in μ L
rCutSmart™ Buffer (NEB)	5 μ L
Plasmid DNA	5 μ g
BamHI-HF (NEB)	1 μ L
EcoRI-HF (NEB)	1 μ L
ddH ₂ O	Up to 50 μ L
Total Volume	50 μ L

The reaction was incubated at 37°C overnight.

The vector was separated by electrophoresis with 1% agarose gel in 1 × TAE buffer, running at 100 volts for 40 minutes. The target band was about 8000 bp. The single stripe of digested plasmid was purified by the FastPure Gel DNA Extraction Mini Kit (Vazyme).

HA-tagged Foxp1 was cloned into the vector by the BM Seamless Cloning Kit (Biomed) (

Table 2.39).

Table 2.39 Mixture for seamless cloning

Components	Volume in μ L
2 × Seamless Cloning Mix (Biomed)	5 μ L
HA-tagged Foxp1	37.8 ng
Digested plasmid	50 ng
ddH ₂ O	Up to 10 μ L
Total Volume	10 μ L

Deleted: Table 2.38

Formatted: Font: Not Bold

Deleted: Table 2.39

Formatted: Font: Not Bold

The reaction was incubated at 50°C for 30 minutes.

The ligation products were introduced into TOP10 Competent Cells (Biomed) by heat-shock transformation for amplification. A small amount of plasmid was purified using FastPure Plasmid Mini Kit (Vazyme) and the insertion of HA-tagged Foxp1 DNA fragment was validated by restriction digestion ([Table 2.40](#)).

Deleted: Table 2.40

Formatted: Font: Not Bold

Table 2.40 Mixture for pCDH-EF1α-HA-Foxp1-IRES-neo plasmid restriction digestion

Components	Volume in μ L
rCutSmart™ Buffer (NEB)	1 μ L
Plasmid DNA	500 ng
BamHI-HF (NEB)	0.1 μ L
EcoRI-HF (NEB)	0.1 μ L
ddH ₂ O	Up to 10 μ L
Total Volume	10 μ L

The reaction was incubated at 37°C for 2 hours.

The products were separated by electrophoresis with 1% agarose gel in 1x TAE buffer, running at 100 volts for 40 minutes. Plasmids with the HA-tagged Foxp1 insert had two bands at about 8000 bp and 2000 bp. The insert was further identified by Sanger sequencing (Sangon Biotech Co., Ltd.). The plasmid with the correct insert was amplified by transformation and purified for further experiments.

2.5.2 Gel Extraction

DNA was purified from an agarose gel slice using the Gel DNA Extraction Kit (Vazyme). The DNA fragment was excised from the agarose and weighed. Assuming the volume of 100 mg gel slice is approximately 100 μ L, an equal volume of Buffer GDP (Vazyme) was added to dissolve the gel slice under incubation at 55°C. The solution was transferred to the FastPure DNA Mini Columns-G (Vazyme) and centrifuged at 12,000 rpm for 30 seconds. DNA was absorbed on the column and the filtrate was discarded. 300 μ L of Buffer GDP (Vazyme) were added to the

column and incubated at room temperature for 1 minute. The column was centrifuged at 12,000 rpm for 30 seconds and the filtrate was discarded. To completely remove the salt, the column and DNA were washed with 700 μ L of Buffer GW (Vazyme) twice and dried by spinning at 12,000 rpm for 1 minute. The DNA was eluted by 20 μ L of Elution Buffer (Vazyme).

2.6 Transformation

Plasmids or ligation products were mixed into 10 μ L (for plasmids) or 50 μ L (for ligation products) of TOP10 competent cells. The mixture was incubated on ice for 30 minutes followed by a heat shock at 42°C for 45 seconds. The bacteria were recovered on ice for 2 minutes and allowed to grow in 500 μ L of antibiotic-free LB media at 37°C for 45 minutes to 1 hour. After incubation, bacteria were pelleted by centrifugation at 5,000 rpm for 5 minutes and resuspended by 50 μ L of antibiotic-free LB media. The bacteria suspension was plated onto a 10 cm LB agar plate with 100 μ g/mL ampicillin. Bacterial colonies were cultured on agar plates at 37°C overnight (about 14-16 hours).

2.6.1 Plasmid Extraction

FastPure Plasmid Mini Kit (Vazyme) was used to purify plasmids from a small amount of bacteria culture. A single colony was inoculated into 5 mL of LB medium containing 50 μ g/mL ampicillin and the culture was incubated at 37°C and 220 rpm overnight. Bacteria in 2 mL of overnight culture was pelleted by centrifugation at 10,000 rpm for 1 minute. The culture medium was aspirated and the bacteria pellet was dried at RT for a few minutes. The pellet was resuspended by 250 μ L of Buffer P1(Vazyme) and mixed with 250 μ L of Buffer P2 (Vazyme) to lyse the cells. 350 μ L of Buffer P3 (Vazyme) was added to the mixture to neutralize Buffer P2. The flocculent precipitates were removed by centrifugation at 12,000 rpm for 10 minutes and the supernatant was transferred to the FastPure DNA Mini Columns

(Vazyme). The column was centrifuged at 12,000 rpm for 30 seconds and the filtrate was discarded. The plasmid DNA was absorbed on the membrane of the column. The column and DNA were washed with 600 µL of Buffer PW2 (Vazyme) twice and dried by spinning at 12,000 rpm for 1 minute. The DNA was eluted by 100 µL of Elution Buffer (Vazyme).

NucleoBond Xtra Midi kit (MACHEREY-NAGEL) was used to purify plasmids from 100 mL bacteria culture. A single colony was inoculated into 3 mL of LB medium containing 50 µg/mL ampicillin and the culture was incubated at 37°C and 220 rpm for 8 hours. The bacteria culture was diluted to 100 mL with LB medium containing 50 µg/mL ampicillin and incubated at 37°C and 220 rpm overnight. Cells were pelleted by centrifugation at 4,200 rpm for 30 minutes at 4°C. The supernatant was aspirated and the pellet was dried at room temperature for a few minutes. The pellet was resuspended by 8 mL of Buffer RES (MACHEREY-NAGEL) and mixed with 8 mL of Buffer LYS (MACHEREY-NAGEL) to lyse the cells. The mixture was incubated at RT for 5 minutes and the lysis buffer was neutralized by 8 mL of Buffer NEU (MACHEREY-NAGEL). The lysate was applied to the equilibrated NucleoBond® Xtra Column Filter (MACHEREY-NAGEL) inserted in a NucleoBond® Xtra Column (MACHEREY-NAGEL). The column was equilibrated by 12 mL of Buffer EQU (MACHEREY-NAGEL) before the lysate loading. After the column was emptied by gravity flow, 5 mL of Buffer EQU (MACHEREY-NAGEL) was used to wash the filter and column. The filter was removed after the first wash and the column was washed with 8 mL of Buffer WASH (MACHEREY-NAGEL). The plasmid DNA was eluted with 5 mL of Buffer ELU (MACHEREY-NAGEL). The elution was mixed with 3.5 mL of isopropanol and centrifuged at 4,200 rpm for 30 minutes at 4°C. The DNA pellet was washed once with 2 mL of 70% ethanol and dried at room temperature. The DNA pellet was dissolved in 200 µL of buffer TE (Solarbio).

2.7 Cells

2.7.1 Cell Lines and Maintenance

293T were maintained in DMEM high glucose (GENOM) supplemented with 10% FBS (ExcellBio) and 1 × P/S (TransGen) and passaged when they reached 90% confluence.

For cell passaging, cells were washed with PBS (GENOM) once to remove excess medium and serum. 0.25% trypsin (TransGen) was added to the monolayer and the plate was incubated at 37°C for 2-5 minutes until cells were dissociated. Trypsinization was terminated by FBS or culture medium. Cells were pelleted by centrifugation and resuspended in the culture medium. Cells were seeded at the appropriate density and cultured in the cell incubator (37°C with 5% CO₂).

2.7.2 Thawing and Freezing Cells

Cells were thawed in 37°C water bath, pelleted by centrifugation at 1,500 rpm for 5 minutes and resuspended by culture medium. Cells were plated in cell culture dishes and cultured in the cell incubator (37°C with 5% CO₂).

Cells were frozen with a density of 1-3 × 10⁶ cells/mL when they reached 90% confluence. Cells were dissociated by trypsin and collected by centrifugation. For 293T, cells were resuspended in the freezing medium consisting of 90% 293T culture medium and 10% DMSO (Solarbio) and frozen at -80°C in an automated, controlled-rate freezing apparatus.

2.7.3 Transfection and Lentivirus Concentration

3.5 × 10⁶ 293T cells were seeded in a 10 cm dish and incubated overnight for transfection. GeneTwin™ Transfection Reagent (Biomed) and plasmid DNA were diluted in PBS gently as follow:

Table 2.41 Mixture for 293T transfection

Plasmids/reagents	Amount per 10cm dish
psPAX2	8.60 µg
pMD2.G	2.59 µg
pCDH-EF1α-HA-Foxp1-IRES-neo/	11 µg/
pCDH-IRES-neo	8.5 µg
Transfection Reagent (Biomed)	60 µL
PBS	1 mL

The mixture was incubated at RT for 10 minutes and added to 293T culture. Cells were incubated with the mixture for 8 hours or overnight. After transfection, the medium containing the transfection reagent was aspirated and replaced by 293T culture medium. Lentivirus was harvested at 48 hour and 72 hour after the onset of transfection. The lentivirus-containing supernatant was filtered by a 0.45 µm membrane to remove detached cells and lentivirus were concentrated by GML-PC™ Lentivirus Concentration Kit (Genomeditech). 1 volume of GML-PCTM lentivirus concentrator was combined to 3 volumes of clarified supernatant and the mixture was incubated at 4°C overnight. Lentivirus was pelleted by centrifugation at 4,200 rpm and 4°C for 45 min. The supernatant was aspirated and the virus pellet was resuspended by PBS.

2.7.4 Transduction and Antibiotic Selection

Lentivirus transduction was performed when cells reached 70% confluency. Lentivirus suspension and polybrene (YEASEN) were added to the culture medium. The final concentration of polybrene in the culture medium is 8 µg/mL. The second transduction was performed after 8 hours or overnight. After transduction, the medium containing virus particles was replaced by the fresh culture medium.

Antibiotic selection started from 48 hour after the first transduction by changing the culture medium to the selection medium (culture medium supplemented with antibiotics). The screening was terminated when cells in the untransduced plate

completely died.

2.8 Histology

2.8.1 Whole Mount Staining

Abdominal mammary tissues were dissected from the mice and spread on the glass slide. Mammary tissues were fixed in Carnoy's solution at RT overnight. Once the samples were prepared for carmine staining, they were rehydrated through a graded ethanol series (70%, 50%, 20% ethanol and distilled water, 1 hour each). After rehydration, tissues were stained in carmine stain until the whole glands were stained, which usually takes 12-24 hours for mammary glands from nulliparous mice. After staining, the tissues were dehydrated in a graded ethanol series (70%, 90%, 95%, 100%, 1 hour each). The glands were dehydrated in 100% ethanol for another 24 hours to ensure complete dehydration. The glands were transferred to xylenes to clear the fats for 24 hours and stored in methyl salicylate (D&B).

2.8.2 Paraffin Embedding and Sectioning

To ensure proper preservation of tissue architecture, fresh mammary tissues were dissected carefully, spread on the slides and placed in 10% formalin (Biosharp) for fixation at RT overnight. The fixed tissues were transferred to 70% ethanol and sent to Servicebio (China) for paraffin embedding and sectioning. In brief, paraffin embedding and sectioning were performed as follow. Tissues were dehydrated through a graded ethanol series (75% for 4 hours, 85% for 2 hours, 90% for 2 hours, 95% for 1 hour, and two changes of 100% ethanol, 30 minutes each) followed by two changes of xylene (10 minutes each) for clearing. The tissue was then infiltrated with molten paraffin wax at 65°C (three changes, 1 hour each) and embedded in paraffin blocks. During embedding, each tissue was oriented parallel to the surfaces of the paraffin block to ensure consistent sectioning. The blocks were allowed to solidify on a -20°C freezing plate. Paraffin-embedded tissue blocks

were trimmed, and 4 µm thick sections were cut using a microtome. Sections were floated on a 40°C water bath to remove wrinkles, mounted onto glass slides, and dried overnight at 60°C.

2.8.3 Haematoxylin and Eosin (H&E) Staining

H&E staining was performed by Servicebio (China). Sections were deparaffinized in xylene (two changes, 20 minutes each) followed by rehydration in 100% ethanol (two changes, 5 minutes each), 75% ethanol for 5 minutes, and tap water. Tissue sections were stained with Haematoxylin (Servicebio) for 3-5 minutes, rinsed in tap water, differentiated in Haematoxylin Differentiate Solution (Servicebio), rinsed in tap water, blued in Haematoxylin Bluing Solution (Servicebio) and rinsed in tap water. After haematoxylin staining, sections were dehydrated in 85% and 95% ethanol, each for 5 minutes, followed by Eosin (Servicebio) staining for 5 minutes. Sections were dehydrated 100% ethanol (three changes, 5 minutes each), cleared in xylene (two changes, 15 minutes each), and mounted with neutral balsam (Sinopharm). The slides were scanned on a 3D Histech MIDI pannoramic scanner using a 20 × objective lens and images were processed in ImageJ.

2.8.4 Immunohistochemistry (IHC) Staining

Sections were baked in a 60°C incubator for 60 minutes to enhance tissue adhesion to the slides. Sections were deparaffinized in xylene (two changes, 10 minutes each), rehydrated through a graded ethanol series (100%, 95%, 85%, and 75%, 5 minutes each) and immersed into ddH₂O (three changes, 15 minutes each). Antigen retrieval was performed by boiling the sections in diluted 1 × Improved Citrate Antigen Retrieval Solution (Beyotime) for 3 minutes. After cooling the sections and solutions to RT, the tissue sections were immersed in ddH₂O for 5 minutes with two rinses, followed by immersion in PBST for 5 minutes with two rinses. Endogenous peroxidase activity was blocked with 50 µL Enhanced

Endogenous Peroxidase Blocking Buffer (Beyotime) for 15 minutes. Sections were immersed in PBST for 5 minutes and rinsed twice, followed by blocking with 50 µL 10% normal donkey serum (Servicebio) for 30 minutes at RT. Primary antibodies diluted in 10% normal donkey serum, anti-NRG4 antibody (Solarbio) or anti-STAT5 (phospho Y694) antibody (abcam), were applied and sections were incubated overnight at 4°C. After primary antibody incubation, sections were recovered at RT for 40 minutes. After rinsing in PBST as described before, sections were incubated with HRP-conjugated Goat Anti-Rabbit/mouse IgG (Sangon) for 30 minutes at RT. Chromogenic detection was performed using DAB (ZSGB-BIO) for 1 minute, followed by rinsing in ddH₂O to terminate the reaction. Tissue sections were stained with haematoxylin (Biosharp) for 10 minutes, rinsed in ddH₂O, differentiated in 1% acid alcohol, and blued in PBS. Sections were dehydrated in graded ethanol series (75%, 85%, 95% and 100%, 5 minutes each), cleared in xylene (two changes, 10 minutes each) and mounted with neutral balsam (Solarbio). The slides were scanned on a 3D Histech MIDI panoramic scanner using a 20 × objective lens and images were processed in ImageJ.

2.9 Primary Stromal Cells Adipogenesis *In Vitro*

2.9.1 Primary Stromal Cells Isolation

Stromal-vascular fractions (SVFs) were isolated from nulliparous C57BL/6N female mice at 6-8 weeks old. Thoracic and abdominal mammary tissues were harvested and lymph nodes were removed. The tissues were briefly washed with PBS, minced into small pieces and digested in 10-20 mL primary SVFs digestion buffer for 2h at 37°C with shaking at 200 rpm. Midway through the digestion, the solution was homogenized by pipetting up and down a few times. To remove undigested pellets, digested tissues were pipetted up and down and passed through a 100 µm cell strainer. Cells were collected by centrifugation at 600 × g at RT for 5 minutes. Red blood cells were removed by ACK Lysing Buffer (Gibco) through incubation at

RT with handshaking for 3-5 minutes. Red blood cell lysis was terminated by 10 mL wash buffer (2% FBS in PBS), and the remaining cells were passed through a 70 μ m cell strainer. Cells were collected by centrifugation at 600 \times g for 5 minutes at RT. SVFs were resuspended and cultured in the SVF culture medium. Stromal cells were attached to the culture dish after 12 hours and unattached cells were washed by PBS. Primary stromal cells were maintained in the SVF culture medium. Stromal cells were passaged when they reached 90% confluence.

2.9.2 FOXP1 Overexpression

To overexpress *Foxp1* in stromal cells, 2×10^5 of stromal cells were seeded in a 6 cm culture dish. Lentivirus transduction was performed when cells were 70% confluent. 48 hours after transduction, the SVF culture medium was replaced by the G418 selection medium (SVF culture medium with 1 mg/mL G418 sulfate). Antibiotics were removed when the cells in the untransduced well completely died, which took about 5 days. Lentivirus produced from plasmid without HA-tagged *Foxp1* insertion served as the control group to compare with FOXP1 overexpression group. The efficiency of FOXP1 overexpression was detected by qPCR.

2.9.3 Adipogenesis

Primary stromal cells were seeded in a 6-well (10^5 per well) or 12-well (5×10^4 per well) plate and cultured with SVF culture medium for 4 days. To induce adipogenesis, cells were treated with adipogenesis induction medium for 2 days, followed by adipogenesis differentiation medium for 6 days.

2.9.4 Oil Red O Staining and Imaging

Cells were washed once with PBS and fixed in 4% paraformaldehyde (Biosharp) for 30 min. After fixation, PFA were removed and cells were stained with oil red O

staining solution for 1h. After staining, wash the wells with ddH₂O three times. Cells were kept under water for imaging. After microscopy imaging, cells were dried and the whole well was scanned.

2.10 Primary Mammary Organoid Lipogenesis *In Vitro*

2.10.1 Primary Mammary Organoid Isolation

Mammary organoid isolation was performed according to the established protocol with modifications (Nguyen-Ngoc et al., 2015). Mammary organoids were isolated from C57BL/6N wild-type (WT) female mice at mid-pregnancy (pregnancy day 13-15). To maximize organoid yield, all plastic surfaces used in the following steps were precoated with 2.5% BSA. Thoracic and abdominal mammary tissues were harvested and lymph nodes were removed. The tissues were minced until the tissue relaxed and digested in a primary mammary organoid digestion buffer for 40-60 min at 37°C with shaking at 150 rpm. Digested tissues were centrifuged at 1,500 rpm for 10 minutes at RT and the solution was separated into three layers. The fatty layer on top was preserved and transferred into a new tube and the aqueous layer was aspirated. The pellet on the bottom was resuspended by 10 mL Advanced DMEM/F12 (Gibco) and combined with the fatty layer. The pellet and the fatty layer were homogenized by pipetting up and down vigorously to release the organoids within the digested tissues. The cell clusters were collected by spinning at 1,500 rpm for 10 minutes at RT. The supernatant was aspirated and the cell pellet was resuspended by 4 mL Advanced DMEM/F12 (Gibco). To break up the organoid clusters and detach organoids from stromal cells, 40 µL of 1 mg/mL DNase I solution (Stem cell) was added into the suspension and the cell suspension was incubated at RT with gentle inversion for 2-5 minutes. The reaction was terminated by 6 mL Advanced DMEM/F12 (Gibco) and the suspension was pipetted up and down thoroughly to detach the organoids from stromal cells. The suspension was centrifuged at 1,500 rpm for 10 minutes at RT and the supernatant

was aspirated. The pellet was resuspended by 10 mL Advanced DMEM/F12 (Gibco) and mixed thoroughly. The suspension was centrifuged for 3-4 seconds at 1,500 rpm and the supernatant was aspirated. The differential centrifugation was repeated three more times to remove stromal cells from epithelial organoids. The organoids were resuspended in Advanced DMEM/F12 (Gibco) for counting. Organoids were seeded in Matrigel (Corning) for culture and further lipogenesis induction. 500 or 1000 organoids per dome (50 μ L Matrigel) were seeded in a 24-well plate for whole mount staining and gene expression analysis, respectively. Each well contained one dome and 500 μ L culture medium. Primary mammary organoids were maintained in basal organoid medium (BOM) before inducing lipogenesis.

2.10.2 Lipogenesis Induction

After incubation in BOM overnight, lipogenesis of the mammary organoids was induced by the lactation medium. For the STAT5 inhibition group, the lactation medium was supplemented with 100 μ M STAT5-IN-1 (MCE), a STAT5 phosphorylation inhibitor. The same volume of DMSO was added in the control group. Mammary organoids were treated with the lactation medium for 6 days, and the lactation medium was changed every three days.

2.10.3 Staining and Imaging

The mammary organoids were harvested and stained as described (Dekkers et al., 2019). The culture medium was aspirated and the Matrigel was washed by ice-cold PBS once. To release organoids from the Matrigel, the Matrigel were incubated with 1 mL ice-cold Cell Recovery Solution (Corning) on ice with horizontal shaking for 40-60 minutes until the Matrigel was completely dissolved. To minimize organoid loss, all plastic surfaces used in the following steps were precoated with 2.5% BSA. The organoids were transferred into a 15 mL centrifuge tube and

allowed to stand for 2 minutes followed by centrifugation at $70 \times g$ for 3 min at 4°C . In the following step, organoids were collected under the same conditions. Organoids were resuspended and fixed in 1 mL 4% PFA on ice for 45 min. After fixation, 9 mL of 0.1% PBST were added to the organoids and mixed with cell suspension gently. The organoids were incubated in PBST on ice for 10 min and collected by centrifugation. To visualize the lipid droplets in the mammary organoids, they were stained in 10 μM BODIPY (GLPBIO) and 1 $\mu\text{g/mL}$ DAPI (US EVERBRIGHT, #D4054) at RT for 30 min. After staining, organoids were collected and washed with 1 mL of OWB three times. After the last wash, the organoids were resuspended in 30 μL fructose-glycerol clearing solution for 20 min. Organoids and the clearing solution were transferred to the slides for imaging. To maintain the 3D structure of organoids, 2 layers of double-sided sticky tape were placed at both sides of the $1 \times 2\text{-cm}$ rectangle drawn by hydrophobic barrier pen (ACD) on the slides. Organoids were placed in the rectangle, and coverslips were placed on top and attached to the sticky tape. The slides were imaged on a Nikon A1 Confocal Microscope using a $20 \times$ objective lens and images were processed in ImageJ.

2.11 Primary Preadipocytes Adipogenesis *In Vitro*

2.11.1 Primary Preadipocyte Isolation

Preadipocytes were isolated from nulliparous C57BL/6N WT female mice at 6-8 weeks old. Thoracic and abdominal mammary tissues were harvested and lymph nodes were removed. The tissues were briefly washed with PBS, minced into small pieces and digested in a primary preadipocyte digestion buffer for 1h at 37°C and 200 rpm. Digested tissues were homogenized by pipetting up and down. Single cells were collected by passing the digested tissues through a 100 μm cell strainer followed by centrifugation at $250 \times g$ for 5 minutes. For the subsequent centrifugation procedures, conditions were maintained under the same condition unless noted. Red blood cells were removed by ACK Lysing Buffer (Gibco) through

incubation at RT with handshaking for 3-5 minutes. Red blood cell lysis was terminated by 10 mL wash buffer (2% FBS in PBS). The suspension was passed through a 70 µm cell strainer and cells were pelleted by centrifugation.

To remove epithelial cells, cells were resuspended by 100 µL wash buffer supplemented with 2.5-5 µg/mL anti-EpCAM-biotin antibody (Invitrogen) and incubated on ice for 30 minutes. To remove excess antibodies, cells were pelleted by centrifugation and the antibody-containing wash buffer was aspirated. The cell pellets were washed with 500 µL of wash buffer once and resuspended with 100 µL of wash buffer. Streptavidin magnetic beads (NEB) were used to pull down Epcam⁺ cells. 20 µL streptavidin magnetic beads were pulled down by the magnet and the supernatant was aspirated. The beads were washed with 200 µL wash buffer once and resuspended with 100 µL wash buffer. The cell suspension was mixed with the beads and incubated at RT for 5 minutes. EpCAM⁺ cells were pulled down by the magnet through interaction between biotin in the antibody and streptavidin magnetic beads. The magnet was applied to the side of the tube containing cell-bead mixture for 3 minutes and the cell suspension was collected. The beads pellet was washed with 100 µL wash buffer three times and the supernatant was collected and combined with the EpCAM⁻ cell suspension. The EpCAM⁻ cells were collected by centrifugation and cultured in the preadipocyte culture medium. Preadipocytes were attached to the culture dish after 12 hours and unattached cells were washed by PBS. Primary preadipocytes were maintained in the preadipocyte culture medium and were passaged when they reached 90% confluence.

2.11.2 Adipogenesis

Adipogenesis of preadipocytes was the same as adipogenesis of SVFs. Preadipocytes were treated with 500 ng/mL IL15 (R&D System) at the beginning of adipogenesis induction. The same volume of PBS was added to the medium for

the control group.

2.11.3 Staining and Imaging

Lipid droplets in differentiated preadipocytes were stained in the same processes as oil red O staining of differentiated stromal cells.

2.12 Single-Nuclei RNA Sequencing Analysis

2.12.1 Mammary Tissue Harvest for Sequencing

Wild-type C57BL/6N female mice were mated with males and allowed to litter to obtain mammary tissues at pregnancy day 13.5 (P13.5) and lactation day 5 (L5). Abdominal mammary tissues from nulliparous mice at 8 weeks of age (virgin), P13.5 and L5 were harvested and lymph nodes were removed. Harvested mammary tissues were frozen and stored in nitrogen. snRNA-seq of frozen mammary tissues were performed on 10X Genomics platform (virgin and P13.5: LC-Bio Technology Co., Ltd; L5: Gene Denovo Biotechnology Co., Ltd).

For snRNA-seq of mammary tissues from mice fed by HFD or normal diet (ND), abdominal mammary tissues were harvested at 10 weeks and processed in the same way. snRNA-seq was performed by LC-Bio Technology Co., Ltd.

2.12.2 Pre-processing and Clustering

snRNA-seq data from mammary tissues at different time points were analysed separately. Raw data were processed by the CellRanger software and analysed by Seurat (v4.2.1) following the standard pipeline. Low quality cells were filtered by abnormal unique feature counts and percentage of mitochondrial genes. To remove low-quality cells and doublets, thresholds for unique feature counts were set as follow: 200-8000 for virgin and P13.5, and 200-6000 for L5. In addition, cells with the high percentage of mitochondrial genes were defined as dying cells and

were removed from the following analysis: 5% for virgin, 1% for P13.5 and 2% for L5. After discarding low quality cells, a total number of 17,947 cells were left (5,034 for virgin, 6,684 for P13.5 and 6,229 for L5). Feature expression values for each cell were normalized and highly variable features between cells were identified. The number of highly variable features was determined by the distribution of feature counts observed in the majority of cells within each dataset (3,000 for virgin, 2,000 for P13.5 and L5), ensuring a balance between retaining biological variation and minimizing technical noise in downstream analyses. Linear transformation was applied to all features to scale and centre features and avoid domination of highly-expressed genes. Principal components analysis (PCA) was performed on the scaled data and highly variable features determined previously were used to compute PCA. Principal components were ranked according to the percentage of variance. The first 15 principal components were selected for downstream analysis based on the Elbow Plot method, which identified the inflection point where the cumulative variance plateaued, balancing cell-type differences and technical noise. These 15 principal components were used to calculate cell-cell distance. Cells were clustered with a resolution of 0.2 to prioritize broader clustering patterns, intentionally merging subpopulations with similar characteristics, thereby facilitating robust identification of major cell types while avoiding over-segmentation. Clustered cells were projected into two dimensions by non-linear dimensional reduction, uniform manifold approximation and projection (UMAP). Cell types were defined by their expression of canonical markers (

Table 2.42) and clusters annotated to the same cell type were merged. Six types of cells were identified from three datasets, including luminal cells, basal cells, adipocytes, stromal cells, immune cells and endothelial cells.

The decontamination procedure was implemented with the R package scCDC, and this analysis was carried out by Weijian Wang, Yihui Cen and Zezhen Lu (W. Wang

Deleted: Table 2.42

Formatted: Font: Not Bold

et al., 2024). Decontaminated data were processed and clustered by repeating normalization, highly variable feature identification, scaling, principal component analysis, clustering and dimensional reduction steps. To integrate data from different time points, they were integrated using Seurat and the integrated data were re-clustered. 3755 features which were repeatedly variable across datasets were selected for finding anchors to integrate the datasets. Standard workflow including scaling, PCA, clustering and dimensional reduction was run on the integrated data for visualization and clustering. Cell types were defined by the expression of canonical markers.

To further examine the cell fate transitions of luminal cells, luminal clusters were further divided into luminal progenitor cells, proliferating luminal cells, ductal cells, hormone sensing cells and alveolar cells ([Figure 4.4A](#)). First 15 principal components were used to calculate cell-cell distance and cells were clustered with a resolution of 0.1. Similarly, the stromal cluster was divided into 4 clusters ([Figure 4.1A](#)).

Deleted: Figure 4.4

Formatted: Font: Not Bold

Deleted: Figure 4.1

snRNA-seq data from mammary tissues of mice fed by HFD and ND were analysed in similar ways. In brief, raw data were processed and analyzed by Seurat. Cells with features lower than 200 or higher than 6000, and cells with over 5% of mitochondrial genes were removed. Data was scaled by linear transformation and PCA was performed on the scaled data. Cell-cell distance was calculated based on the first 15 principal components and cells were clustered with a resolution of 0.1 to avoid over-segmentation. Non-linear dimensional reduction UMAP was performed for visualization and cell types were defined by markers. Decontamination was performed by scCDC and the decontaminated data were integrated and processed by repeating the Seurat standard pipeline. Seven types of cells were identified, including luminal progenitors, basal cells, hormone sensing cells, adipocytes, stromal cells, immune cells and endothelial cells ([Figure 6.2A](#)).

Deleted: Figure 6.2

Proportions of each cell type were computed within each group by normalizing the cell counts to relative frequencies and visualized by bar plots.

2.12.3 Visualisation

Clusters with annotated cell types were visualized by scatter plots where cells were embedded based on the UMAP reduction and coloured by annotated cell types. Gene expression of each cell was visualized in a similar plot with colour gradient representing the levels of gene expression. The average gene expression across different cell types was visualized by DotPlot where the dot size represented the proportion of cells within a cluster expressing a given gene, and the colour intensity of each dot corresponded to the gene expression level. Proportions of each cell type were computed within each stage by normalizing the cell counts to relative frequencies and visualized by bar plots.

2.12.4 Cell Type Identification

To identify the cell type of each cluster, differential expressed genes (DEGs) of each cluster were identified by statistically comparing gene expression levels between the target cell cluster and all other clusters. Significant expression differences were detected by the Wilcoxon rank sum test. Genes with high log-fold change and expression prevalence were regarded as cluster markers. Identified cluster markers were cross-referenced with canonical markers to reveal cell identities. Expression of those marker genes in each cluster was visualized by plot to confirm the cell type of each cluster. Cell types in mammary tissue and their marker genes were listed as follow:

Table 2.42 Canonical markers used for cell type identification

Cell type	Genes
Basal cells	<i>Pdpn, Etv5, Acta2</i>
Luminal cells	<i>Krt18, Gata3, Elf5, Wfdc18, Csn2, Csn3</i>

Luminal progenitors	<i>Aldh1a3, Kit</i>
Alveolar cells	<i>Csn2, Csn3</i>
Hormone sensing cells	<i>Esr1, Prlr, Pgr</i>
Immune cells	<i>Ptprc, Dock2, Cd74</i>
Stromal cells	<i>Col3a1, Col5a1, Fn1</i>
Endothelial cells	<i>Eng, S1pr1, Emcn</i>
Adipocytes	<i>Adipoq, Gpat3, Dgat1</i>

In addition, gene ontology (GO) enrichment analysis of DEGs across subdivided luminal clusters was performed using the enrichGO function in the clusterProfiler package (v3.18.1). This analysis revealed the classification of luminal subpopulations based on canonical markers.

2.12.5 Deconvolution

snRNA-seq data and scRNA-seq data (GSE106273) were used to estimate cell type abundance from bulk mammary tissue RNA sequencing (GSE37646) by CIBERSORTx. For the scRNA-seq datasets, expression profiles of mammary glands from mice at nulliparous, gestation day 14.5 and lactation day 6 were used. The transcriptome profiles of scRNA-seq and bulk RNA sequencing were obtained from the GEO repository. In the scRNA-seq data, subtypes of luminal cells including hormone sensing progenitors, hormone sensing differentiated cells, luminal progenitors, alveolar progenitor cells and alveolar differentiated cells, were defined as luminal cells for the deconvolution analysis. Similarly, subtypes of basal cells, including myoepithelial cells and Procr⁺ basal cells, were defined as basal cells.

The log-transformed gene expression matrices of 8,000 randomly sampled cells from snRNA-seq and scRNA-seq were used as the reference to calculate cell type abundance of bulk mammary tissue samples. Signature matrix files were built from scRNA-seq data and snRNA-seq data respectively. The proportion of different cell

types in bulk RNA sequencing of mammary tissues was inferred based on the signature matrix files. The results from the samples with the same genotype and developmental stage were merged and the imputed cell proportion was visualized by bar plot.

2.12.6 Correlation Analysis

To assess the potential relationships between different cell populations, pairwise correlations were calculated based on their average gene expression profiles. The average expression matrix was computed for each cell population by aggregating the integrated expression values across all cells within a cell type. To focus on the most variable genes driving population differences, the top 1,000 genes with the highest standard deviation across clusters were selected for correlation calculation as these genes were likely to exhibit significant expression changes among cell populations and were informative for correlation analysis. Pairwise spearman correlations were computed between the average expression profiles of the selected genes for each cell population. The correlation matrix was visualized as a heatmap where rows and columns represented cell populations and the colour intensity indicated the strength of the correlation. In addition, clustering was applied to group cell populations with similar expression profiles, revealing patterns of transcriptional similarity and divergence.

2.12.7 Identification of Differentiation Trajectory

The Monocle package (v2.18.0) in R was employed to calculate the differentiation trajectories of stromal cells into luminal, basal, and adipocyte lineages respectively. The integrated expression matrix and cell type annotations from snRNA-seq data were incorporated into Monocle-compatible objects. Size factors were estimated to normalize library sizes across cells and gene dispersions were calculated to identify highly variable genes. Genes expressed in at least 10 cells were retained

for downstream analysis. t-SNE was applied to reduce the data to two dimensions, followed by unsupervised clustering to group transcriptionally similar cells. Differential gene expression analysis across clusters identified genes significantly associated with cellular states. These genes were regarded as ordering genes and were used to infer the trajectory using the DDRTree algorithm, which constructed a principal graph embedding the developmental continuum. Cells were ordered along pseudotime, which predicted their progression through the differentiation trajectory. The inferred trajectories were visualized with cells coloured by their annotated cell types or gene expression levels.

The calculateDiffusionMap function from the scater package (v1.18.6) in R was employed to analyse the differentiation trajectory of luminal cells, including luminal progenitors, proliferating luminal cells and alveolar cells. Diffusion map is a nonlinear dimensional reduction technique that captures the high-dimensional gene expression profiles to establish a pseudotemporal ordering which reflects their biological progression. This method is effective in scRNA-seq data, as it preserves continuous trajectories. The diffusion map was computed based on the integrated expression matrix, generating low-dimensional embeddings where cell-to-cell distances reflected the underlying differentiation paths. To visualize the inferred differentiation trajectory, cells were mapped in the diffusion space with colour assigned according to cell types or colour gradients representing the regulon activity.

2.12.8 Comparison of Top Transcriptional Regulators among Clusters

Gene regulatory networks of luminal subpopulations and stromal subpopulations were inferred by SCENIC. Filtered raw counts of cells were used to perform pySCENIC following the standard workflow. The analysis began with the co-expression module inference step, where potential relationships between transcription factors and target genes were identified using the GRNBoost2

algorithm. Next, each transcription factor and its target genes were regarded as a regulon, which was refined by pruning non-target genes using cis-regulatory motif analysis with the RcisTarget database. After this step, only target genes with the corresponding transcription factor binding motifs were retained, ensuring that the inferred regulons are supported by both expression data and regulatory motifs. Once the regulons were defined, the activity of each regulon was quantified using the AUCell algorithm, which calculated the area under the curve (AUC) for each regulon across cells and provided a score that reflected the activity levels of the regulons in each cell. The pySCENIC outputs were further analysed and visualised by SCopeLoomR, which enabled the identification of key transcription factors and regulatory networks by comparing the regulon activity across the luminal populations. The average regulon activity for each cell type was calculated according to the AUCell scores and the mean activity of each regulon within each cell type was computed to generate a regulon activity matrix across cell types. The regulon activity matrix was normalized and the relative activity of selected regulons was visualized by heatmap.

2.12.9 Identification of Intercellular Communications

Intercellular communications between the cells in the mammary tissue were constructed and visualized CellChat and iTALK.

For cell-cell communications analysed by CellChat (v1.1.3), the database for mouse was used. Over-expressed ligand-receptor interactions were identified based on gene expression. The communication probability of ligand-receptor pairs was computed based on gene expression levels, binding affinities, and pathway coherence. The aggregated network was calculated and its centrality scores were computed to identify dominant interactions. Ligand-receptor pairs were visualized by chord plots or bubble plots. To compare the changes in cell-cell communications across developmental stages, the CellChat datasets from different stages were

merged and the interaction strength of each signalling pathway at different stages was compared. The top signalling pathways between mammary epithelial cells and adipocytes at virgin, P13.5 and L5 were identified.

For cell-cell communication analysed by iTALK (v0.1.0), genes in datasets were converted to human homologues as iTALK only provided a database for human. Ligand-receptor pairs were identified based on gene expression. Ligand-receptor interactions between cell types were quantified and their significance was assessed by statistical tests. Significant communication networks were visualized by circle plots.

2.13 Quantification and Statistical Analysis

Differences in cell proportions across different stages or groups in snRNA-seq were analysed by bootstrapping followed by the Wilcoxon rank sum test. For each dataset, 1,000 bootstrap replicates were generated by randomly sampling cells with replacement to match the original dataset size. The proportions of target cell types were recalculated within each iteration to produce an empirical distribution of proportion estimates. 95% confidence intervals were derived from 2.5%-97.5% of these distributions to quantify uncertainty. Statistical significance was assessed using Wilcoxon rank sum tests.

Experimental data were presented as mean \pm standard deviation (SD). Significance was assessed by statistical tests.

To evaluate differences in gene expression in undifferentiated and differentiated primary stromal cells with or without FOXP1 overexpression, ANOVA for multiple-group comparisons were used. While comparing the expression of adipogenesis-related genes, gene expression levels in differentiated cells were normalized to the undifferentiated cells in each group. While comparing the expression of *Foxp1* and epithelial-related genes, gene expression levels in the FOXP1 overexpression

group were normalized to the control group. Bonferroni's multiple comparisons test was used to compare the differences between the FOXP1 overexpression group and the control group.

To evaluate differences in fluorescent intensity and gene expression in mammary organoids with or without treatment of STAT5 phosphorylation inhibitor, the t-test for two-group comparisons was used. Fluorescent intensity and gene expression in STAT5 phosphorylation inhibition group were normalized to the control group.

To evaluate differences in the gene expression in differentiated primary adipocytes with or without IL15 treatment, the t-test for two-group comparisons was used. The expression levels of adipogenesis-related genes in differentiated cells were normalized to the undifferentiated cells.

To evaluate differences in pup weight between litters nursed by NRG4 knockout dams and wild-type dams, the nested t-test was applied for each separated time point. This statistical approach accounted for the hierarchical structure of the data that pups were nested within dams when comparing the two maternal groups. In addition, the chi-square test was used to evaluate intra-litter weight variability which represented the differences among pups from the same dam, irrespective of maternal genotype.

To evaluate differences in body weight between the control group and the experimental group in HFD studies, ANOVA for multiple-group comparisons was used. Bonferroni's multiple comparisons test was used to compare the differences between the control group and the experimental group at each time point.

To evaluate the differences in ductal elongation, branching frequency, TEB density, ductal width and NRG4 expression between wild-type and NRG4 knockout mice or between high-fat diet-fed and normal diet-fed mice, the t-test was used. The NRG4 expression in NRG4 knockout mice or high-fat diet-fed mice were normalized to

wild-type mice or normal-diet fed mice, respectively.

Chapter 3

Single-Nucleus Sequencing Profiles Cell Map in Mammary Tissue

3.1 Introduction

scRNA-seq technology reveals the heterogeneity of transcriptomes of individual cells, contributing to understanding the dynamics of gene expressions and regulatory factors. In addition, scRNA-seq helps unravel the cell compositions and their interactions within tissues. Previous studies perform scRNA-seq on murine mammary tissues, revealing regulatory mechanisms, differentiation dynamics and cell-cell communications within the mammary tissue. scRNA-seq of mammary epithelial cells from different developmental stages demonstrates the differentiation hierarchy of basal and luminal compartments during puberty, pregnancy and lactation (Bach et al., 2017; Regan & Smalley, 2020). Single-cell transcriptome analysis of mouse mammary tissue also indicates the contributions of stromal cells on mammary gland organizations and interactions between mammary epithelial cells and stromal cells during these processes (Kanaya et al., 2019; Yoshitake et al., 2022). In addition, scRNA-seq identifies subpopulations of luminal cells and macrophages and uncovers the alterations of cell proportions in the mammary gland microenvironment associated with aging (C. M.-C. Li et al., 2020).

Although scRNA-seq in previous studies provides insights into transcriptomic atlas and regulatory networks of various cell populations in the mammary tissue, one of the major cell populations, white adipocytes, has not been studied by scRNA-seq due to their buoyant and fragile nature. About 90% of white adipocytes are occupied by lipid droplets, which increases difficulties in dissociating adipose tissues into single-cell suspension. Furthermore, high lipid content in white

adipocytes may affect enzymatic reactions during sequencing. Recently, with the development of snRNA-seq, adipocytes with large lipid droplets are allowed to be included in single-cell studies.

To study the cell-cell communications and regulatory networks within cell populations in the mammary tissues during pregnancy and lactation, snRNA-seq was used to generate the transcriptional profiles of murine mammary tissues. snRNA-seq of the whole tissue allows the inclusion of adipocytes, which enables exploration of heterogeneity and dynamics of adipocytes in the mammary tissue during mammary gland development. This chapter focuses on the preliminary analysis of snRNA-seq data of mammary tissues, including clustering and differential expression analysis. Furthermore, this section compares the differences between snRNA-seq and scRNA-seq of the mammary gland in the same development stages by applying transcriptomic data to estimate the abundances of cell populations from bulk RNA sequencing.

3.2 Single-Nucleus Sequencing Experimental Design

To study the dynamics of cells within the mammary tissue across three developmental stages, including nulliparous, pregnancy and lactation, snRNA-seq was performed on mammary tissues obtained at these stages ([Figure 3.1](#)). The mammary tissues from mice at nulliparous (virgin), pregnancy day 13.5 (P13.5) and lactation day 5 (L5) were harvested for nuclei extraction. RNA sequencing was performed on the 10X Chromium platform and the datasets were processed using the conserved computational pipeline similar to scRNA-seq. Sequencing metrics were analyzed by Seurat to identify clusters and cell types. Cells of interest were selected for further analysis, including inferring differentiation trajectory by DiffusionMap and Monocle, revealing potential important transcription factors and gene regulatory networks by SCENIC, and identifying cell-cell communications through ligand-receptor pairs by CellChat and iTALK.

Deleted: Figure 3.1

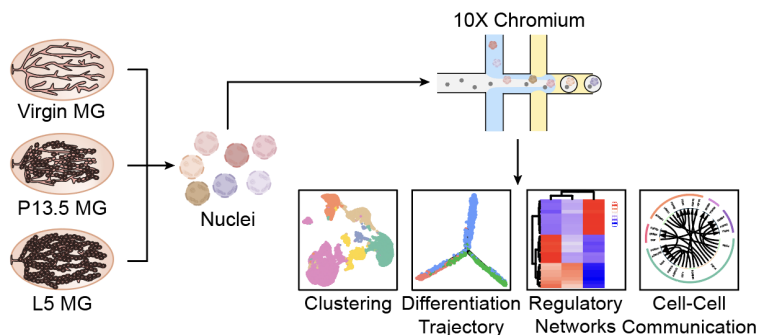


Figure 3.1 Schematic diagram highlighting the experimental design for snRNA-seq and downstream analyses.

P13.5, pregnancy day 13.5; L5, lactation day 5; MG, mammary gland.

3.3 Clustering and Cell Type Identification

snRNA-seq detected 27,516 features from 17,947 individual cells. After pre-processing and decontamination, three datasets, virgin, P13.5 and L5, were integrated for further analysis. UMAP was performed to visualize the integrated data. Cells from the integrated data were dissected into 14 clusters (Figure 3.2A). Biomarkers for each cluster were identified and compared with canonical markers to define the cell types. Based on the expression of *Krt18*, *Gata3*, *Elf5*, *Aldh1a3*, *Kit*, *Wfdc18*, *Csn2*, *Csn3*, *Esr1*, *Pgr* and *Prlr*, cluster 0, 4, 6, 7 and 12 were identified as luminal cells (Bach et al., 2017; C. M.-C. Li et al., 2020) (Figure 3.2B). The heterogeneity of luminal cells resulted in distinct genetic characteristics across subpopulations, as evidenced by divergent biomarker expression. Therefore, the luminal clusters need to be divided into more detailed subpopulations to delineate their functional and molecular diversity. Cells in cluster 3 and cluster 11 expressed *Pdnp*, *Etv5* and *Acta2* were identified as basal cells (Bach et al., 2017) (Figure 3.2B). Cluster 1 and cluster 9 with high expression of *Adipoq*, *Cidec*, and *Pparg* were identified as adipocytes (Dong et al., 2022; Kim et al., 2008) (Figure 3.2B). Cluster 5, 10 and 13 which showed high expression of immune cell markers *Ptprc*,

Deleted: Figure 3.2

Formatted: Default Paragraph Font

Deleted: Figure 3.2

Formatted: Default Paragraph Font

Formatted: Default Paragraph Font

Deleted: Figure 3.2

Deleted: Figure 3.2

Formatted: Default Paragraph Font

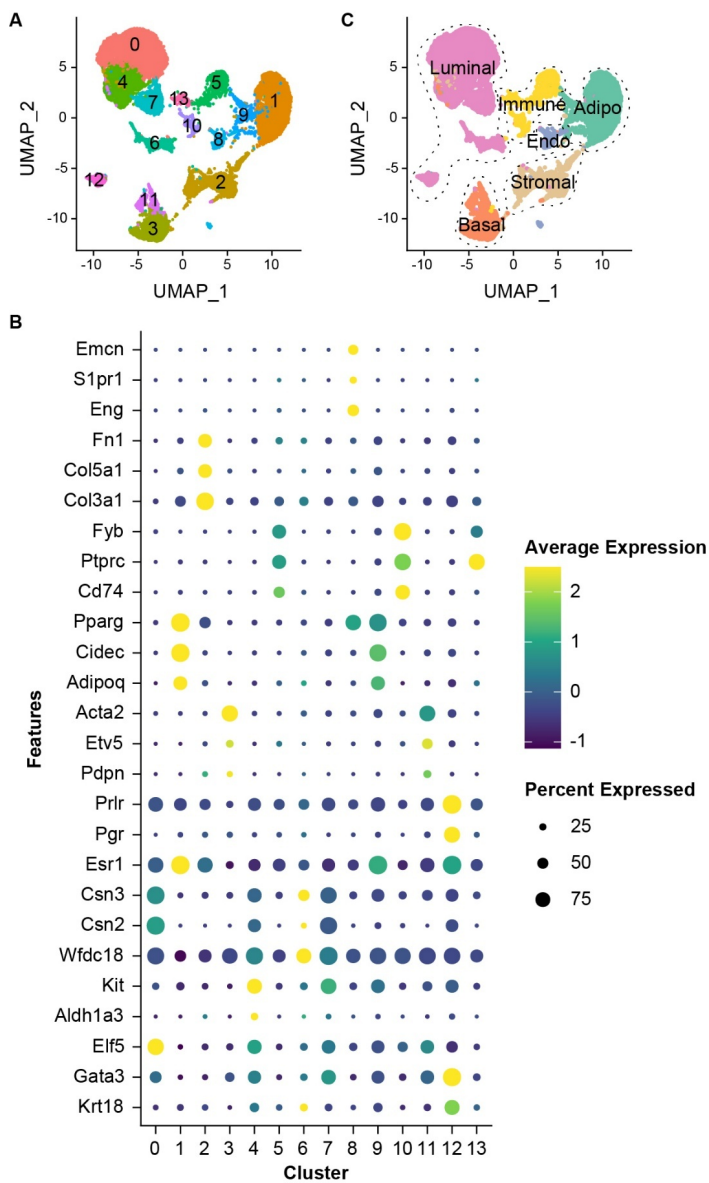


Figure 3.2 snRNA-seq identifies 6 cell types in the mammary tissue.

A. UMAP plot of integrated cells coloured by clusters. B. Expression of canonical markers in cell clusters. C. UMAP plot of integrated cells coloured by cell types. Luminal, luminal cells; Basal, basal cells; Adipo, adipocytes; Stromal, stromal cells; Immune, immune cells; Endo, endothelial cells.

Fyb and *Cd74*, were identified as immune cells (Bach et al., 2017; Valdés-Mora et al., 2021) (Figure 3.2B). Cluster 2 was identified as stromal cells as most of the cells in this cluster expressed markers of fibroblasts, including *Col3a1*, *Col5a1* and *Fn1* (Bach et al., 2017) (Figure 3.2B). Cluster 8 was identified as endothelial cells based on high expression of endothelial cell markers, *Eng*, *S1pr1* and *Emcn* (Bach et al., 2017) (Figure 3.2B).

Deleted: Figure 3.2

Formatted: Default Paragraph Font

Deleted: Figure 3.2

Formatted: Default Paragraph Font

Deleted: Figure 3.2

Formatted: Default Paragraph Font

Cell types were assigned to clusters. Six types of cells were identified within the mammary tissue, including luminal cells and basal cells from mammary epithelium, adipocytes, stromal cells, immune cells and endothelial cells from the mammary fat pad (Figure 3.2C). The proportion of each type of cell at each stage was computed and the significance of the differences in the proportion of luminal, basal, stromal and adipocyte clusters among stages was calculated by bootstrapping and Wilcoxon rank sum tests (Figure 3.3). During pregnancy and lactation, the proportion of mammary epithelial cells increases from about 20% to about 70% and the proportion of other non-epithelial cells decreases. These dynamics of cells are consistent with the morphological changes within the mammary tissue that the mammary fat pad is filled with ducts and alveoli during pregnancy and lactation.

Deleted: Figure 3.2

Formatted: Default Paragraph Font

The luminal cells rapidly expand during pregnancy revealed by the dramatic increase of luminal proportion at P13.5 (about 55%) compared to virgin (about 20%). However, the proportion of luminal cells is similar between P13.5 and L5, suggesting that luminal cells almost finish expansion at P13.5 and switch to differentiation and maturation. In addition, the proportion of basal cells gradually increases from 5% to 20% during pregnancy and lactation. On the contrary, the adipocytes undergo a dramatic reduction at P13.5 (from 45% at virgin to 10% at P13.5), indicating adipocytes vacate their space for epithelial expansion. The proportion of stromal cells and immune cells gradually decreased during pregnancy and lactation (from 30% at virgin to 10% at L5). The proportion of endothelial cells had slight changes in different development stages.

Deleted: Figure 3.3

Formatted: Check spelling and grammar

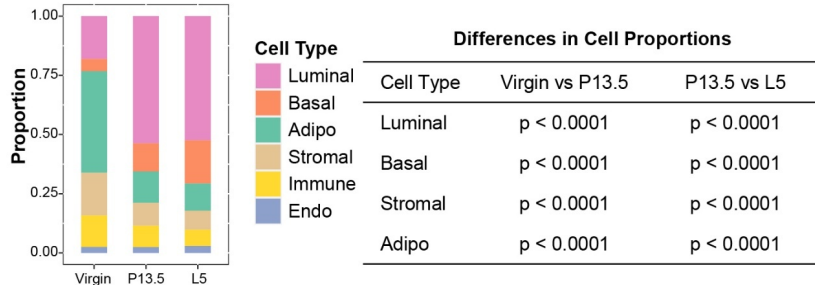


Figure 3.3 Proportion of each cell type at different stages.

Luminal, luminal cells; Basal, basal cells; Adipo, adipocytes; Stromal, stromal cells; Immune, immune cells; Endo, endothelial cells. The p-value is calculated by the Wilcoxon rank sum test.

3.4 Identification of Differential Expressed Genes

To identify markers of each cell type found in snRNA-seq datasets, a list of differentially and highly expressed genes for each type of cell was found. Four DEGs were defined as cell type-specific markers based on their dominant expression levels within distinct cell populations and their functional relevance to the biological roles of those cell types (Figure 3.4). *Csn2*, *ErbB4*, *Csn1s2a* and *Elf5* were defined as markers for luminal clusters. *Csn2* and *Csn1s2a* encode caseins which are milk proteins produced in luminal cells during pregnancy and lactation (L. G. Hennighausen & Sippel, 1982). *ErbB4* encodes the receptor ErbB4 on the luminal cells, which is indispensable for mammary gland maturation during lactation (Jones et al., 1999; Long et al., 2003). *ELF5* encoded by *Elf5* is highly expressed in luminal cells which are prepared to specify into milk-producing cells (Shehata et al., 2012). *Oxtr*, *Acta2*, *Myh11* and *Nrg1* were defined as markers for basal clusters. *Oxtr* encodes oxytocin receptor which is found expressed in myoepithelial cells of the basal lineage in the mammary ductal epithelium and involved in milk production (Kimura et al., 1998). *Acta2* and *Nrg1* are specifically expressed in basal cells in the mammary gland (Forster et al., 2014; Prater et al., 2014). *Myh11* encodes a smooth muscle myosin, indicating the smooth muscle cell

Deleted: Figure 3.4

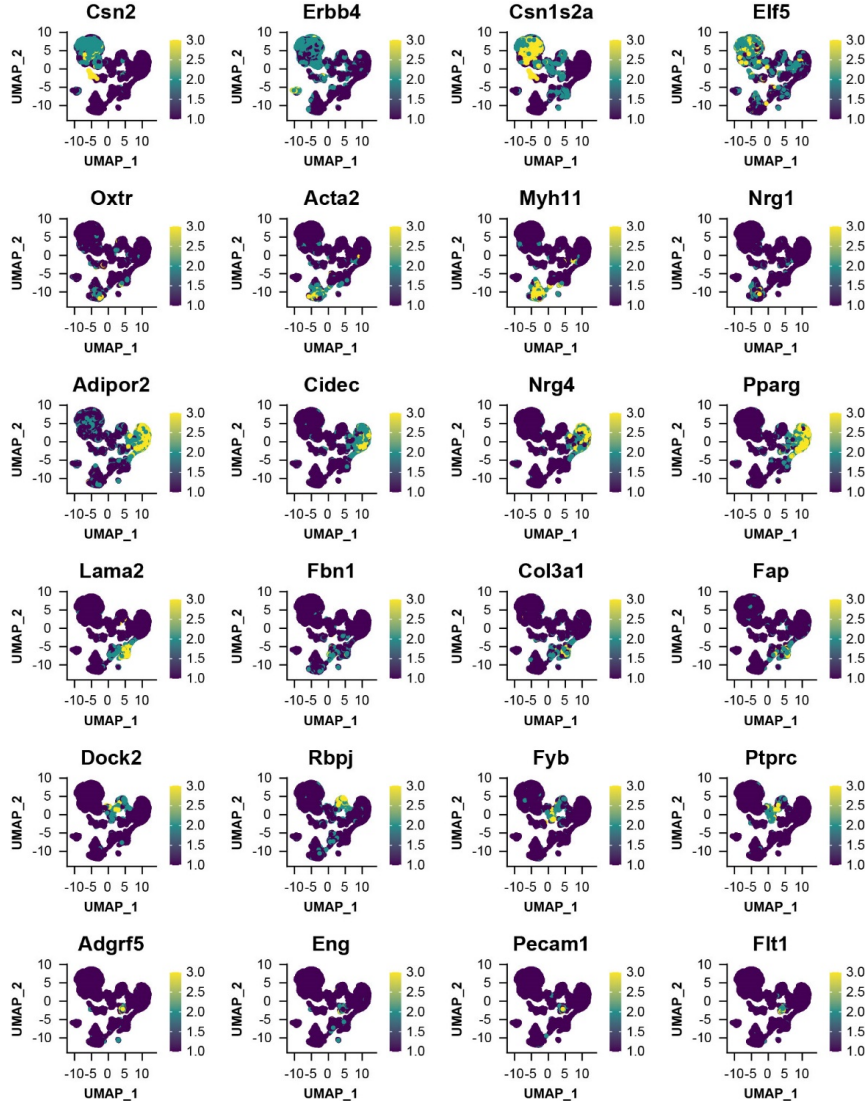


Figure 3.4 Expression of cell type-specific markers identified through snRNA-seq.

characteristics of myoepithelial cells in the basal layers (Mauduit et al., 2024).

Adipor2, *Cidec*, *Nrg4* and *Pparg* were defined as markers for adipocyte clusters.

Adipor2 and *Cidec* encode proteins involved in lipid metabolism in adipocytes (Y.

Li et al., 2018; Ruiz et al., 2023). *Pparg* encodes peroxisome proliferator-activated receptor γ which regulates gene transcription and promotes differentiation of adipocytes (Rosen, 2005). *Nrg4* encodes NRG4 which is an adipokine synthesized and secreted by adipocytes. *Lama2*, *Fbn1*, *Col3a1* and *Fap* were defined as markers for the stromal cluster. Proteins encoded by *Lama2*, *Fbn1* and *Col3a1* are key extracellular matrix components, laminin $\alpha 2$, fibrillin-1 and type III collagen, which interact with stromal cells to maintain the structure of extracellular matrix (Domogatskaya et al., 2012; Hatzirodos et al., 2019; Korsunsky et al., 2022; L. Li et al., 2024; Rodda et al., 2018). The fibroblast activation protein encoded by *Fap* is specially expressed in stromal cells and plays an important role in extracellular matrix remodelling (Huang et al., 2011; Y. Wu et al., 2023). *Dock2*, *Rbpj*, *Fyb* and *Ptprc* were defined as markers for the immune clusters. *Dock2* encodes the dedicator of cytokinesis 2, which is crucial for the migration and immune functions of T cells and B cells (Y. Chen et al., 2021; Randall et al., 2024; Ushijima et al., 2018). *Rbpj* encodes a protein involved in Notch signalling, which plays a critical role in T cells and macrophage development (E. L. Y. Chen et al., 2019; Guo et al., 2024; H. Han et al., 2002). *Fyb* encodes an adaptor molecule Fyn-binding protein that regulates T cell receptor signalling (Krause et al., 2000). *Ptprc*, also known as *Cd45*, is a conserved marker for immune cells (Hermiston et al., 2003). *Adgrf5*, *Eng*, *Pecam1* and *Flt1* were defined as markers for the endothelial cluster. *Adgrf5*, *Eng* and *Pecam1* are highly expressed in endothelial cells and encode proteins responsible for regulating cell adhesion and modulating vascular permeability (Graesser et al., 2002; Jerkic & Letarte, 2015; Niaudet et al., 2015; Rossi et al., 2016). *Flt1* encodes a receptor for vascular endothelial growth factor (VEGF), which is involved in regulating angiogenesis in response to VEGF signalling (Chappell et al., 2016; G. Zeng et al., 2007). Collectively, the markers of each cell type are summarized in Table 3.1.

Table 3.1 Cell type-specific markers identified by snRNA-seq data.

Deleted: Table 3.1

Formatted: Font: Not Bold

Cell type	Genes
Luminal cells	<i>Csn2, Erbb4, Csn1s2a, Elf5</i>
Basal cells	<i>Oxtr, Acta2, Myh11, Nrg1</i>
Adipocytes	<i>Adipor2, Cidec, Nrg4, Pparg</i>
Stromal cells	<i>Lama2, Fbn1, Col3a1, Fap</i>
Immune cells	<i>Dock2, Rbpj, Fyb, Ptprc</i>
Endothelial cells	<i>Adgrf5, Eng, Pecam1, Flt1</i>

3.5 Estimating Cell Fraction of Bulk RNA Sequencing Data

Although scRNA-seq/snRNA-seq provides insight into the heterogeneity and complexity within individual cells, it is more complicated and costly compared to bulk RNA sequencing. A transcriptomic deconvolution tool, CIBERSORT, is developed to estimate cell composition from tissue gene expression profiles based on single-cell reference profiles (Newman et al., 2019). To explore the accuracy of the reference matrix built from snRNA-seq, cell composition from bulk RNA sequencing of mammary tissues was inferred based on the reference matrix built from snRNA-seq (Figure 3.5A). Single-cell gene expression profiles of mammary epithelial cells from previous study was used in comparison to the snRNA-seq dataset (Bach et al., 2017).

Deleted: Figure 3.5

Formatted: Default Paragraph Font

The proportion of luminal cells, basal cells, stromal cells, immune cells and adipocytes were estimated in mammary tissues used for bulk RNA sequencing. When using scRNA-seq data as reference, the proportion of adipocytes is undetectable and the estimated cell fraction in each sample was different compared to imputation based on snRNA-seq data (Figure 3.5). Imputed cell fraction based on snRNA-seq data shows that the proportion of luminal cells decreases in mammary tissues from STAT5A knockout mice and STAT5A/STAT5B double knockout mice (Figure 3.5A). The proportion of luminal cells from the STAT5A/STAT5B double knockout group at lactation day 1 (L1) is only about 25%,

Deleted: Figure 3.5

Formatted: Default Paragraph Font

Deleted: Figure 3.5

Formatted: Default Paragraph Font

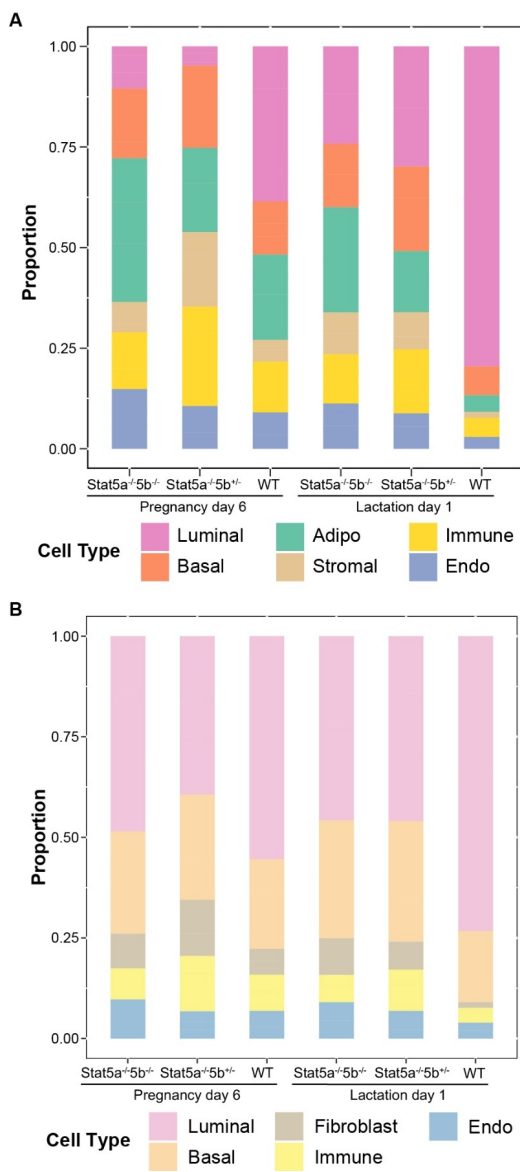


Figure 3.5 Cell fraction imputation of bulk RNA-sequencing data.

A-B. Deconvolution of bulk RNA-Sequencing of mammary tissue using snRNA-Seq (A) and scRNA-Seq (B) as reference. Luminal, luminal cells; Basal, basal cells; Adipo, adipocytes; Stromal, stromal cells; Immune, immune cells; Endo, endothelial cells.

while the proportion of luminal cells from the WT group at L1 is about 80% ([Figure 3.5A](#)). This result is consistent with previous studies that STAT5A deficiency impairs mammary gland development. In addition, the proportion of adipocytes in mammary tissues from WT mice decreases from about 20% at pregnancy day 6 (P6) to about 5% at L1 while the luminal proportion increases from about 10% at P6 to about 80% at L1, indicating that the mammary gland is well-developed in WT mice and adipocytes disappear due to epithelial expansion. Compared to deconvolution analysis based on snRNA-seq data, cell fraction estimated by scRNA-seq reference is less accurate. In the imputation of cell fraction based on scRNA-seq, adipocytes are not detected ([Figure 3.5B](#)). In addition, the proportion of luminal cells in mammary tissues from STAT5A knockout mice and STAT5A/STAT5B double knockout mice has fewer differences compared to that from wild-type mice, which is inconsistent with the morphology of the STAT5 knockout mammary gland in previous studies ([Figure 3.5B](#)). In summary, snRNA-seq provides an accurate reference for deconvolution analysis of bulk RNA sequencing data.

Formatted: Default Paragraph Font

Deleted: Figure 3.5

Deleted: Figure 3.5

Formatted: Default Paragraph Font

Deleted: Figure 3.5

Formatted: Default Paragraph Font

3.6 Discussion

This chapter focused on primary processing of the snRNA-seq data, including clustering and differential expression analysis. Six types of cells were identified in the mammary tissue across three developmental time points and changes in the abundance of mammary epithelial cells and adipocytes were detected during pregnancy and lactation. Compared to the scRNA-seq of mammary epithelial cells in the previous study, where the major cell population detected at lactation is basal cells, the proportion of luminal cells at lactation greatly increased in the snRNA-seq dataset (Bach et al., 2017). One possible reason for these differences is that luminal cells differentiate into lipid-containing alveolar cells at lactation, which share similar characteristics with adipocytes, making them difficult to isolate for single-

cell analysis. Since lipid-containing alveolar cells are less likely to be captured through scRNA-seq, the reference matrix of luminal cells based on scRNA-seq is inaccurate, which lead to a deviated imputation of the luminal fraction. In addition, the snRNA-seq dataset includes transcriptome data of non-epithelial cells such as adipocytes, stromal cells, immune cells and endothelial cells, which are hardly detected in scRNA-seq where cells are screened by EpCAM levels. Although the fractions of stromal cells, immune cells and endothelial cells imputed based on scRNA-seq data were not significantly different from those imputed based on snRNA-seq data, the adipocytes fraction was lost in the cell fraction imputed based on scRNA-seq. Therefore, by enabling accurate imputations of adipocyte and luminal fractions, snRNA-seq of mammary tissues provide a reliable reference for deconvolution analysis of bulk RNA sequencing data.

Despite the advantages, one of the major challenges for snRNA-seq is the contamination of ambient RNA from broken cytoplasm during nuclei extraction. The effects of contamination were minimized during analysis by detecting and correcting the highly contaminating genes using scCDC (W. Wang et al., 2024). Another limitation of snRNA-seq is that it primarily detects nuclear RNAs, leading to the loss of cytoplasmic transcripts and lower gene detection sensitivity. Due to the lower RNA levels in nuclei compared to whole cells, the snRNA-seq data exhibited reduced gene detection sensitivity in certain cell types. For example, compared to the scRNA-seq data, snRNA-seq data demonstrated lower gene detection sensitivity in luminal cells ([Figure 3.6](#)). This limitation might result in failure to detect some biologically significant genes. Consequently, although snRNA-seq successfully captures lipid-containing luminal cells, its lower detection sensitivity might lead to omission of certain lipid metabolism-related genes, potentially resulting in incomplete profiling of lipid metabolic pathways in luminal cells. In addition, the expression levels of RNA transcripts detected in snRNA-seq may slightly differ from those detected in scRNA-seq. Therefore, DEGs for each

Deleted: Figure 3.6

cell type were re-identified based on snRNA-seq in this study and their specificity is supported by previous research.

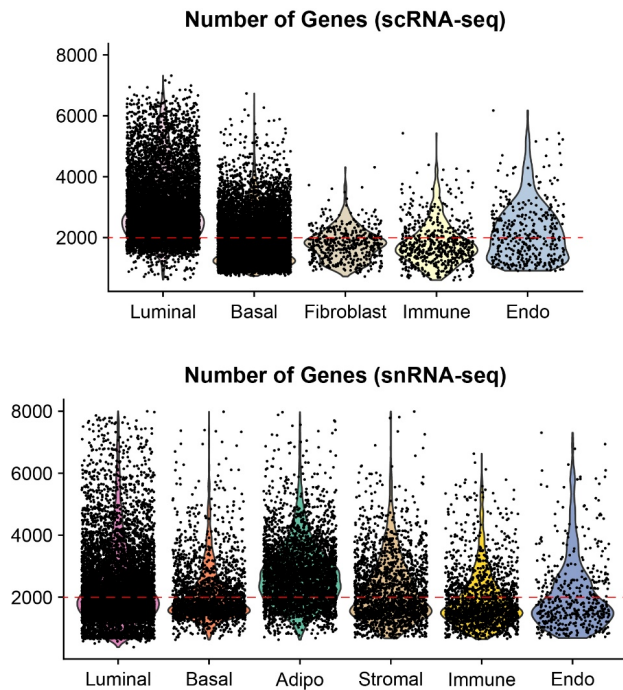


Figure 3.6 The number of detected genes per cell in snRNA-seq versus scRNA-seq data.

Luminal, luminal cells; Basal, basal cells; Adipo, adipocytes; Stromal, stromal cells; Immune, immune cells; Endo, endothelial cells.

General cell types and correlated DEGs were identified in this chapter. To understand the heterogeneity of each cell population and potential regulators involved in cell fate transitions, cell clusters require further division. Pseudotime analysis and regulatory network inference were performed to infer the changes in cell fates during mammary gland development and the potential regulators involved in these processes.

Chapter 4

Identification of Potential Transcription Factors in Mammary Epithelial Cell Fate Determination

4.1 Introduction

Transcriptome profiles of cells in the mammary tissue help identify potential transcription factors that drive the differentiation of mammary epithelial cells. It is found that mammary epithelial cells could be generated from PDGFR α^+ stromal adipocyte progenitors (Joshi et al., 2019). The stromal-epithelial transition occurs during both early development and pregnancy (Joshi et al., 2019). Although it is figured out that the stromal-epithelial transition could be driven by PDGFC derived from mammary epithelial cells, transcriptional changes within the stromal cells are not identified. As mammary epithelial cells expand rapidly during mid-pregnancy and luminal cells derived from PDGFR α^+ stromal cells were detected at mid-pregnancy, a population of stromal cells at the intermediate state of transition is likely to be detected at mid-pregnancy. In addition to stromal adipocyte progenitors, progenitors of mammary epithelial cells also undergo differentiation during pregnancy. Luminal progenitors differentiate into milk-producing alveolar cells during pregnancy and lactation. The mechanisms of alveolar cell specification are illustrated by previous research. However, these studies pay little attention on the regulation of lipid formation in differentiated luminal cells. In addition, as lipid-containing luminal cells are hardly captured in scRNA-seq studies, the transcriptome profiles of these cells remain unclear.

This section focuses on identifying the potential transcription factors that drive the stromal-epithelial transition and lipid-containing luminal cell specification. The

trajectories of stromal-epithelial transition and luminal differentiation were inferred by monocle and diffusion map, respectively. Potential transcription factors are identified by SCENIC and validated by in vitro models.

4.2 Bi-Directional Differentiation of Stromal Cells

4.2.1 A Stromal Cell Population with Mammary Epithelial Characteristics

To figure out the population of stromal cells that have the ability to transit into epithelial cells, the stromal cells were further divided into four clusters as described in section 2.11.2 ([Figure 4.1A](#)). The proportion of sub-divided clusters in each developmental stage was computed to identify the populations that increased during pregnancy. Furthermore, the correlation between stromal clusters and other cell types as well as the expression of epithelial markers in stromal clusters were used to predict the stromal population undergoing stromal-epithelial transition.

Deleted: Figure 4.1

The abundance of stromal_C3 increased at P13.5 and L5 ([Figure 4.1B](#)). Compared to the other three clusters, the molecular features of stromal_C3 were more similar to luminal and basal cells, supported by the higher expression of epithelial markers *Epcam*, *Erbb4*, *Kit*, *Acta2*, *Myh11* and *Nrg1* ([Figure 4.1C, D](#)). Compared to stromal_C3 and stromal_C4, stromal_C1 and stromal_C2 showed higher expression of stromal markers, even though expression levels of *Lama2*, *Fap* and *Col3a1* were higher in stromal_C2 while the expression level of *Fbn1* was higher in stromal_C1 ([Figure 4.1D](#)). In addition, a large proportion of cells in stromal_C2 highly expressed *Pdgfra*, which marks mesenchymal progenitors in the stromal population that transits into mammary epithelial cells during pregnancy (Joshi et al., 2019) ([Figure 4.1D](#)). Cells in stromal_C4 were possibly in the intermediate state of adipocyte differentiation as they expressed low levels of stromal cell markers (*Lama2*, *Fbn1*, *Fap* and *Col3a1*) and high levels of adipocyte markers (*Adipoq* and *Pparg*) ([Figure 4.1D](#)).

Deleted: Figure 4.1

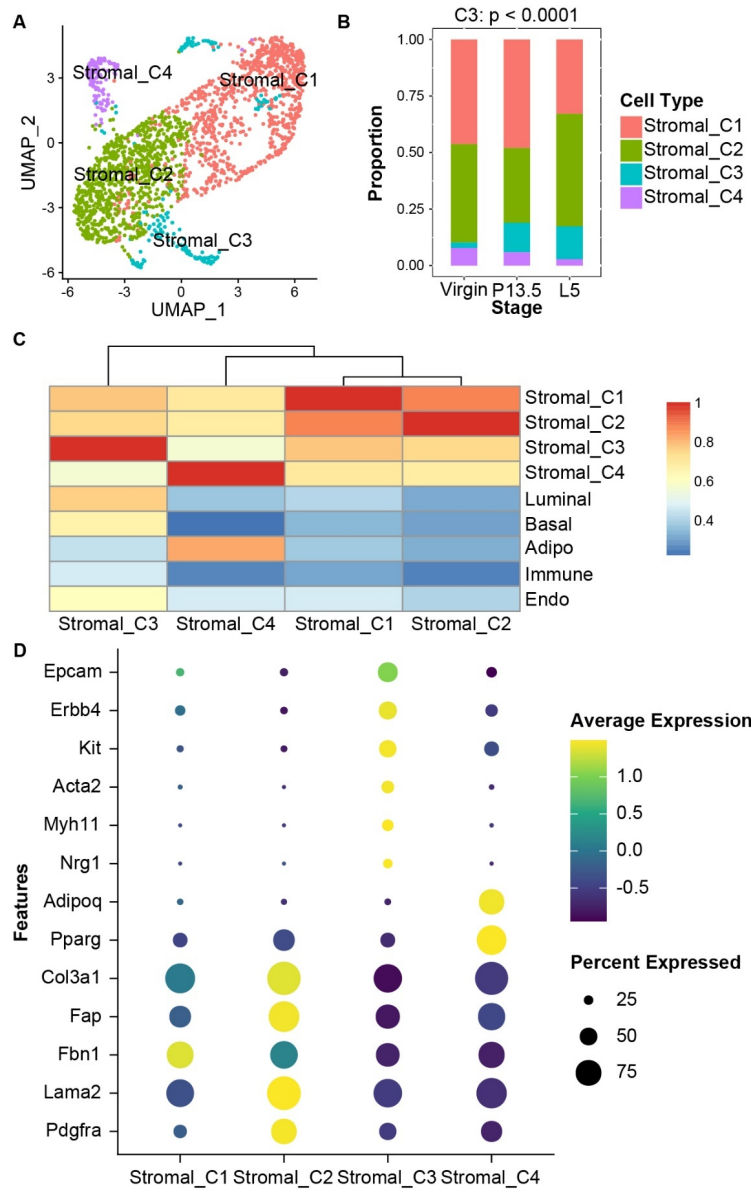


Figure 4.1 Identification of a stromal subpopulation with epithelial features.

A. UMAP plot of stromal cell clusters. B. Proportion of each cluster of stromal cells. The p-value is calculated by the Wilcoxon rank sum test. C. Correlation between stromal cells and other types of cells. D. Expression of epithelial, stromal and adipocyte markers in stromal cell clusters. Luminal, luminal cells; Basal, basal cells;

Adipo, adipocytes; Stromal, stromal cells; Immune, immune cells; Endo, endothelial cells; P13.5; pregnancy day 13.5; L5, lactation day 5.

4.2.2 Potential Transcription Factors Controlling Stromal Cell Differentiation

To investigate the trajectory of stromal-epithelial transition and stromal-adipocyte differentiation, time-series analyses were performed on stromal cells, luminal cells, basal cells and adipocytes by monocle ([Figure 4.2A-C](#)). Most cells in stromal_C1 showed low expression of *Pdgfra*, indicating that stromal_C1 might belong to another differentiation branch. Therefore, this cluster was excluded in the following time-series analyses. In addition, as cells in stromal_C3 had more similar expression patterns to mammary epithelial cells while cells in stromal_C4 obtained molecular features more similar to adipocytes, stromal_C3 was included in the trajectory analysis of stromal and mammary epithelial cells and stromal_C4 was included in the analysis of stromal cells and adipocytes. Stromal_C3 served as an intermediated state between stromal_C2 and mammary epithelial cells ([Figure 4.2A, B](#)). This supported the assumption that stromal_C3 represents stromal cells that are able to transit into epithelial cells under hormonal control during pregnancy. Similarly, stromal_C4 was in the intermediate stages between stromal_C2 and adipocytes, suggesting that cells in stromal_C4 are precursors of adipocytes.

Transcription factors are responsible for the determination of cell fate. To identify transcription factors involved in the transition from stromal cells to mammary epithelial cells, the activities of transcription factors and their downstream targets for each stromal cluster are calculated by SCENIC. Through analysing the expression matrix of stromal cells from mammary tissue at P13.5, regulons with high activity in stromal_C2, stromal_C3 and stromal_C4 were identified. High activities of Egr1, Etv1 and Zeb1 regulons were found in stromal_C2 ([Figure 4.2D](#)). These transcription factors are involved in regulating different functions of stromal cells. EGR1 is important to restore the stemness of adipose-derived stromal cells

Deleted: Figure 4.2

Formatted: Default Paragraph Font

Formatted: Default Paragraph Font

Deleted: Figure 4.2

Deleted: Figure 4.2

Formatted: Default Paragraph Font

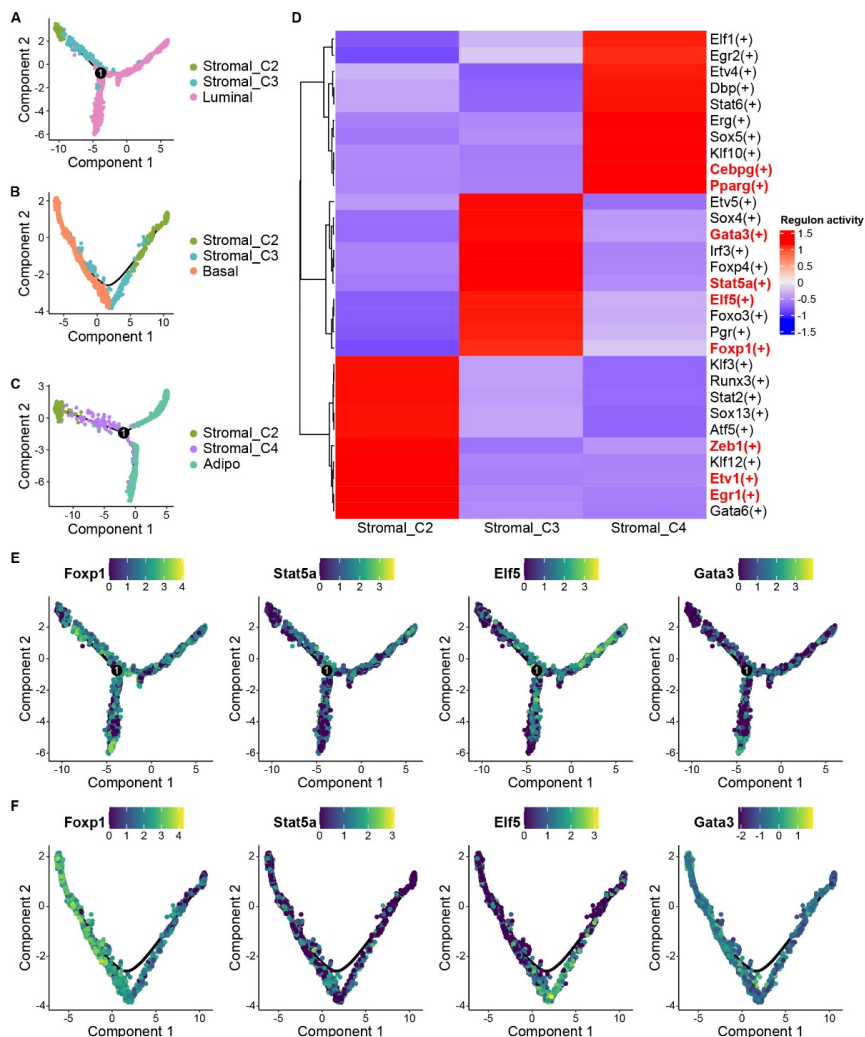


Figure 4.2 Potential transcription factors involved in stromal-epithelial transition.

A-C. Pseudotime trajectory of (A) stromal cells and luminal cells, (B) stromal cells and basal cells, (C) stromal cells and adipocytes. D. Heatmap of regulon activity in stromal clusters C2, C3 and C4 at pregnancy day 13.5. E-F. Expression of *Foxp1*, *Stat5a*, *Elf5* and *Gata3* in stromal clusters C2, C3 and (E) luminal cells or (F) basal cells. Luminal, luminal cells; Basal, basal cells; Adipo, adipocytes; Stromal, stromal cells.

(C. Wang et al., 2024). ETV1 mediates the expansion of stromal cells and promotes tumour metastasis through inducing epithelial-mesenchymal transition (Heeg et al., 2016). ZEB1 expressed in stromal fibroblasts promotes the formation of mammary epithelial tumours (R. Fu et al., 2019). High activities of Pparg and Cebpg regulons were detected in stromal_C4 (Figure 4.2D). PPARy and C/EBP-gamma are involved in adipogenic differentiation (Ou-yang & Dai, 2023). Foxp1, Elf5, Stat5a and Gata3 regulons showed high activity in stromal_C3 (Figure 4.2D). ELF5, STAT5A and GATA3 are proved to regulate luminal specification (Kouros-Mehr et al., 2006; H. J. Lee et al., 2011; Yamaji et al., 2009). FOXP1 maintains the repopulating activity of MaSCs, which is crucial for mammary gland development (N. Y. Fu et al., 2018). Loss of FOXP1 in mammary epithelial cells severely impairs both ductal elongation and lobuloalveolar development of the mammary gland (N. Y. Fu et al., 2018). Compared to *Elf5*, *Stat5a* and *Gata3*, *Foxp1* expressed throughout the transition trajectory from stromal cells to luminal and basal cells (Figure 4.2E, F). Expression levels of *Elf5*, *Stat5a* and *Gata3* were much lower in basal cells than in luminal cells, as transcription factors encoded by these genes are mainly involved in specification of luminal lineage. Since FOXP1 is indispensable for the maintenance of MaSCs, which give rise to both the basal population and luminal population, it can be inferred that high expression of *Foxp1* in stromal cells could drive their transition into epithelial cells. Further exploration of the role of *Foxp1* in stromal-epithelial transition was performed.

Deleted: Figure 4.2

Formatted: Default Paragraph Font

Deleted: Figure 4.2

Formatted: Default Paragraph Font

Deleted: Figure 4.2

Formatted: Default Paragraph Font

4.2.3 Effects of FOXP1 Overexpression on Stromal Cell Specification

To investigate the function of FOXP1 on stromal-epithelial transition, FOXP1 was overexpressed in stromal cells isolated from the SVFs of the mammary tissue from 8-week-old female mice. In undifferentiated stromal cells, *Foxp1* expression increased over 2-fold in the overexpression (FOXP1 OE) group, but the differences between the control and FOXP1 OE group were not significant (Figure 4.3A). After

Deleted: Figure 4.3

Formatted: Check spelling and grammar

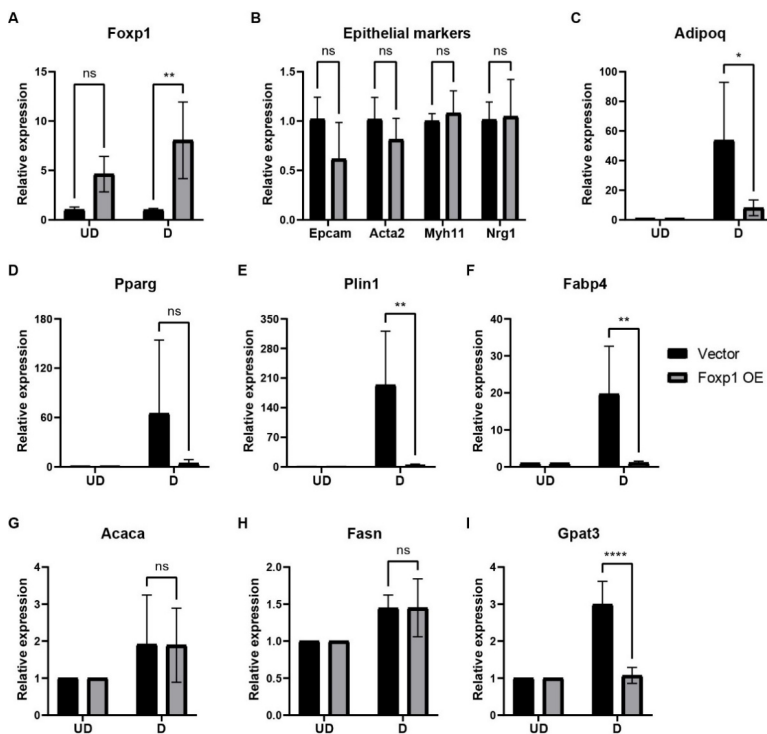


Figure 4.3 Overexpression of FOXP1 suppressed adipogenesis of stromal cells.

A. Efficiency of FOXP1 overexpression. B. Expression of mammary epithelial markers in undifferentiated stromal cells. C-I. Expression of adipogenesis-related markers in stromal cells before and after differentiation. UD, undifferentiated; D, differentiated. n = 4. *P < 0.05, **P < 0.01, ****P < 0.0001. ns, not significant. p values were calculated by two-way ANOVA with post hoc Bonferroni's multiple comparisons test.

inducing adipogenesis, *Foxp1* expression in the FOXP1 OE group was significantly higher than the control group (Figure 4.3A). This situation might result from the downregulation of endogenous FOXP1 after differentiation, which accentuates the functional impact of FOXP1 overexpression. In undifferentiated stromal cells, expression levels of epithelial-related biomarkers had insignificant differences between the FOXP1 OE group and the control group, indicating that

Deleted: Figure 4.3

Formatted: Check spelling and grammar

overexpressing merely FOXP1 in stromal cells was not enough to promote the stromal-epithelial transition.

Another major differentiation direction of stromal cells is adipogenesis. To explore whether overexpression of FOXP1 affects adipocyte differentiation from stromal cells, primary stromal cells were induced adipogenesis *in vitro*. Although overexpressing *Foxp1* had no dominant effect on stromal-epithelial transition, FOXP1 overexpression in stromal cells strongly suppressed adipogenesis and lipid metabolism (Figure 4.3C-I). Expression levels of *Adipoq*, *Plin1*, *Fabp4* and *Gpat3* were significantly lower in the differentiated stromal cells from the FOXP1 OE group than the control group (Figure 4.3C, E, F and I). Adiponectin encoded by *Adipoq* is a signature for mature adipocytes. *Gpat3* encodes an enzyme involved in triglyceride synthesis (Shan et al., 2010). *Fabp4* encodes a fatty acid binding protein and *Plin1* encodes a lipid binding protein, which is essential for lipid metabolism in adipocytes (Queipo-Ortuño et al., 2012; Tansey et al., 2001). Expression levels of *Acaca* and *Fasn*, which encode enzymes involved in the fatty acid synthesis, were slightly upregulated after differentiation and showed insignificant differences between the FOXP1 OE group and control group (Figure 4.3G, H). In summary, FOXP1 overexpression suppressed the adipogenic direction of stromal cells.

Deleted: Figure 4.3

Formatted: Check spelling and grammar

Deleted: Figure 4.3

Formatted: Check spelling and grammar

Deleted: Figure 4.3

Formatted: Check spelling and grammar

4.3 STAT5 Phosphorylation Regulates Alveolar Cells Lipogenesis

4.3.1 Identification of Alveolar Cell in Single-Nucleus Sequencing Data

To identify the lipid-containing luminal cells, the luminal clusters were further divided into 5 clusters (Figure 4.4A). Specific cell types were identified based on the expression of canonical markers (Figure 4.4B). Gene Ontology (GO) analysis was performed using biomarkers identified in several clusters, which helped further confirm their cell types (Figure 4.4D, E and Figure 4.5A). The cluster widely expressed relatively high levels of genes encoding milk proteins (*Csn2* and *Csn3*)

Deleted: Figure 4.4

Formatted: Default Paragraph Font

Deleted: Figure 4.4

Formatted: Default Paragraph Font

Deleted: Figure 4.4

Deleted: Figure 4.5

Formatted: Default Paragraph Font

Formatted: Default Paragraph Font

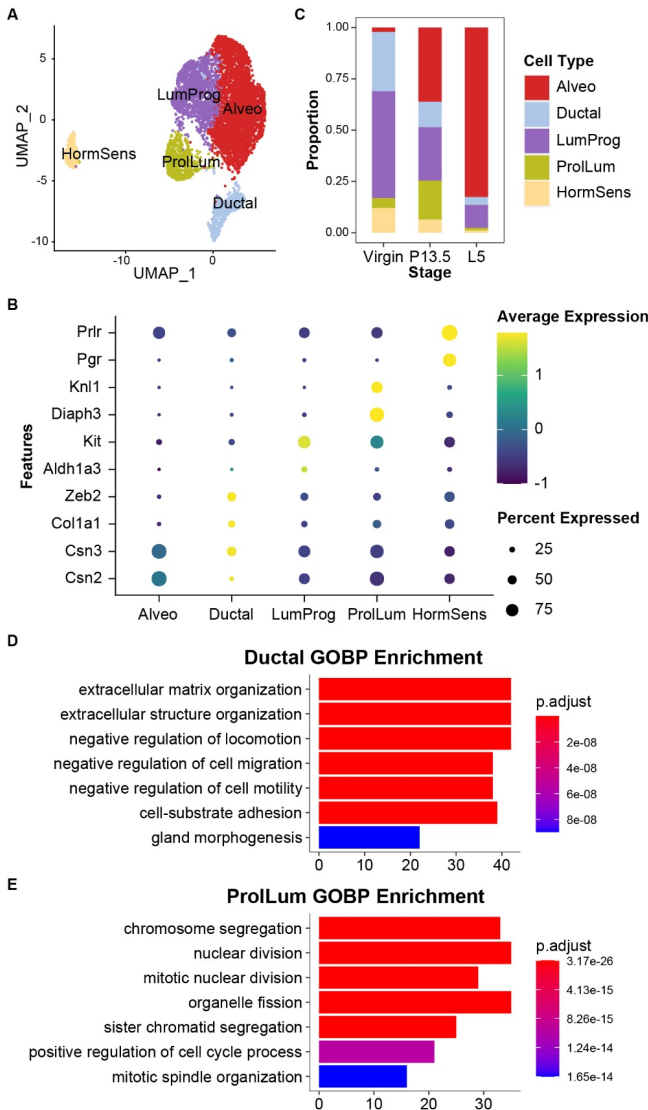


Figure 4.4 Identification of lipid-containing alveolar cells in luminal clusters.

A. UMAP plot of subdivided luminal cells. Cells were coloured by clusters. B. Expression of canonical markers in luminal clusters. C. Proportion of each type of luminal cell at different stages. D-E. GO analysis of (D) ductal cells and (E) proliferating luminal cells. Alveo, alveolar cells; Ductal, ductal cells; LumProg, luminal progenitor; ProlLum, proliferating luminal cell; HormSens, hormone sensing cells; P13.5; pregnancy day 13.5; L5, lactation day 5.

was identified as alveolar cells. The cluster expressing relatively high levels of *Aldh1a3* and *Kit* was identified as luminal progenitors. The cluster with high expression of *Col1a1* and *Zeb2*, which are biomarkers of stromal cells, was defined as ductal cells (Figure 4.4B, D) (Chua et al., 2007; C. M.-C. Li et al., 2020). This cluster of luminal cells might originate from stromal cells during mammary development at early age (Joshi et al., 2019). The cluster with high expression levels of *Diaph3* and *Knl1* was defined as proliferating luminal cells, as biomarkers of this cluster are closely related to cell division (Figure 4.4B, E) (Damiani et al., 2016; DeWard & Alberts, 2009; Shepperd et al., 2012; Yamagishi et al., 2012). The cluster with dominant expression of *Prlr* and *Pgr* was identified as hormone sensing cells. The abundance of each type of luminal cells at different stages was computed (Figure 4.4C). The proportion of alveolar cells increased during pregnancy and lactation, finally accounting for about 80% of the total luminal cell population at L5. By contrast, the proportion of luminal progenitor decreased from 50% at virgin to 10% at L5, indicating that luminal progenitors differentiated into alveolar cells during this process. In addition, the proportion of proliferating luminal cells increased to about 20% at P13.5, suggesting that luminal cells rapidly expand during pregnancy.

GO analysis of biomarkers identified in the alveolar cluster demonstrated that biological processes related to lipid synthesis and metabolism were enriched in alveolar cells (Figure 4.5A). Furthermore, alveolar cells expressed genes encoding proteins involved in lipid synthesis in the mammary epithelium, including *Ppard*, *Acaca*, *Fasn*, *Olah*, *Fabp3*, *Gpat4* and *Plin2* (Figure 4.5B-H). *Ppard* encoding peroxisome proliferator-activated receptor delta and *Fabp3* encoding fatty acid binding protein 3 are involved in regulating lipid formation in mammary epithelial cells from goat (H. B. Shi et al., 2017; Y. Sun et al., 2016). *Olah* encodes oleoyl-ACP hydrolase, which is responsible for the synthesis of medium-chain fatty acid in the mammary gland (Smith, 1980). In addition, *Acaca* and *Fasn*, which encode

Deleted: Figure 4.4

Formatted: Default Paragraph Font

Deleted: Figure 4.4

Formatted: Default Paragraph Font

Deleted: Figure 4.4

Formatted: Default Paragraph Font

Deleted: Figure 4.5

Formatted: Default Paragraph Font

Deleted: Figure 4.5

Formatted: Default Paragraph Font

enzymes regulating fatty acid synthesis in adipocytes, also showed dominant expression in alveolar clusters (Figure 4.5C, D) (Suburu et al., 2014). *Gpat4* encodes *sn*-Glycerol-3-phosphate acyltransferase, which is crucial for the production of milk fats in mice (Beigneux et al., 2006). *Plin2* encodes perilipin-2, a lipid binding protein that is expressed in murine mammary alveoli and facilitates lipid secretion (Monks et al., 2022; Russell et al., 2011). In summary, cells in the alveolar cluster were lipid-containing luminal cells.

Deleted: Figure 4.5

Formatted: Default Paragraph Font

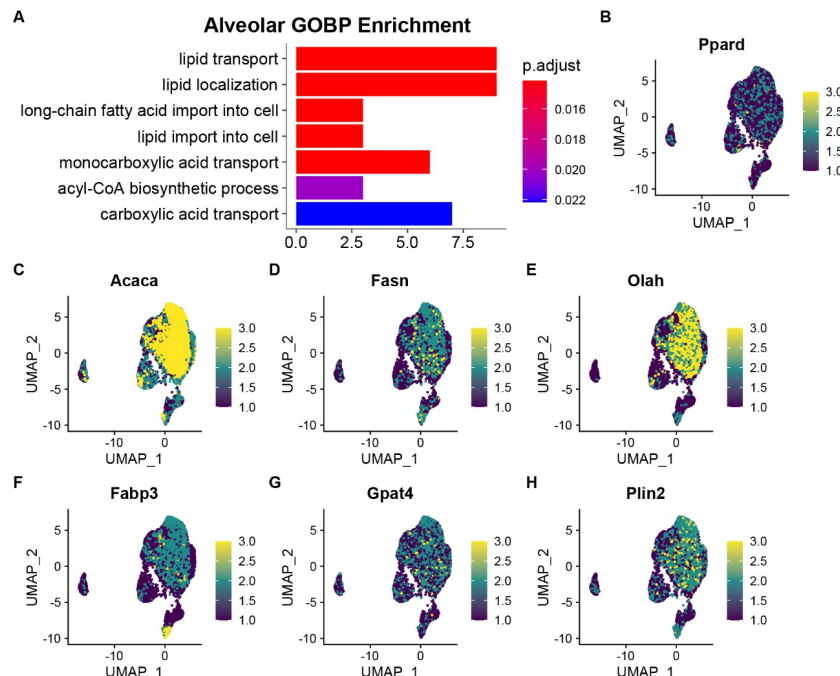


Figure 4.5 Identification of alveolar-specific lipogenesis genes.

A. GO analysis of alveolar cells. B-H. Expression of alveolar-specific lipogenesis-related genes in luminal clusters.

4.3.2 Potential Transcription Factors Directing Lipid Production in Alveolar Cells

To identify the transcription factors involved in the specification of alveolar cells,

time-series analysis and gene-regulatory network analysis were performed on luminal clusters. Since ductal cells and hormone sensing cells are possibly involved in distinct differentiation pathways, only luminal progenitors, proliferating luminal cells and alveolar cells were included in these analyses. From the diffusion map of luminal cells, it can be inferred that luminal progenitors differentiate into alveolar cells (Figure 4.6A). Proliferating luminal cells could be the intermediate state of luminal differentiation (Figure 4.6A). Proliferating luminal cells with high expression of mitosis-related genes were enriched in pregnancy, suggesting that proliferating luminal cells are mitotic luminal progenitors which differentiate into alveolar cells after mitosis (Figure 4.4E).

Deleted: Figure 4.6

Deleted: Figure 4.6

Deleted: Figure 4.4

Formatted: Font: Not Bold

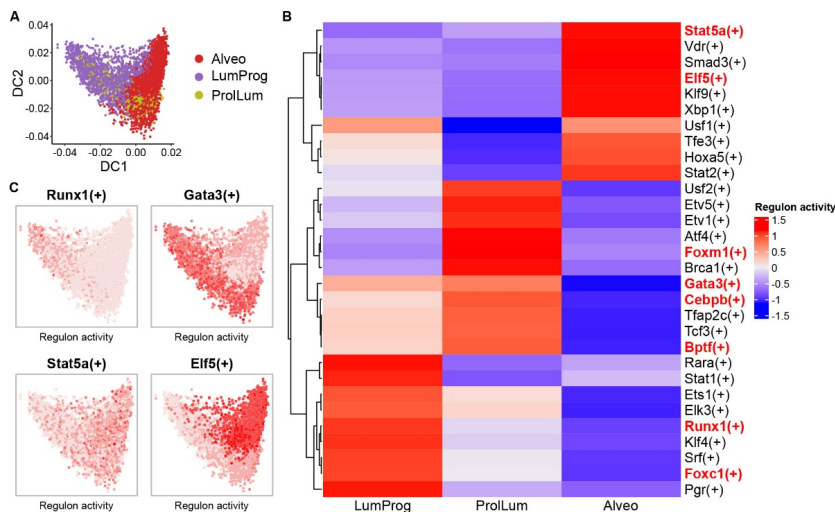


Figure 4.6 Potential transcription factors promoting differentiation and lipid production of alveolar cells.

A. Diffusion map of luminal cells from virgin, P13.5 and L5. Alveo, alveolar cells; LumProg, luminal progenitor; ProlLum, proliferating luminal cell. B. Heatmap of regulon activity in three luminal progenitors, proliferating luminal cells and alveolar cells. C. Diffusion map of luminal cells coloured by regulon activity.

Regulons with high activity in luminal progenitors, proliferating luminal cells and alveolar cells were identified by SCENIC (Figure 4.6B). Foxc1 and Runx1 regulons

Deleted: Figure 4.6

were enriched in luminal progenitors and Bptf, Cebpb and Foxm1 regulons were enriched in proliferating luminal cells (Figure 4.6B, C). FOXC1 and FOXM1 are found enriched in luminal progenitors (Carr et al., 2012; Sizemore et al., 2013). Overexpression of FOXC1 and FOXM1 promotes the expansion of luminal progenitors and inhibits luminal differentiation (Carr et al., 2012; Gao et al., 2017). RUNX1, BPTF and C/EBP-beta function as regulators to maintain stem cell properties and proliferation of mammary epithelial cells (Frey et al., 2017; LaMarca et al., 2010; Matsuo et al., 2022). Loss of BPTF suppresses the specification of luminal cell fate (Frey et al., 2017). Deletion of C/EBP-beta in mammary epithelial cells results in the reduction of luminal progenitors and the increase of differentiated luminal cells (LaMarca et al., 2010). Gata3 regulon was enriched in both luminal progenitors and proliferating luminal cells, aligning with its role in maintaining the luminal lineages reported in previous studies (Figure 4.6B, C) (Asselin-Labat et al., 2007; Kouros-Mehr et al., 2006). Stat5a and Elf5 regulons were specifically enriched in alveolar cells, consistent with their importance in alveolar specification reported in previous studies (Figure 4.6B, C) (Liu et al., 1997; Oakes et al., 2008; Yamaji et al., 2013). Although the functions of STAT5A and ELF5 in alveolar specification are well-investigated, their potential roles in regulating lipid synthesis within these cells have received less attention. Nevertheless, emerging evidence suggests that STAT5 plays a role in regulating lipid synthesis in mammary epithelial cells. For instance, in bovine mammary epithelial cells, STAT5 interacts with promoter III to regulate the expression of *Acaca*, a key gene encoding an enzyme involved in fatty acid synthesis (Mao et al., 2002). Moreover, IL-1 β has been shown to suppress lipid production in mammary epithelial cells by inactivating STAT5, further implicating its involvement in alveolar lipogenesis (Matsunaga et al., 2018). Therefore, this study primarily focused on validating the role of STAT5 in regulating lipid synthesis in mammary epithelial cells.

Deleted: Figure 4.6

Deleted: Figure 4.6

Deleted: Figure 4.6

4.3.3 Effects of Inhibiting STAT5 Phosphorylation on *In Vitro* Mammary Organoid Lipogenesis

To validate the function of STAT5 in the alveolar lipogenesis, lipid formation in mammary epithelial cells was induced *in vitro* with administration of a STAT5 phosphorylation inhibitor, STAT5-IN-1, which significantly reduced STAT5 activity by inhibiting STAT5 phosphorylation within mammary epithelial cells ([Figure 4.7](#)).

Deleted: Figure 4.7

Formatted: Default Paragraph Font

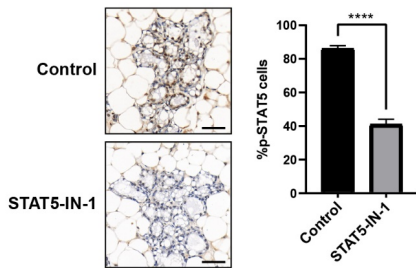


Figure 4.7 Efficiency of STAT5 phosphorylation inhibitor STAT5-IN-1.

IHC staining of phosphorylated STAT5 in mammary tissues from mice at pregnancy day 18.5. Mice in the STAT5-IN-1 group received STAT5 phosphorylation inhibitor (11 μ g/g) at pregnancy day 12.5, 14.5, 15.5, 16.5 and 17.5 through intraperitoneal injection while the control group received PBS. Scale bar = 50 μ m. ***P < 0.0001. The p-value was calculated by t-test. (Data provided by Teng Wang)

Mammary organoids were isolated from female mice at mid-pregnancy. Lipogenesis was induced *in vitro* with prolactin and hydrocortisone, the same condition as inducing lactation *in vitro* (Sumbal et al., 2020). The lipid synthesis in mammary organoids was detected by BODIPY, a green fluorescent dye for neutral lipid staining. After induction with prolactin and hydrocortisone, lipid droplets were detected in the organoids ([Figure 4.8A](#)). The effect of STAT5 phosphorylation inhibitor was validated by the significant reduction of *Wap* expression, which is a downstream target of STAT5 (Shin et al., 2016). Lipid formation in mammary organoids was suppressed by the administration of STAT5-IN-1 ([Figure 4.8A](#)). The BODIPY intensity in organoids treated with STAT5-IN-1 was much lower than that

Deleted: Figure 4.8

Formatted: Check spelling and grammar

Deleted: Figure 4.8

Formatted: Check spelling and grammar

in the control group. Furthermore, the expression of lipogenesis-related genes was significantly reduced with the administration of STAT5-IN-1 (Figure 4.8C-I). These results suggest that STAT5 plays a crucial role in lipogenesis in alveolar cells.

Deleted: Figure 4.8

Formatted: Check spelling and grammar

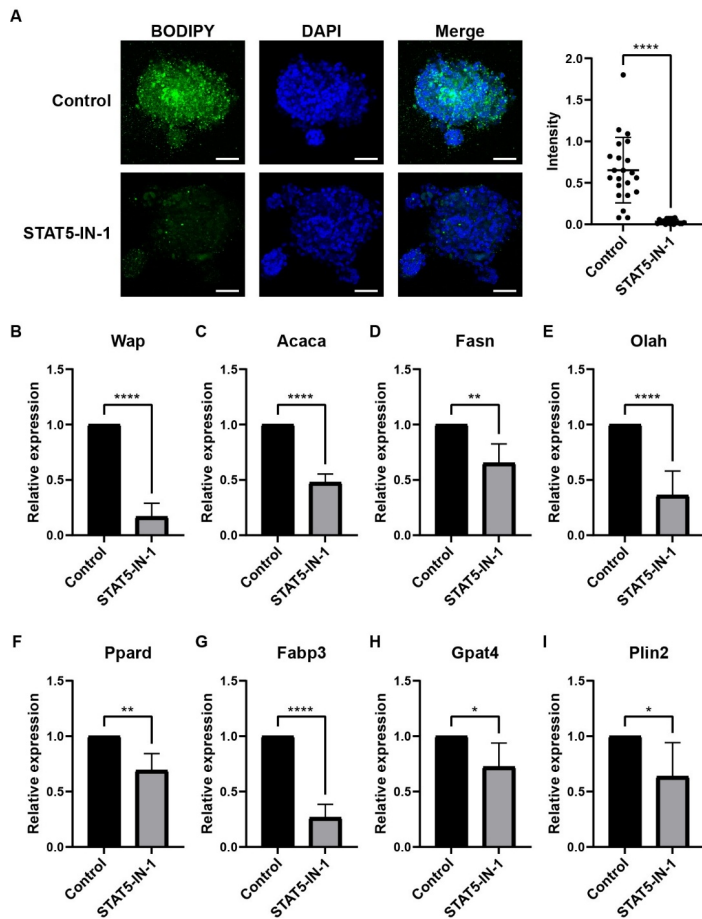


Figure 4.8 Inhibiting STAT5 phosphorylation suppressed lipid production in mammary organoids.

A. BODIPY staining of neutral lipids in mammary organoids. Control, n = 22; STAT5-IN-1, n = 19. Scale bar = 50 μ m. B-I. Expression of milk protein genes and lipogenesis-related genes in mammary organoids. *P < 0.05, **P < 0.01, ***P < 0.001, ****P < 0.0001. p-values were calculated by the two-tailed unpaired t-test.

4.4 Discussion

This chapter investigated transcription regulators that participate in mammary epithelial specification during pregnancy and lactation. A stromal population abundant at mid-pregnancy shared similar transcriptional characteristics with mammary epithelial cells. As previous study reveals that PDGFR α^+ stromal cells are more likely to give rise to luminal cells during pregnancy, molecular features of stromal_C3 were more similar to luminal cells than basal cells (Figure 4.1C, D) (Joshi et al., 2019). Nevertheless, some cells in stromal_C3 still show high expression of basal markers such as *Acta2*, *Myh11* and *Nrg1* (Figure 4.1D). By analysing the expression levels of transcription factors and their downstream targets in stromal cells, transcription factor FOXP1 and its target genes show high activity in the stromal population with epithelial properties. In addition, *Foxp1* expresses throughout the transition from PDGFR α^+ stromal cells to mammary epithelial cells, including basal and luminal cells. Overexpressing *Foxp1* in primary stromal cells isolated from mammary tissue only suppress adipogenesis of stromal cells but failed to induce the epithelial properties in stromal cells. Although previous study reveals that FOXP1 is necessary for MaSCs to exit from quiescence, FOXP1 may not direct further differentiation into basal and luminal cells (N. Y. Fu et al., 2018).

Deleted: Figure 4.1

Deleted: Figure 4.1

The major change in mammary epithelium during pregnancy and lactation is the specification of milk-secreting alveolar cells. Alveolar cells responsible for synthesis of milk proteins and lipids was identified from the luminal clusters. In addition to genes encoding milk proteins, alveolar cells demonstrate high expression levels of genes involved in lipid synthesis and lipid transport. Consistency with previous studies, transcription factors STAT5A and ELF5 were enriched in alveolar cells. Inhibiting STAT5 phosphorylation in primary mammary organoids isolated from mid-pregnant mice suppresses lipid formation, indicating that STAT5 also regulates expression of alveolar-specific lipogenic genes.

Transcription factors usually serve as downstream regulators of signalling pathways, indicating that intercellular signalling also plays important roles in cell fate determination. To investigate the effects of intercellular signalling on cell fate determination, cell-cell communications within the mammary tissue across different developmental stages were analysed.

Chapter 5

Identification of Potential Cell-Cell Communication Signals in Mammary Tissue

5.1 Introduction

Activation of transcription factors could be mediated by upstream signalling pathways, indicating the importance of paracrine signalling through cell-cell communications. Previous research demonstrates that mammary adipocytes undergo dedifferentiation during lactation, transitioning from lipid-rich white adipocytes to a regressed state characterised by reduced or even loss of lipid deposition (Q. A. Wang et al., 2018). However, the underlying mechanisms of adipocyte dedifferentiation during lactation remain unclear. Adipocyte dedifferentiation can be driven by signalling pathways or mechanical stress, which might be exerted by expanding and differentiating mammary epithelial cells. Therefore, elucidating their crosstalk during lactation is critical to deciphering the mechanisms of adipocyte dedifferentiation. On the other hand, although signalling pathways inducing alveolar specification are well-studied, the roles of adipocytes in the process are not fully understood. As the necessity of adipocytes in mammary gland development during puberty is proved, it is possible that adipocytes induce alveolar specification through paracrine signalling (Brenot et al., 2020).

This section aims to identify the intercellular signalling pathways between adipocytes and mammary epithelial cells which determine their cell fate at different developmental stages. Cell-cell communications between adipocytes and mammary epithelial cells were calculated according to the expression of ligands and receptors in these cells. Subsequently, the functions of identified signalling

molecules were validated by *in vitro* or *in vivo* experiments.

5.2 Effects of Alveolar Cell-Produced Interleukin-15 on Adipocyte Dedifferentiation During Lactation

5.2.1 Crosstalk Between Mammary Epithelial Cells and Adipocytes at Lactation

To determine whether mammary epithelial cells regulate adipocyte dedifferentiation through intercellular signalling, upregulated signalling pathways between mammary epithelial cells and adipocytes at lactation were identified ([Figure 5.1A](#),

B). Luminal progenitors, proliferating luminal cells, alveolar cells and basal cells served as senders and adipocytes served as the receiver of the signalling pathways. Compared to virgin and P13.5, the communication probability of FGF, CCL and VISFATIN signalling pathways were upregulated at lactation ([Figure 5.1A](#),

B). The ligand-receptor pairs involved in these signalling pathways and their expression levels in epithelial cells and adipocytes at different developmental stages were illustrated ([Figure 5.1C, D](#)). In the FGF signalling pathway, FGF1 was

the ligand secreted by basal cells, and FGFR1 and FGFR2 were receptors expressed by adipocytes ([Figure 5.1C](#)). In the CCL signalling pathway, CCL25 was

the ligand secreted by luminal progenitors, proliferating luminal cells and alveolar cells, and ACKR4 was the receptor on adipocytes ([Figure 5.1C](#)). In the VISFATIN signalling pathway, NAMPT was the ligand secreted by luminal progenitors and alveolar cells, and INSR was the receptor expressed on adipocytes ([Figure 5.1C](#)).

Although the communication probability of the CCL signalling pathway upregulated in L5 when compared to P13.5, the strength of CCL25-ACKR4 interaction between luminal cells and adipocytes was still weak at L5 ([Figure 5.1B, C](#)). Even though the expression level of *Nampt* rose in alveolar cells at lactation, *Nampt* was also expressed by adipocytes in virgin mammary tissue ([Figure 5.1D](#)). In addition, the NAMPT expression level in adipocytes increased during adipogenesis, suggesting

Deleted: Figure 5.1

Formatted: Default Paragraph Font

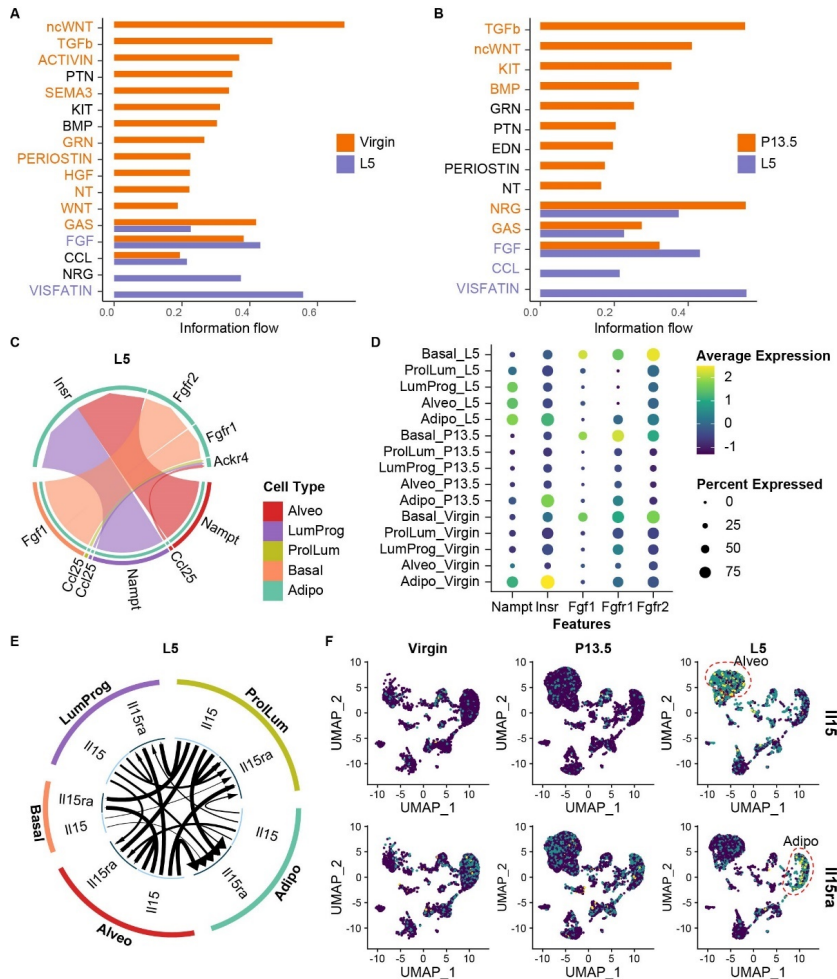


Figure 5.1 Potential epithelial-derived signals inducing dedifferentiation of adipocytes during lactation.

A-B. Comparisons of signalling pathways between mammary epithelial cells and adipocytes enriched at (A) virgin and (B) P13.5 versus L5. C. Ligand-receptor interactions between mammary epithelial cells and adipocytes at L5. D. Expression of Nampt, Insr, Fgf1, Fgfr1 and Fgfr2 in mammary epithelial cells and adipocytes at different stages. E. Ligand-receptor interactions between mammary epithelial cells and adipocytes at L5. F. Expression levels of *II15* and *II15ra* in cells in mammary tissue at different stages. Alveo, alveolar cells; LumProg, luminal progenitor; ProlLum, proliferating luminal cell; Basal, basal cells; Adipo, adipocytes.

that NAMPT contributes to adipocyte differentiation rather than inducing dedifferentiation (Mitani et al., 2020; Park et al., 2024). *Fgf1* was specifically expressed in basal cells and the expression levels increased at lactation (Figure 5.1D). However, expression levels of *Fgfr1* and *Fgfr2* were low in adipocytes and FGF1-FGFR1 is reported as an inducer of adipogenesis (Figure 5.1D) (S. Wang et al., 2020). Therefore, the FGF and VISFATIN signalling pathways are less likely to induce adipocyte dedifferentiation at lactation.

The CellChat software usually requires the co-expression of all subunits within a receptor complex to validate an interaction, which could lead to false negatives when one subunit is expressed below the analytical threshold. Since some genes may not be captured by snRNA-seq due to low abundance or technical noise, certain ligand-receptor interactions that are upregulated during lactation may not be detected by CellChat due to its reliance on simultaneous detection of all receptor subunits. Therefore, another analytical approach, iTALK, was used to detect individual ligand-receptor pairs that differ among development stages. Interactions between luminal cells and adipocytes through IL15 and IL15 receptor α (IL15R α) were identified at L5. Luminal cells served as senders to secrete IL15 and adipocytes served as receivers expressing IL15R α . While IL15R α expression in adipocytes was detected throughout three stages, IL15 was specifically expressed at lactation (Figure 5.1F). Moreover, as IL15 has been found to suppress lipid deposition in adipocytes, luminal cells might regulate lipogenesis and dedifferentiation of adipocytes through IL15 during lactation (Barra et al., 2010).

5.2.2 Effects of IL15 on Adipogenesis of Preadipocytes

To validate the function of IL15 on adipocyte dedifferentiation, whether adipogenesis can be suppressed by exogenous IL15 was examined. As it is reported that administration of 500ng/mL IL15 when inducing adipogenesis of human primary adipocytes *in vitro* reduces lipid deposition, a parallel experiment

Formatted: Default Paragraph Font

Deleted: Figure 5.1

Deleted: Figure 5.1

Formatted: Default Paragraph Font

Deleted: Figure 5.1

Formatted: Default Paragraph Font

using murine primary preadipocytes was conducted to investigate this phenomenon in an alternative model system (Barra et al., 2010). Primary preadipocytes were isolated from female mammary tissues and adipogenesis was performed *in vitro*. Preadipocytes were treated with exogenous human recombinant IL15 at the onset of adipogenesis induction. After inducing adipogenesis for 8 days, lipid deposition was detected by Oil Red O ([Figure 5.2A](#)).

Deleted: Figure 5.2

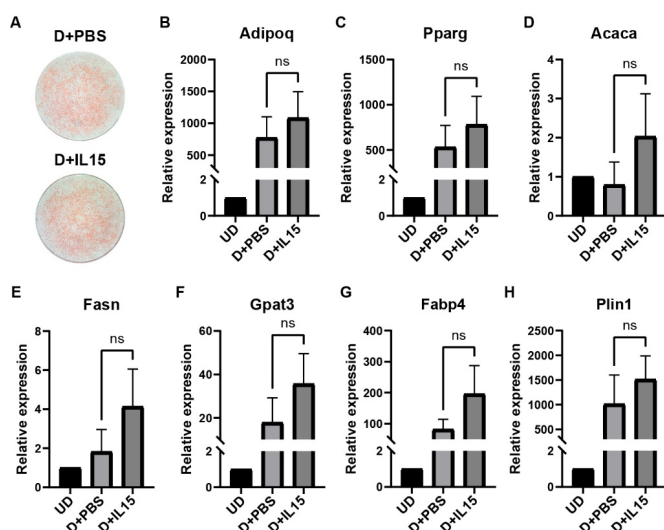


Figure 5.2 Effects of IL15 on lipid synthesis of preadipocytes.

A. Oil Red O staining of neutral lipids in differentiated preadipocytes. B-G. Expression of adipogenesis-related genes in differentiated preadipocytes. UD, undifferentiated preadipocytes; D+PBS: differentiated preadipocytes; D+IL15, preadipocytes differentiated with 500ng/mL IL15. n = 3. ns, not significant. p-values were calculated by two-tailed unpaired t-test.

Exogenous IL15 unexpectedly failed to suppress the lipid deposition ([Figure 5.2A](#)).

Deleted: Figure 5.2

Expression levels of adipogenesis-related genes were measured to further assess the effects of IL15 in adipogenesis ([Figure 5.2B-G](#)). Expression of adipogenesis-related genes increased after incubating the preadipocytes in differentiation media ([Figure 5.2B-G](#)). Particularly, expression levels of *Adipoq*, *Pparg*, *Fabp4* and *Plin1*

Deleted: Figure 5.2

Deleted: Figure 5.2

Deleted: Figure 5.2

increased over 100-fold after inducing adipogenesis, confirming lipid accumulation in differentiated preadipocytes (Figure 5.2B, C, G and H). However, a significant difference in expression levels of adipogenesis-related genes was not detected between the control group and IL15 treated group (Figure 5.2B-G). Furthermore, expression levels of adipogenesis-related genes in the IL15 treated group exhibited an upregulated tendency (Figure 5.2B-G). These results suggested an opposite role of IL15 in adipogenesis of murine preadipocytes.

Deleted: Figure 5.2

Deleted: Figure 5.2

Deleted: Figure 5.2

5.3 Effects of Adipocyte-Derived Neuregulin-4 on Mammary Gland Development

5.3.1 Potential Regulatory Role of Adipocyte-Derived NRG4-ERBB4 Signalling in Alveolar Specification

To identify adipocyte-derived molecules involved in regulating luminal differentiation and alveolar specification, significant interactions from adipocytes to luminal cells were identified by CellChat (Figure 5.3A-C). Communication probabilities of ligand-receptor pairs were calculated based on the expression levels of ligands and receptors, as well as the proportions of sender and receiver cell populations. Luminal cells, including luminal progenitors, proliferating luminal cells and alveolar cells serve as receivers, whereas adipocytes serve as senders. Notably, the NRG4-ERBB4 pair exhibited the most predominant communication probability across virgin, P13.5 and L5 (Figure 5.3A-C). NRG4 serves as the ligand secreted by adipocytes while ERBB4 serves as the receptor expressed by luminal cells, both of which were dominantly expressed across three development stages (Figure 5.3D). Given the indispensable role of ERBB4 in lobuloalveolar development, it can be inferred that adipocytes promote alveolar specification through NRG4-ERBB4 signalling (Long et al., 2003).

Deleted: Figure 5.3

Deleted: Figure 5.3

Deleted: Figure 5.3

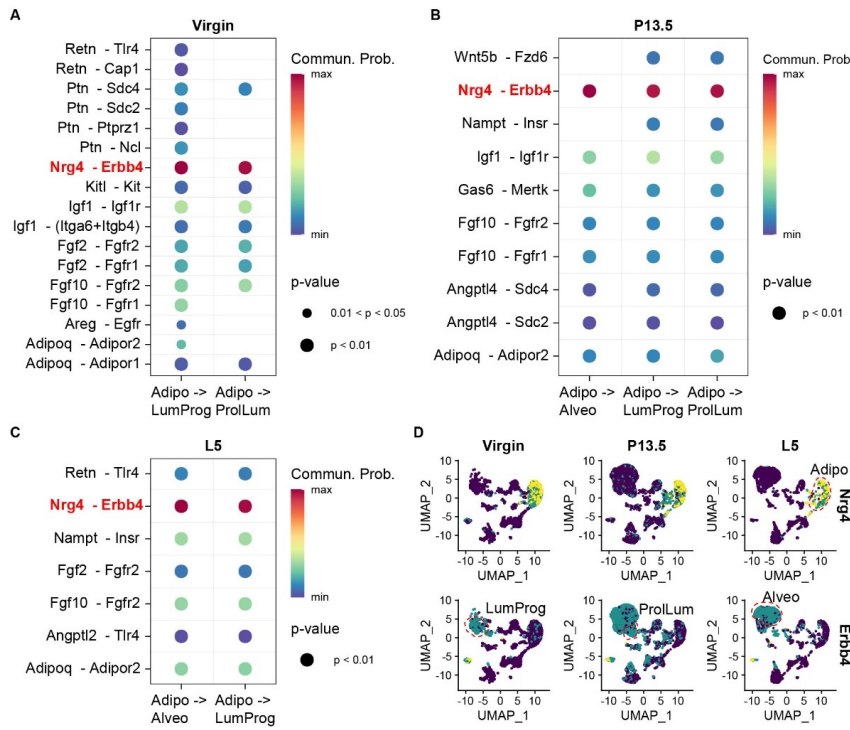


Figure 5.3 Potential adipocyte-derived signals promoting luminal growth and differentiation.

A-C. Significant ligand-receptor interactions between adipocytes and luminal cells in mammary tissue at (A) virgin, (B) P13.5 and (C) L5. D. Expression of Nrg4 and Erbb4 in cells in mammary tissue at different stages. Alveo, alveolar cells; LumProg, luminal progenitor; ProlLum, proliferating luminal cell; Adipo, adipocytes; P13.5, pregnancy day 13.5; L5, lactation day 5.

5.3.2 Effects of NRG4 on Alveogenesis and Breastfeeding

To validate the importance of adipocyte-derived NRG4 on alveogenesis, the *Nrg4* knockout (KO) mouse model was used. In this *Nrg4* KO mouse model, the *Nrg4* gene was knocked out globally. The knockout efficiency in this mouse model was validated at the RNA level ([Figure 5.5H](#)). The weight of pups nursed by KO or WT dams was measured to evaluate the lactating functions and alveolar maturation of

Deleted: Figure 5.5

the females. Pup weight was used as a robust indirect metric to evaluate the functional maturation of maternal mammary alveolar structures due to its intrinsic correlation with lactogenic capacity. Alveolar development directly governs milk synthesis and secretion during lactation and insufficient alveolar maturation compromises the volumetric and biochemical composition of milk, thereby manifesting as reduced pup weight gain (Flint et al., 2005; Gregor et al., 2013).

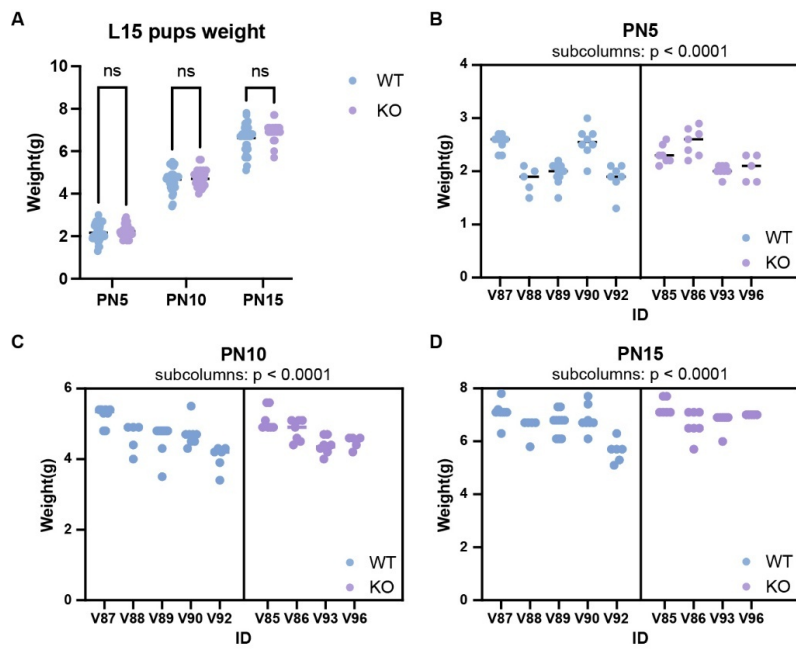


Figure 5.4 Effects of global NRG4 knockout on lactating functions of the mammary gland.

A. Body weight of pups nursed by wild-type and Nrg4 KO mice. WT, n > 37; NRG4-KO, n > 26. PN5/10/15, postnatal day 5/10/15. p values were calculated by two-tailed nested t-test. B-D. Body weight of pups nursed by wild-type and Nrg4 KO mice at postnatal day 5 (B), day 10 (C) and day 15 (D), separated by dams. ns, not significant. p-values were calculated by chi-square test.

When comparing the pup weight at postnatal day 5, 10, or 15, no significant differences were observed between WT and KO groups ([Figure 5.4A](#)). Pups

Deleted: Figure 5.4

exhibited age-dependent weight gain, indicating that they grew up normally (Figure 5.4A). However, inter-litter comparisons revealed substantial variability in pup weights across different litters (Figure 5.4B-D). Notably, even within litters nursed by dams with the same genotype, differences in intra-litter weight were significant and increased with postnatal age (Figure 5.4B-D). These results suggest that NRG4 plays a minimal role in alveogenesis and lactogenesis, and its deletion does not exert a significantly greater impact than that of other intrinsic or extrinsic factors.

Deleted: Figure 5.4

Deleted: Figure 5.4

Deleted: Figure 5.4

5.3.3 Effects of NRG4 on Mammary Gland Development During Puberty

Since previous studies demonstrate that adipose tissue exerts a greater influence on pubertal mammary gland development than on alveogenesis and the NRG4-ERBB4 signalling is possibly present in non-pregnant mice, *Nrg4* knockout models were employed to investigate the role of NRG4 in pubertal mammary morphogenesis. Mammary glands were harvested at 6 weeks of age for quantitative analysis of ductal elongation, branching frequency, TEB density, and ductal width. NRG4 expression was undetectable in mammary tissue from KO mice, confirming the knockout efficiency (Figure 5.5C). No significant difference in ductal elongation, branching frequency, TEB density, or ductal width was observed between KO and WT groups (Figure 5.5A, D-G). However, KO mice exhibited insignificant trends toward increased ductal elongation, branching frequency, and TEB density (Figure 5.5D-F). Histological staining further confirmed that no overt structural difference in the ductal architecture of the mammary glands between KO and WT groups was observed (Figure 5.5B). Collectively, these data suggested that NRG4 deletion may subtly accelerate ductal growth dynamics without achieving statistical or biological significance.

Deleted: Figure 5.5

Deleted: Figure 5.5

Deleted: Figure 5.5

Deleted: Figure 5.5

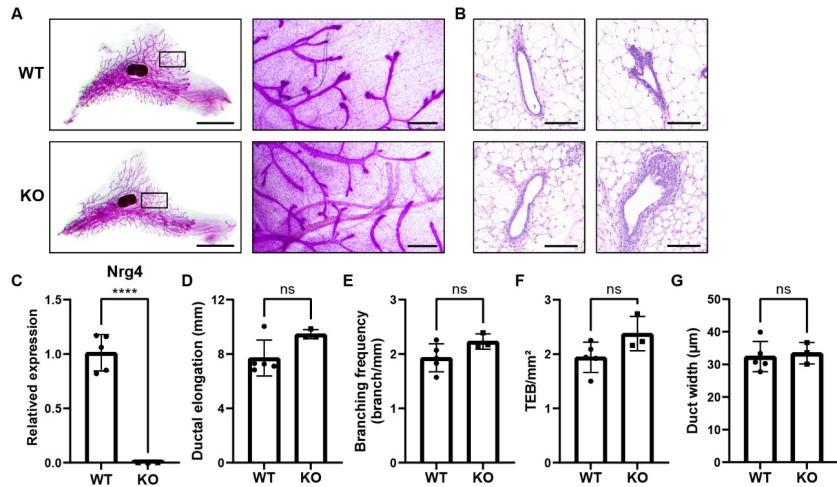


Figure 5.5 Effects of global Nrg4 KO on mammary gland development during puberty.

A. Whole mount staining of mammary tissue from wild-type and Nrg4 KO mice. Scale bar, 5 mm (left) and 500 μm (right). B. H&E staining of mammary tissue sections representing the structure of duct (left) and TEB (right). Scale bar, 100 μm. C. Expression of Nrg4 in mammary tissue. WT, n = 5; KO, n=3. ****P < 0.0001. The p-values was calculated by two-tailed unpaired t-test. D-G. Quantifications of ductal elongation (D), branching frequency (E), TEB density (F) and ductal width (G) from whole mount staining samples. WT, n = 5; KO, n=3. ***P < 0.0001. ns, not significant. p-values were calculated by two-tailed unpaired t-test.

5.4 Discussion

This chapter identified cell-cell communications between luminal cells and adipocytes, providing insights into the roles of IL15 and NRG4 signalling during mammary gland development. While IL15/IL15R α interactions between luminal cells and adipocytes was specifically detected at L5, functional validation experiments revealed unexpected discrepancies that recombinant IL15 failed to suppress lipid deposition in murine preadipocytes *in vitro*, contrasting with previous study in human primary adipocytes (Barra et al., 2010). This discrepancy may arise

from interspecies differences in IL15 receptor affinity or signalling mechanisms, as murine adipocytes might exhibit divergent responsiveness to human IL15. Moreover, the *in vivo* physiological relevance of luminal-derived IL15 remains uncertain. Epithelial-derived IL15 could act through paracrine mechanisms involving stromal mediators such as immune cells which is absent in simplified *in vitro* model. Future studies employing epithelial-specific IL15 knockout models or intra-mammary IL15 delivery during lactation are warranted to resolve this paradox.

Similarly, despite robust expression of NRG4-ERBB4 signalling across developmental stages, no statistically significant alterations in lactation performance or pubertal ductal morphogenesis were observed in NRG4 knockout mice. It is possible that the effects of NRG4 deletion was compensated by NRG1 derived by basal cells, which have been found crucial for luminal differentiation and lactogenesis (Forster et al., 2014). In addition, NRG4 knockout mice showed a modest tendency toward increased ductal elongation and branching as well as TEB formation, indicating that subtle differences might be masked by insufficient statistical power due to small sample sizes. Although the biological effects of luminal-derived IL15 on adipocyte dedifferentiation and adipocyte-derived NRG4 on luminal differentiation remained unvalidated, experimental results highlighted the importance of the complex regulating network within the mammary tissue, where single-molecule approaches failed to recapitulate physiological complexity.

Chapter 6

Single-Nucleus Sequencing Reveals the Mechanisms of HFD-Induced Mammary Gland Development Defects

6.1 Introduction

Obesity driven by HFD consumption impairs ductal morphogenesis and lactation efficiency of the mammary gland (Flint et al., 2005; Kamikawa et al., 2009). HFD reduces ductal branching, compromises myoepithelial cell integrity, and alters the mammary microenvironment via adipocyte hypertrophy, collagen deposition, and immune infiltration (Kamikawa et al., 2009). During lactation, diet-induced obesity impairs milk synthesis by downregulating critical milk proteins and reducing lipid storage capacity, resulting in delayed pup growth (Flint et al., 2005; Saben et al., 2014). While these observations highlight obesity-driven developmental defects in the mammary gland, the molecular pathways linking adipocytes to mammary gland maldevelopment remain unclear.

NRG4 was identified as a potential mediator of adipocyte-epithelial communication. In addition, HFD suppresses *Nrg4* expression while NRG4 overexpression mitigates weight gain caused by HFD (Y. Ma et al., 2016; G.-X. Wang et al., 2014). Therefore, while loss of NRG4 does not markedly impair mammary gland development under normal conditions, its regulatory role may be accentuated under HFD-induced metabolic stress, where compensatory mechanisms are overwhelmed. This chapter aims to identify the effects of NRG4 on mammary developmental defects induced by HFD.

6.2 High-Fat Diet Affects Mammary Gland Development During Puberty

To investigate the impacts of HFD-induced obesity on mammary gland development, an HFD-induced obesity mouse model was developed. Mice were fed by HFD or ND from 3 weeks of age and significant differences in body weight between groups were detected from week 8 (Figure 6.1A, B). HFD-fed mice exhibited enlarged adipose tissue and slightly reduced ductal density compared to ND controls (Figure 6.1D). Furthermore, the HFD group demonstrated diminished ductal branching and reduced ductal width compared to the ND group (Figure 6.1E, F), consistent with findings in previous research (Kamikawa et al., 2009). Notably, while the HFD group displayed a trend toward thicker collagen layers compared to the ND group, intergroup differences failed to reach statistical significance (Figure 6.1G, H). This observation contrasted with the previous study reporting significant alterations in collagen deposition (Kamikawa et al., 2009). This discrepancy is potentially attributed to the relatively short HFD exposure duration in this study, 10 weeks versus 20 weeks in Kamikawa et al. 2009. Collectively, these findings indicated that HFD impairs the morphogenesis of the mammary gland. Since NRG4 is found to regulate diet-induced metabolic dysregulation, *Nrg4* expression levels were quantified in mammary tissues (Figure 6.1C). Although the HFD group exhibited a marginal reduction in NRG4 expression, the difference did not reach statistical significance (Figure 6.1C).

To elucidate the underlying mechanisms of HFD-induced mammary developmental defects, snRNA-seq was performed on mammary tissues from ND-fed and HFD-fed mice. snRNA-seq enables comprehensive profiling of cell type-specific transcriptome alterations under diet-induced obesity. Cell types were annotated based on the expression of marker genes identified in this study (Figure 6.2A, B). Consistent with the histological observations, snRNA-seq data revealed a reduced proportion of mammary epithelial cells along with a moderate increase in adipocyte abundance in the HFD group relative to the ND group (Figure 6.2C). Notably, HFD

Deleted: Figure 6.1

Formatted: Default Paragraph Font

Deleted: Figure 6.2

Deleted: Figure 6.2

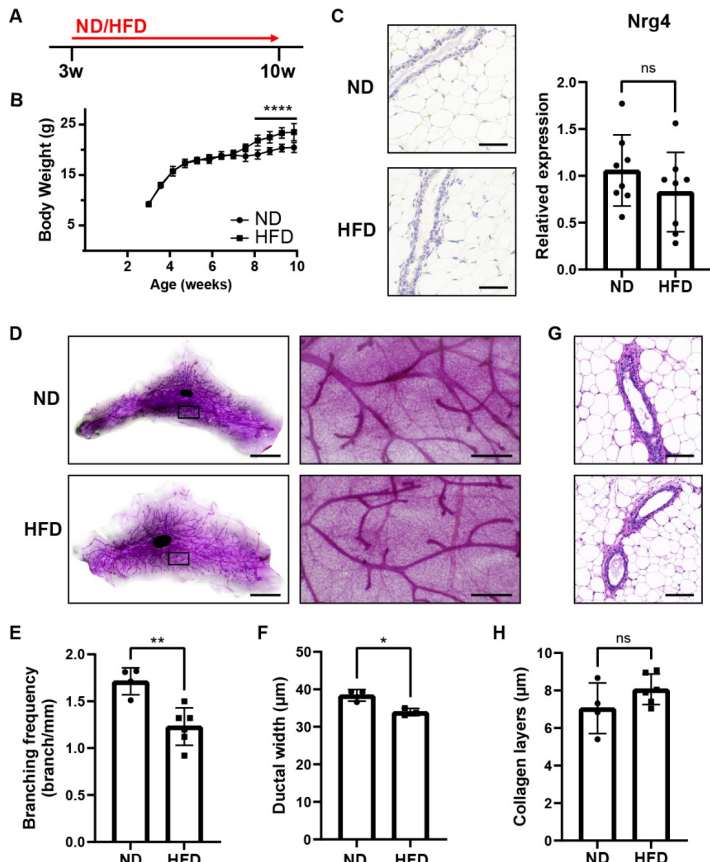


Figure 6.1 HFD induces weight gain and abnormal mammary gland development.

A. Experimental design of developing HFD-induced obesity model in wild-type mice. B. Body weight of mice from 3 weeks to 10 weeks of age. p-values were calculated by two-way ANOVA with the post hoc Bonferroni's multiple comparisons test. C. IHC staining of NRG4 (left) and expression of *Nrg4* quantified by qPCR (right). Scale bar, 50 μm. D. Whole mount staining of mammary tissues. Scale bar, 5 mm (left) and 500 μm (right). E-F. Quantifications of branching frequency (E) and ductal width (F) from whole mount staining samples. G. H&E staining of mammary tissue. Scale bar, 100 μm. H. Quantification of the thickness of collagen layers. ND and HFD, n ≥ 3. *P < 0.05, **P < 0.01. ns, not significant. p-values were calculated by two-tailed unpaired t-test.

mice exhibited a marked expansion of immune cell populations ([Figure 6.2C](#)), aligning with a previous study that diet-induced obesity promotes macrophage infiltration in mammary stroma (Kamikawa et al., 2009).

Deleted: Figure 6.2

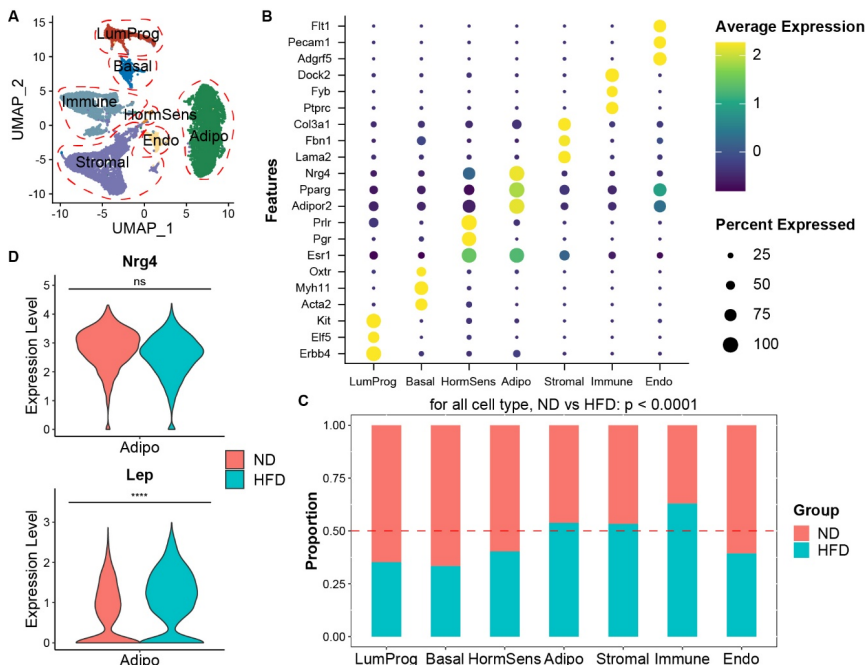


Figure 6.2 snRNA-seq of cells in mammary tissues from mice fed by HFD and ND.

A. UMAP plot of cells coloured by cell type. B. Expression of markers used for cell type identification. C. The proportion of each type of cell in the HFD group and the ND group. The p-value was calculated by the Wilcoxon rank sum test. D. Expression levels of Nrg4 and Lep in adipocytes. ***P < 0.0001. ns, not significant. p-values were calculated by t-test.

To further explore the changes in adipocytes driven by HFD, the expression level of NRG4 in adipocytes was compared between the HFD group and the ND group. Consistent with qPCR findings from bulk tissue analyses ([Figure 6.1C](#)), insignificant downregulation of NRG4 was observed in adipocytes from the HFD group ([Figure 6.2D](#)). In contrast, adipocytes in the HFD group displayed significant

Deleted: Figure 6.1

Formatted: Default Paragraph Font

Deleted: Figure 6.2

upregulation in leptin expression (Figure 6.2D), consistent with previous findings that leptin is upregulated in obese mice and suppresses the growth of mammary epithelial cells (Kamikawa et al., 2009). Although HFD did not significantly reduce *Nrg4* expression in mammary adipocytes, NRG4 may play a fundamental role in mammary gland development or metabolic regulation. Additionally, HFD could influence mammary development through other mechanisms, where NRG4 potentially acts as an indirect mediator in this process. Further investigations are required to determine whether the absence of NRG4 exacerbates HFD-induced developmental defects in the mammary gland, thereby uncovering its potential protective function.

Deleted: Figure 6.2

6.3 Effects of NRG4 Deletion on Mammary Gland Development of High-Fat Diet Fed Mice

To investigate the effects of NRG4 deletion on mammary gland development under the HFD condition, WT and *Nrg4* KO mice were fed by HFD from 3 to 10 weeks of age (Figure 6.3A, G). Although previous studies demonstrate that NRG4 overexpression attenuates HFD-induced obesity, *Nrg4* KO mice exhibited no significant differences in body weight compared to WT mice (Figure 6.3B). Consistently, NRG4 deletion did not alter the size of adipose depot (Figure 6.3D). Moreover, loss of NRG4 does not affect the ductal morphogenesis or epithelial architecture of the mammary gland (Figure 6.3C-F). Notably, reduced ductal width was observed in the mammary gland from KO mice, though this trend did not reach statistical significance (Figure 6.3F). These results indicated that NRG4 deficiency does not exert measurable impacts on HFD-induced obesity or mammary developmental defects within this experimental timeframe.

Deleted: Figure 6.3

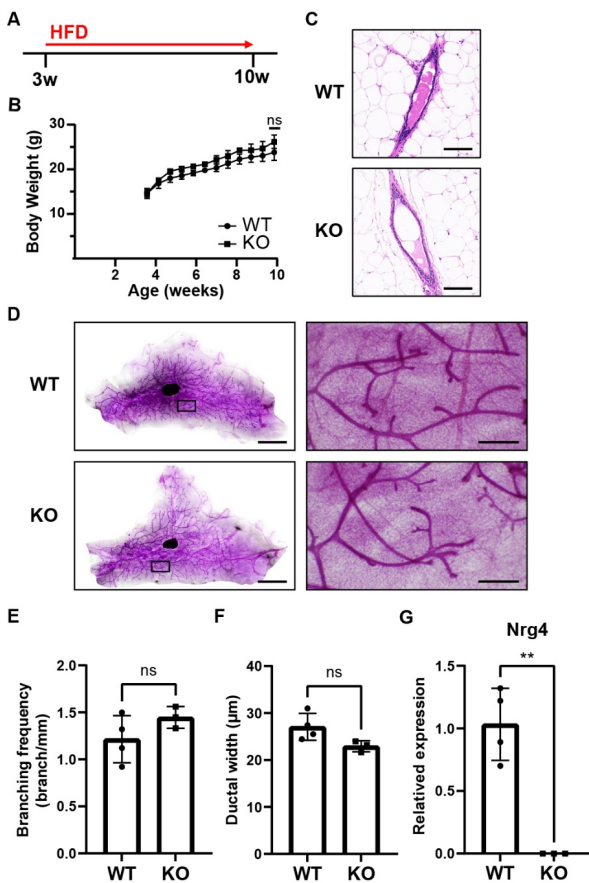


Figure 6.3 Effects of global Nrg4 knockout on ductal morphogenesis of the mammary gland under HFD.

A. Experimental design of developing HFD-induced obesity model in WT and Nrg4 KO mice. B. Body weight of mice from 3 weeks to 10 weeks of age. WT, n = 4; KO, n = 3. ns, not significant. The p-value was calculated by two-way ANOVA with the post hoc Bonferroni's multiple comparisons test. C. H&E staining of mammary tissue. Scale bar, 100 μm . D. Whole mount staining of mammary tissues. Scale bar, 5 mm (left) and 500 μm (right). E-F. Quantifications of branching frequency (E) and ductal width (F) from whole mount staining samples. G. Expression of Nrg4 in mammary tissues. WT, n = 4; KO, n = 3. **P < 0.01. ns, not significant. p-values were calculated by two-tailed unpaired t-test.

6.4 Discussion

This chapter revealed the impacts of HFD on mammary gland development and the role of NRG4 in this process. An HFD mouse model which induces mammary developmental defects was developed to study how diet-induced obesity impairs mammary gland morphogenesis. Notably, abnormalities in ductal morphogenesis similar to those reported in the previous study emerged after only 7 weeks of HFD exposure, suggesting that even short-term dietary lipid overload during puberty is sufficient to impair the ductal morphogenesis of the mammary gland (Kamikawa et al., 2009). However, the absence of significant differences in collagen deposition between the HFD group and the ND group which is contrary to the previous study, possibly reflects the truncated HFD duration in this study. Collagen remodelling is a progressive process and requires sustained inflammatory signalling (Kamikawa et al., 2009). Therefore, extended dietary interventions could be necessary to elicit significantly increased collagen deposition.

snRNA-seq provided critical insights into the multicellular pathophysiology of HFD-driven mammary developmental defects. snRNA-seq data confirmed histological observations, including the reduction in mammary epithelial cells and the expansion of adipocytes. While this study focused on adipocyte-specific transcriptional changes, it comprehensively captured obesity-driven shifts in epithelial and stromal compartments, which is a valuable resource for future investigations. Identifying transcriptional alterations of stromal and epithelial cells in response to HFD helps illustrate the underlying mechanisms of HFD-induced abnormal mammary gland development and provides therapy for this situation.

Since previous studies demonstrate that NRG4 plays a protective role against metabolic dysregulation induced by HFD, the HFD mouse model and the *Nrg4* KO mouse model were combined to study the effects of NRG4 on mammary gland development under HFD (Y. Ma et al., 2016). The combination of the HFD and the

Nrg4 KO mouse model yielded unexpectedly subtle phenotypes. Despite evidence that NRG4 overexpression mitigates metabolic dysfunction, global NRG4 deletion has no significant impact on HFD-induced obesity or mammary developmental defects (Z. Chen et al., 2017; Y. Ma et al., 2016). It is possible that a short-term HFD treatment is insufficient to unmask the protective role of NRG4, as prolonged HFD treatment amplifies metabolic and developmental defects. For example, 16-week HFD treatment results in more predominant weight gain and developmental defects of the mammary gland (Kamikawa et al., 2009). Moreover, inadequate sample size might also mask the potential statistical significance between groups. Future studies with larger sample sizes and extended HFD timelines could clarify these issues.

Collectively, these findings underscore the multifactorial nature of obesity-driven mammary developmental defects, where altered adipocyte signalling, immune dysregulation, and stromal remodelling collectively impair epithelial growth and mammary ductal morphogenesis. Although the role of NRG4 remains unclear, snRNA-seq data provides insights into the cellular mechanisms by which a HFD suppresses mammary gland development.

Chapter 7

Discussion and Future Perspectives

In this study, snRNA-seq and functional analyses were applied to unravel cellular dynamics, transcription regulatory networks, and intercellular signalling networks within the mammary tissue during mammary gland development under normal physiology and HFD conditions. snRNA-seq data provided a comprehensive view of the cellular dynamics during pregnancy and lactation, characterized by a significant expansion of epithelial cells accompanied by a reduction in stromal and adipocyte populations. In nulliparous mice, non-epithelial cells comprised over 75% of the mammary tissue, with adipocytes accounting for more than half of this population ([Figure 3.3](#)). This cellular composition underwent dramatic remodelling during pregnancy. Extensive epithelial expansion led to a substantial increase in mammary epithelial content, particularly luminal cells, which reach over 50% of the total cellular composition by P13.5 ([Figure 3.3](#)). This epithelial expansion continued into late pregnancy and lactation. Notably, while the proportion of luminal cells remained stable after P13.5, the proportion of basal cells increases significantly by L5, suggesting a specific expansion of myoepithelial cells within the basal lineage to support milk ejection during lactation ([Figure 3.3](#)). This period of epithelial expansion involves not only increased proliferation but also cellular differentiation. snRNA-seq analysis revealed that luminal progenitors differentiated into alveolar cells during this process. This epithelial expansion coincided with stromal regression, where adipocytes and other non-epithelial components exhibited marked declines throughout pregnancy and lactation ([Figure 3.3](#)). Notably, emerging evidence indicates that stromal cells undergo phenotypic transitions to support epithelial expansion, whereas adipocytes experience marked shrinkage

Deleted: Figure 3.3

Deleted: Figure 3.3

Deleted: Figure 3.3

Deleted: Figure 3.3

and dedifferentiation (Joshi et al., 2019; Q. A. Wang et al., 2018; Zwick et al., 2018). These changes reflect spatial remodelling to facilitate accommodation for the proliferating epithelial populations required for lactation. Remodelling of the mammary tissue is primarily governed by hormonal changes, which direct the specification of mammary epithelial cells from progenitor cells.

Oestrogen and progesterone stimulate the stromal-epithelial transition in stromal cells, driving their differentiation into epithelial lineages during pregnancy (Joshi et al., 2019). This phenomenon is further supported by the identification of the stromal subpopulation displaying epithelial-like features at P13.5 in snRNA-seq data ([Figure 4.1](#)). Furthermore, regulatory network analysis identified several transcription factors that are highly active in the stromal subpopulation positioned at the transcriptional interface between stromal and epithelial cells. Notably, FOXP1 exhibited broad expression across the entire putative differentiation trajectory toward both luminal and basal lineages ([Figure 4.2](#)). In addition, previous studies have demonstrated that FOXP1 is essential for MaSC maintenance and morphogenesis of the mammary gland, highlighting its potential as a key regulator of stromal-epithelial transition (N. Y. Fu et al., 2018). Given the importance of FOXP1 in mammary epithelial development, it is reasonable to explore whether it can drive stromal-epithelial transition. Previous studies have demonstrated that forced expression of specific transcription factors can reprogram stromal cells into epithelial lineages. For instance, overexpression of FOXN1 has been shown to reprogram fibroblasts into thymic epithelial-like cells (Z. Ma et al., 2024). Similarly, human fibroblasts overexpressing defined “core transcription factors” adopt corneal epithelial-like characteristics (Kitazawa et al., 2019). In addition, GRHL2 overexpression in mesenchymal cells can induce the expression of E-cadherin, a hallmark epithelial marker (Cieply et al., 2012). These findings provide a strong rationale for testing whether overexpressing FOXP1 in stromal cells can facilitate stromal-epithelial transition. However, FOXP1 overexpression in stromal cells

Deleted: Figure 4.1

Deleted: Figure 4.2

Formatted: Font: Not Bold

failed to induce expression of epithelial marker genes, though it effectively suppressed stromal differentiation toward adipocytes, consistent with its established role in inhibiting adipogenesis (H. Li et al., 2017). Notably, FOXP1 physically interacts with recombination signal binding protein for immunoglobulin kappa J region (RBPJ) to repress Notch signalling, a pathway critical for luminal differentiation (H. Li et al., 2017). In addition, RBPJ deletion in mammary epithelial cells disrupts luminal maturation during pregnancy and promotes basal-like features (Buono et al., 2006). These findings suggest that FOXP1 may help maintain the proliferative state of mammary epithelial cells rather than promote their differentiation. This is further supported by evidence showing that loss of FOXP1 in alveolar cells have no effect on lactation, implying its role is more prominent during earlier stages of mammary gland development (N. Y. Fu et al., 2018). Indeed, loss of FOXP1 disrupts pubertal mammary gland development, a period when PDGFR α ⁺ stromal-derived epithelial cells are particularly abundant (N. Y. Fu et al., 2018; Joshi et al., 2019). Collectively, these findings support the notion that FOXP1 is a critical transcription factor mediating stromal-epithelial transition, even though its overexpression alone may not be sufficient to induce epithelial gene expression. In addition to FOXP1, snRNA-seq analysis revealed the enrichment of multiple epithelial lineage-determining transcription factors within the stromal subpopulation, including STAT5A, ELF5, and GATA3. These results suggest that stromal-epithelial transition is regulated by a network of synergistic transcription factors rather than a single determinant. Future work should co-express these transcription factors in stromal cells to determine which combination of them can drives the stromal-epithelial transition. Moreover, inhibition or deletion of these transcription factors specifically in PDGFR α ⁺ stromal cells *in vivo* will also help validate their necessity in stromal-epithelial transition. If knockdown or knockout of these transcription factors in PDGFR α ⁺ stromal cells suppresses the transition, they are the major regulators in the stromal-epithelial transition process.

In parallel, luminal cells differentiate into alveolar cells during pregnancy and lactation under the control of hormones. These cells are specialized for the synthesis of milk proteins and lipids. snRNA-seq analysis revealed that alveolar cells were abundant at L5 and exhibited high expression of lipogenesis-related genes ([Figure 4.4B](#), [Figure 4.5](#)). Further analysis suggested that these alveolar cells were differentiated from luminal progenitors and showed enriched expression of STAT5 and its downstream target genes ([Figure 4.6](#)). Given the potential involvement of STAT5 in lipid synthesis in mammary epithelial cells, an *in vitro* lipogenesis model was established to directly investigate its functional role (Mao et al., 2002; Matsunaga et al., 2018). Since STAT5 is known to regulate luminal cell maturation and its inhibition impairs alveolar cell formation, mammary organoids containing differentiated alveolar cells isolated from mid-pregnant mice was employed to assess the role of STAT5 in lipogenesis. This model specifically enabled the assessment of the direct role of STAT5 in lipogenesis, while avoiding confounding effects associated with defective cell differentiation that would otherwise impair lipogenesis. Functional validation confirmed the pivotal role of STAT5 in driving lipid synthesis in mammary epithelial cells, as inhibiting STAT5 phosphorylation suppressed lipogenesis in mammary organoids ([Figure 4.8](#)). To further investigate underlying mechanisms of STAT5 in regulating the expression of lipogenesis-related genes, future studies can first map STAT5 binding sites within regulatory elements of these genes using chromatin immunoprecipitation. Subsequently, targeted deletion of STAT5-binding sites at lipid synthesis gene loci could be performed to assess the impact on the expression of alveolar-specific lipogenic genes. This approach would determine whether STAT5 directly controls lipid synthesis gene transcription. In addition to STAT5, other transcription factors, such as ELF5, were also enriched in alveolar cells, warranting future investigation into their roles in lipid metabolism.

During lactation, the mammary tissue is densely populated by epithelial cells, while

Deleted: Figure 4.4

Deleted: Figure 4.5

Formatted: Font: Not Bold

Formatted: Font: Not Bold

Deleted: Figure 4.6

Deleted: Figure 4.8

the adipocyte population markedly reduces. Previous studies have demonstrated that adipocytes shrink and lose their lipid droplets during lactation (Q. A. Wang et al., 2018; Zwick et al., 2018). Furthermore, inhibition of adipocyte lipid synthesis has been associated with enhanced milk production (Gregor et al., 2013). These findings suggest that reduced lipid synthesis in adipocytes may facilitate lactation by providing both structural space and metabolic resources. In addition, the loss of lipid droplets in mammary adipocytes occur concomitantly with epithelial expansion, suggesting a potential regulatory role of mammary epithelial cells in this process. In this context, snRNA-seq analysis identified elevated expression of IL15 in luminal cells at lactation and its potential signalling to adjacent adipocytes ([Figure 5.1](#)). Previous studies have illustrated that IL15 promotes lipolysis in adipocytes by enhancing lipase activity, thereby reducing lipid accumulation (Alvarez et al., 2002; Barra et al., 2010; Zhang, Zhao, et al., 2023). Therefore, luminal-derived IL15 may suppress lipid synthesis in adipocytes to redirect lipid substrates toward epithelial utilization. Although the inhibitory effects of IL15 in lipogenesis have been demonstrated in various adipocyte progenitors, such as human adipose-derived stem cells, cattle bone marrow-derived mesenchymal stem cells, and murine 3T3-L1 cell line, its role in mammary adipocytes remains to be defined (Almendro et al., 2009; Barra et al., 2010; Fuster et al., 2011; M. Shi et al., 2019). To investigate the functions of IL15 in mammary adipocytes, primary preadipocytes isolated from nulliparous mice were induced to differentiate *in vitro* under IL15 treatment. However, the *in vitro* model failed to validate the role of IL15 in regulating lipid synthesis, which may be attributed to several factors ([Figure 5.2](#)). One possibility is that the exogenous IL15 was ineffective. This could be addressed in future studies by assessing the activation of IL15 downstream signalling targets to determine whether IL15 is functionally active. Previous studies have shown that IL15 treatment upregulates the expression of calcineurin at both the mRNA and protein levels in 3T3-L1 cells (Almendro et al., 2009). In addition, IL15 has been

Formatted: Font: Not Bold

Deleted: Figure 5.1

Deleted: Figure 5.2

reported to enhance STAT5 activity in adipocytes (Akieda-Asai et al., 2018; Fuster et al., 2011; M. Shi et al., 2019). Therefore, evaluating calcineurin expression and STAT5 phosphorylation in IL15-treated differentiated primary preadipocytes could help confirm pathway engagement. Another possible explanation is that IL15 does not exert direct effects on adipocytes but instead acts through indirect mechanisms. Although previous studies have shown that IL15 treatment reduces body weight in lymphocyte-deficient mice, suggesting that its effects on adipose tissue are mainly independent of immune cells, the potential involvement of other cell types or microenvironmental factors within the mammary tissue cannot be excluded (Barra et al., 2012). Therefore, to further verify the function of IL15, a conditional knockout mouse model targeting IL15 specifically in mammary epithelial cells could be established. Analysis of adipocyte morphology in the lactating mammary gland, along with evaluation of lactation performance and milk lipid content in IL15-deficient females, would help clarify the regulatory role of IL15 during lactation.

While the investigation of IL15 function was limited to *in vitro* models, the absence of *in vivo* validation highlights the necessity of using animal models to fully understand the complex interactions within the mammary tissue. Mouse models are particularly valuable in biomedical research because they allow precise genetic modifications while maintaining physiological similarities to humans. Mice and humans possess comparable mammary cell types across developmental stages. During puberty, both species maintain a rudimentary ductal network that begins to expand once hormonal signals rise, leading to the formation of highly proliferative terminal structure that drive extensive ductal extension and branching into the stromal fat pad (Hovey et al., 2002). In the mature virgin human breast, terminal duct lobular units (TDLUs) are already present at the ends of ducts, whereas in mice, lobular structures typically do not form until pregnancy begins (Hovey et al., 2002). With the onset of pregnancy, luminal progenitors in both species expand and differentiate into secretory alveolar cells, while basal cells remain to provide

structural support (Twigger et al., 2022). Regulation of these developmental processes relies on conserved hormonal and transcriptional networks. For instance, prolactin activates the JAK2-STAT5 signalling pathway to drive lactation-related gene expression in both mouse and human milk-secreting luminal cells (Twigger et al., 2022). In addition to epithelial components, the composition of the stromal compartment is generally similar between mice and humans, although a notable structural distinction exists (Reed et al., 2023). The mouse mammary fat pad is predominantly composed of adipose tissue, whereas human breasts contain a denser, collagen-rich interlobular stroma with relatively fewer adipocytes (Kumar et al., 2023). Despite the differences in the mammary stroma between species, obesity adversely affects mammary gland function in both mouse and human. HFD-induced obesity results in impaired ductal morphogenesis and lactation performance in mice (Flint et al., 2005; Saben et al., 2014). Similarly, a decreased breastfeeding and lactation performance was also observed among obese women (Bever Babendure et al., 2015; Turcksin et al., 2014). Overall, the mouse model robustly mirrors core epithelial lineage progression and STAT5-dependent differentiation, thus offering high predictive value for fundamental developmental mechanisms. However, species-specific differences, particularly in adipocyte plasticity or stromal composition, must be considered when extrapolating findings. Validation using human organoid systems or clinical cohorts remains essential for ensuring translational relevance. Nonetheless, mouse models still provide a powerful platform for *in vivo* dissection of interactions between adipocytes and epithelial cells, as demonstrated in the following studies.

Adipocytes, as the most abundant non-epithelial component of the mammary tissue, play a key role in mammary gland development. In this study, snRNA-seq analysis identified NRG4-ERBB4 as a potential signalling pathway between adipocytes and luminal cells ([Figure 5.3](#)). A *Nrg4* KO mouse model was employed to investigate whether adipocytes regulate mammary gland development via NRG4

Deleted: Figure 5.3

signalling. Unexpectedly, loss of NRG4 did not result in lactation defects, possibly due to compensation by NRG1, a closely related ligand also regulating luminal differentiation (Forster et al., 2014). To further explore NRG4 function, a mammary organoid model could be used to assess whether NRG4 supplementation can activate JAK/STAT5 signalling and whether this suffices to induce luminal differentiation. In addition, although NRG4 knockout mice showed a mild trend toward enhanced ductal growth during puberty, the differences were not statistically significant, potentially due to high inter-individual variability (Figure 5.5). Increasing sample size may help confirm these trends. Moreover, the global knockout strategy could involve interference from other cell types that also express NRG4. Previous studies illustrate that NRG4 is also expressed by brown adipocytes and depletion of brown adipocytes accelerates mammary ductal branching and TEB formation (Gouon-Evans & Pollard, 2002; Rosell et al., 2014). Therefore, the observed trends toward enhanced ductal growth in KO mice might reflect indirect metabolic reprogramming. Conditional knockout of *Nrg4* in specific adipocyte populations could more precisely define its role in pubertal mammary gland development.

Deleted: Figure 5.5

To further investigate the impact of adipocyte-derived signals on mammary gland development under HFD conditions, a mouse model fed HFD from weaning (3 weeks of age) through puberty was established. After seven weeks of HFD exposure, mice in the HFD group exhibited increased body weight and impaired mammary ductal morphogenesis when compared to the ND group (Figure 6.1). A snRNA-seq dataset generated from these mammary tissues was established for subsequent mechanism-related investigations (Figure 6.2). Although this study focused on changes in adipocytes after HFD and their potential impact on mammary development, HFD-driven defects in mammary ductal morphogenesis might relate to fibroblast expansion and increased immune cell infiltration. Further analysis of snRNA-seq data not only clarifies the impacts of HFD on other cell populations in the mammary tissue but also identifies potential signalling mediators

Deleted: Figure 6.1

Formatted: Font: Not Bold

Deleted: Figure 6.2

through which adipocytes regulate mammary gland development.

As NRG4 has been reported to mitigate HFD-induced metabolic dysregulation, it may contribute to the regulation of mammary development under HFD conditions (Y. Ma et al., 2016). However, no significant aggravation or mitigation of HFD-induced developmental defects was observed in *Nrg4* KO mice, which may be attributed to the relatively short duration of dietary exposure ([Figure 6.3](#)). An earlier study has indicated that *Nrg4* KO mice fed a HFD for less than 10 weeks exhibit no significant changes in plasma triglyceride or non-esterified fatty acid levels (Z. Chen et al., 2017). However, NRG4 deletion has been reported to cause excessive lipid accumulation in the liver even after a short-term HFD (Z. Chen et al., 2017). These findings bring up another possibility that the importance of NRG4 differs among tissues. In addition, the global knockout strategy may involve systemic interference. Both HFD and NRG4 deficiency alters the functions of brown adipocytes, which itself modulates mammary gland development via undefined mechanisms (Gouon-Evans & Pollard, 2002; Kotzbeck et al., 2018; Rosell et al., 2014). Additionally, since compensatory mechanisms may mask NRG4 knockout phenotypes, overexpressing secretory NRG4 in mammary epithelial cells is a preferred strategy to validate its hypothesized role in counteracting obesity-driven mammary developmental defects. To overcome these limitations, future studies could extend HFD treatment to develop a more robust obesity model. It has been illustrated that prolonged HFD exposure results in more pronounced mammary phenotypic alterations, thereby clearly reflecting the inhibitory effects of obesity on mammary development (Kamikawa et al., 2009). Accordingly, extending HFD exposure in NRG4-deficient mice is likely to accelerate ectopic lipid accumulation within the mammary adipose tissue, which in turn may trigger metabolic and inflammatory disturbances that further constrain ductal morphogenesis. In addition, a NRG4-overexpressing mouse model should be generated to assess whether enhanced NRG4 activity can mitigate HFD-induced developmental defects in the

Deleted: Figure 6.3

mammary gland. Taken together, extending HFD duration while employing tissue-specific NRG4 overexpression or knockout models may offer a more definitive understanding of the protective potential of NRG4 against obesity-driven mammary developmental defects.

In summary, this study applied snRNA-seq to delineate cellular dynamics during mammary gland development in pregnancy and lactation, as well as under HFD conditions during puberty. Compared to previous scRNA-seq studies focusing on mammary epithelial cells, snRNA-seq in this study enabled a more comprehensive characterization of cell types, particularly lipid-rich populations, and uncovered putative intercellular signalling networks between different types of cells within the mammary tissue. snRNA-seq analysis identified key transcription factors involved in the specification of mammary epithelial cells. FOXP1 marked stromal cells undergoing stromal-epithelial transition and STAT5 promoted lipid synthesis in alveolar cells. Though FOXP1 alone insufficiently drove stromal-epithelial transition, regulatory networks suggested synergistic roles with other transcription factors such as GATA3, STAT5 and ELF5. On the other hand, analyses of cell-cell communications identified IL15 and NRG4 as candidate mediators of crosstalk between luminal epithelial cells and adipocytes, though functional validation revealed limited roles for these signals. In the context of nutritional stress, short-term HFD exposure during puberty impaired ductal morphogenesis of the mammary gland. Despite NRG4 deletion failing to alter HFD phenotypes, snRNA-seq provides information for further investigation. Future directions should focus on dissecting cooperative transcriptional networks involved in stromal-epithelial transition, clarifying STAT5 downstream targets in lipogenesis, and validating the roles of IL15 and NRG4 using refined genetic models.

These findings bring new insights into mammary gland plasticity and create a framework for further studies on lactation biology and public health interventions.

Investigating STAT5/ELF5-mediated lipid synthesis could reveal strategies to optimize infant nutrition. Modulating this pathway could enhance milk lipid composition, particularly levels of long-chain polyunsaturated fatty acids essential for neurodevelopment, under suboptimal lactation conditions. Such approaches might be translated into dietary or pharmacological interventions aimed at supporting lactating mothers with impaired milk production, thereby improving neonatal outcomes. Meanwhile, if the role of IL15 in mammary adipocytes is confirmed, it could offer a novel therapeutic approach for lactation-related metabolic disorders. Targeted delivery of IL15 may help reduce pathological lipid accumulation while maintaining mammary gland function. This is particularly relevant for obese mothers, in whom mammary adipocyte hypertrophy and impaired lipid turnover have been linked to poor breastfeeding outcomes. For instance, obesity is associated with elevated leptin levels which can attenuate oxytocin-induced contractility of human myometrium (Moynihan et al., 2006). Since oxytocin also stimulates contraction of mammary myoepithelial cells during milk ejection, it is plausible that elevated leptin levels in obese women may contribute to lactation difficulties. Furthermore, IL15 has been shown to suppress leptin expression in 3T3-L1-derived adipocytes, raising the possibility that enhancing local IL15 activity within the mammary gland could help restore milk release in obese mothers and improve breastfeeding outcomes (Almendro et al., 2009; Fuster et al., 2011). Moreover, exploring NRG4 supplementation during puberty may provide preventive therapies against obesity-related breastfeeding challenges. If NRG4 overexpression within the mammary gland promotes mammary gland development in the context of HFD exposure, targeted NRG4 supplementation could facilitate pubertal mammary development, thereby reducing the risk of lactation deficiencies in adulthood. [Beyond NRG4, systematic analysis of snRNA-seq datasets could help identify additional signalling molecules through which HFD-induced obesity impairs pubertal mammary development. By comparing](#)

intercellular communication networks between normal and HFD conditions, critical ligand-receptor pairs disrupted by metabolic stress may be uncovered. Functional validation of these candidates could inform targeted pharmacological or nutritional interventions aimed at optimizing mammary gland development during puberty in obese individuals. For instance, identified signalling pathways could be modulated through small molecule inhibitors or monoclonal antibodies to restore normal mammary morphogenesis. With potential translational relevance to both clinical and research fields, this work supports the development of nutritional guidelines aimed at promoting healthy mammary development during puberty, ultimately reducing lifelong risks of metabolic diseases. Collectively, this study holds strong translational potential for advancing maternal and infant health.

References

- Akieda-Asai, S., Ida, T., Miyazato, M., Kangawa, K., & Date, Y. (2018). Interleukin-15 derived from Guanylin–GC-C-expressing macrophages inhibits fatty acid synthase in adipocytes. *Peptides*, 99, 14–19. <https://doi.org/10.1016/j.peptides.2017.10.012>
- Almendro, V., Fuster, G., Ametller, E., Costelli, P., Pilla, F., Busquets, S., Figueras, M., Argilés, J. M., & López-Soriano, F. J. (2009). Interleukin-15 increases calcineurin expression in 3T3-L1 cells: Possible involvement on in vivo adipocyte differentiation. *International Journal of Molecular Medicine*, 24(04). https://doi.org/10.3892/ijmm_00000252
- Alvarez, B., Carbó, N., López-Soriano, J., Drivdahl, R. H., Busquets, S., López-Soriano, F. J., Argilés, J. M., & Quinn, L. S. (2002). Effects of interleukin-15 (IL-15) on adipose tissue mass in rodent obesity models: Evidence for direct IL-15 action on adipose tissue. *Biochimica et Biophysica Acta (BBA) - General Subjects*, 1570(1), 33–37. [https://doi.org/10.1016/S0304-4165\(02\)00148-4](https://doi.org/10.1016/S0304-4165(02)00148-4)
- Asselin-Labat, M.-L., Sutherland, K. D., Barker, H., Thomas, R., Shackleton, M., Forrest, N. C., Hartley, L., Robb, L., Grosveld, F. G., Van Der Wees, J., Lindeman, G. J., & Visvader, J. E. (2007). Gata-3 is an essential regulator of mammary-gland morphogenesis and luminal-cell differentiation. *Nature Cell Biology*, 9(2), 201–209. <https://doi.org/10.1038/ncb1530>
- Bach, K., Pensa, S., Grzelak, M., Hadfield, J., Adams, D. J., Marioni, J. C., & Khaled, W. T. (2017). Differentiation dynamics of mammary epithelial cells revealed by single-cell RNA sequencing. *Nature Communications*, 8(1), 2128. <https://doi.org/10.1038/s41467-017-02001-5>
- Barra, N. G., Chew, M. V., Reid, S., & Ashkar, A. A. (2012). Interleukin-15 Treatment

- Induces Weight Loss Independent of Lymphocytes. *PLoS ONE*, 7(6), e39553. <https://doi.org/10.1371/journal.pone.0039553>
- Barra, N. G., Reid, S., MacKenzie, R., Werstuck, G., Trigatti, B. L., Richards, C., Holloway, A. C., & Ashkar, A. A. (2010). Interleukin-15 Contributes to the Regulation of Murine Adipose Tissue and Human Adipocytes. *Obesity*, 18(8), 1601–1607. <https://doi.org/10.1038/oby.2009.445>
- Beigneux, A. P., Vergnes, L., Qiao, X., Quatela, S., Davis, R., Watkins, S. M., Coleman, R. A., Walzem, R. L., Philips, M., Reue, K., & Young, S. G. (2006). Agpat6—A novel lipid biosynthetic gene required for triacylglycerol production in mammary epithelium. *Journal of Lipid Research*, 47(4), 734–744. <https://doi.org/10.1194/jlr.M500556-JLR200>
- Beleut, M., Rajaram, R. D., Caikovski, M., Ayyanan, A., Germano, D., Choi, Y., Schneider, P., & Brisken, C. (2010). Two distinct mechanisms underlie progesterone-induced proliferation in the mammary gland. *Proceedings of the National Academy of Sciences*, 107(7), 2989–2994. <https://doi.org/10.1073/pnas.0915148107>
- Bever Babendure, J., Reifsnyder, E., Mendias, E., Moramarco, M. W., & Davila, Y. R. (2015). Reduced breastfeeding rates among obese mothers: A review of contributing factors, clinical considerations and future directions. *International Breastfeeding Journal*, 10(1), 21. <https://doi.org/10.1186/s13006-015-0046-5>
- Bi, P., Yue, F., Karki, A., Castro, B., Wirbisky, S. E., Wang, C., Durkes, A., Elzey, B. D., Andrisani, O. M., Bidwell, C. A., Freeman, J. L., Konieczny, S. F., & Kuang, S. (2016). Notch activation drives adipocyte dedifferentiation and tumorigenic transformation in mice. *Journal of Experimental Medicine*, 213(10), 2019–2037. <https://doi.org/10.1084/jem.20160157>
- Bouras, T., Pal, B., Vaillant, F., Harburg, G., Asselin-Labat, M.-L., Oakes, S. R., Lindeman, G. J., & Visvader, J. E. (2008). Notch Signaling Regulates

- Mammary Stem Cell Function and Luminal Cell-Fate Commitment. *Cell Stem Cell*, 3(4), 429–441. <https://doi.org/10.1016/j.stem.2008.08.001>
- Brenot, A., Hutson, I., & Harris, C. (2020). Epithelial-adipocyte interactions are required for mammary gland development, but not for milk production or fertility. *Developmental Biology*, 458(2), 153–163. <https://doi.org/10.1016/j.ydbio.2019.11.001>
- Briskin, C., Park, S., Vass, T., Lydon, J. P., O'Malley, B. W., & Weinberg, R. A. (1998). A paracrine role for the epithelial progesterone receptor in mammary gland development. *Proceedings of the National Academy of Sciences*, 95(9), 5076–5081. <https://doi.org/10.1073/pnas.95.9.5076>
- Buitenhuis, M., Verhagen, L. P., Cools, J., & Cofer, P. J. (2007). Molecular Mechanisms Underlying FIP1L1-PDGFR α -Mediated Myeloproliferation. *Cancer Research*, 67(8), 3759–3766. <https://doi.org/10.1158/0008-5472.CAN-06-4183>
- Buono, K. D., Robinson, G. W., Martin, C., Shi, S., Stanley, P., Tanigaki, K., Honjo, T., & Hennighausen, L. (2006). The canonical Notch/RBP-J signaling pathway controls the balance of cell lineages in mammary epithelium during pregnancy. *Developmental Biology*, 293(2), 565–580. <https://doi.org/10.1016/j.ydbio.2006.02.043>
- Carr, J. R., Kiefer, M. M., Park, H. J., Li, J., Wang, Z., Fontanarosa, J., DeWaal, D., Kopanja, D., Benevolenskaya, E. V., Guzman, G., & Raychaudhuri, P. (2012). FoxM1 Regulates Mammary Luminal Cell Fate. *Cell Reports*, 1(6), 715–729. <https://doi.org/10.1016/j.celrep.2012.05.005>
- Carraway III, K. L., Weber, J. L., Unger, M. J., Ledesma, J., Yu, N., Gassmann, M., & Lai, C. (1997). Neuregulin-2, a new ligand of ErbB3/ErbB4-receptor tyrosine kinases. *Nature*, 387(6632), 512–516. <https://doi.org/10.1038/387512a0>
- Chakrabarti, R., Wei, Y., Romano, R.-A., DeCoste, C., Kang, Y., & Sinha, S. (2012).

- Elf5 Regulates Mammary Gland Stem/Progenitor Cell Fate by Influencing Notch Signaling. *Stem Cells*, 30(7), 1496–1508.
<https://doi.org/10.1002/stem.1112>
- Chappell, J. C., Cluceru, J. G., Nesmith, J. E., Mouillesseaux, K. P., Bradley, V. B., Hartland, C. M., Hashambhoy-Ramsay, Y. L., Walpole, J., Peirce, S. M., Mac Gabhann, F., & Bautch, V. L. (2016). Flt-1 (VEGFR-1) coordinates discrete stages of blood vessel formation. *Cardiovascular Research*, 111(1), 84–93.
<https://doi.org/10.1093/cvr/cvw091>
- Chen, E. L. Y., Thompson, P. K., & Zúñiga-Pflücker, J. C. (2019). RBPJ-dependent Notch signaling initiates the T cell program in a subset of thymus-seeding progenitors. *Nature Immunology*, 20(11), 1456–1468.
<https://doi.org/10.1038/s41590-019-0518-7>
- Chen, Y., Chen, Y., Yin, W., Han, H., Miller, H., Li, J., Herrada, A. A., Kubo, M., Sui, Z., Gong, Q., & Liu, C. (2021). The regulation of DOCK family proteins on T and B cells. *Journal of Leukocyte Biology*, 109(2), 383–394.
<https://doi.org/10.1002/JLB.1MR0520-221RR>
- Chen, Z., Wang, G.-X., Ma, S. L., Jung, D. Y., Ha, H., Altamimi, T., Zhao, X.-Y., Guo, L., Zhang, P., Hu, C.-R., Cheng, J.-X., Lopaschuk, G. D., Kim, J. K., & Lin, J. D. (2017). Nrg4 promotes fuel oxidation and a healthy adipokine profile to ameliorate diet-induced metabolic disorders. *Molecular Metabolism*, 6(8), 863–872. <https://doi.org/10.1016/j.molmet.2017.03.016>
- Choi, Y. S., Chakrabarti, R., Escamilla-Hernandez, R., & Sinha, S. (2009). Elf5 conditional knockout mice reveal its role as a master regulator in mammary alveolar development: Failure of Stat5 activation and functional differentiation in the absence of Elf5. *Developmental Biology*, 329(2), 227–241. <https://doi.org/10.1016/j.ydbio.2009.02.032>
- Chua, H. L., Bhat-Nakshatri, P., Clare, S. E., Morimiy, A., Badve, S., & Nakshatri, H. (2007). NF-κB represses E-cadherin expression and enhances epithelial

- to mesenchymal transition of mammary epithelial cells: Potential involvement of ZEB-1 and ZEB-2. *Oncogene*, 26(5), 711–724. <https://doi.org/10.1038/sj.onc.1209808>
- Ciarloni, L., Mallepell, S., & Brisken, C. (2007). Amphiregulin is an essential mediator of estrogen receptor α function in mammary gland development. *Proceedings of the National Academy of Sciences*, 104(13), 5455–5460. <https://doi.org/10.1073/pnas.0611647104>
- Cieply, B., Riley, P., Pifer, P. M., Widmeyer, J., Addison, J. B., Ivanov, A. V., Denvir, J., & Frisch, S. M. (2012). Suppression of the Epithelial–Mesenchymal Transition by Grainyhead-like-2. *Cancer Research*, 72(9), 2440–2453. <https://doi.org/10.1158/0008-5472.CAN-11-4038>
- Cinti, S. (2018). Pink Adipocytes. *Trends in Endocrinology & Metabolism*, 29(9), 651–666. <https://doi.org/10.1016/j.tem.2018.05.007>
- Côté, J. A., Lessard, J., Pelletier, M., Marceau, S., Lescelleur, O., Fradette, J., & Tchernof, A. (2017). Role of the TGF- β pathway in dedifferentiation of human mature adipocytes. *FEBS Open Bio*, 7(8), 1092–1101. <https://doi.org/10.1002/2211-5463.12250>
- Cui, Y., Riedlinger, G., Miyoshi, K., Tang, W., Li, C., Deng, C.-X., Robinson, G. W., & Hennighausen, L. (2004). Inactivation of Stat5 in Mouse Mammary Epithelium during Pregnancy Reveals Distinct Functions in Cell Proliferation, Survival, and Differentiation. *Molecular and Cellular Biology*, 24(18), 8037–8047. <https://doi.org/10.1128/MCB.24.18.8037-8047.2004>
- Damiani, D., Goffinet, A. M., Alberts, A., & Tissir, F. (2016). Lack of Diaph3 relaxes the spindle checkpoint causing the loss of neural progenitors. *Nature Communications*, 7(1), 13509. <https://doi.org/10.1038/ncomms13509>
- DaSilva, L., Rui, H., Erwin, R. A., Zack Howard, O. M., Kirken, R. A., Malabarba, M. G., Hackett, R. H., Larner, A. C., & Farrar, W. L. (1996). Prolactin recruits STAT1, STAT3 and STAT5 independent of conserved receptor tyrosines

- TYR402, TYR479, TYR515 and TYR580. *Molecular and Cellular Endocrinology*, 117(2), 131–140. [https://doi.org/10.1016/0303-7207\(95\)03738-1](https://doi.org/10.1016/0303-7207(95)03738-1)
- Dekkers, J. F., Alieva, M., Wellens, L. M., Ariese, H. C. R., Jamieson, P. R., Vonk, A. M., Amatngalim, G. D., Hu, H., Oost, K. C., Snippert, H. J. G., Beekman, J. M., Wehrens, E. J., Visvader, J. E., Clevers, H., & Rios, A. C. (2019). High-resolution 3D imaging of fixed and cleared organoids. *Nature Protocols*, 14(6), 1756–1771. <https://doi.org/10.1038/s41596-019-0160-8>
- DeWard, A. D., & Alberts, A. S. (2009). Ubiquitin-mediated Degradation of the Formin mDia2 upon Completion of Cell Division. *Journal of Biological Chemistry*, 284(30), 20061–20069. <https://doi.org/10.1074/jbc.M109.000885>
- Dogaru, C. M., Nyffenegger, D., Pescatore, A. M., Spycher, B. D., & Kuehni, C. E. (2014). Breastfeeding and Childhood Asthma: Systematic Review and Meta-Analysis. *American Journal of Epidemiology*, 179(10), 1153–1167. <https://doi.org/10.1093/aje/kwu072>
- Domogatskaya, A., Rodin, S., & Tryggvason, K. (2012). Functional Diversity of Laminins. *Annual Review of Cell and Developmental Biology*, 28(1), 523–553. <https://doi.org/10.1146/annurev-cellbio-101011-155750>
- Dong, H., Sun, W., Shen, Y., Baláz, M., Balázová, L., Ding, L., Löfller, M., Hamilton, B., Klöting, N., Blüher, M., Neubauer, H., Klein, H., & Wolfrum, C. (2022). Identification of a regulatory pathway inhibiting adipogenesis via RSPO2. *Nature Metabolism*, 4(1), 90–105. <https://doi.org/10.1038/s42255-021-00509-1>
- Elias, J. J., Pitelka, D. R., & Armstrong, R. C. (1973). Changes in fat cell morphology during lactation in the mouse. *The Anatomical Record*, 177(4), 533–547. <https://doi.org/10.1002/ar.1091770407>
- Farmer, S. R. (2006). Transcriptional control of adipocyte formation. *Cell*

- Metabolism*, 4(4), 263–273. <https://doi.org/10.1016/j.cmet.2006.07.001>
- Fata, J. E., Chaudhary, V., & Khokha, R. (2001). Cellular Turnover in the Mammary Gland Is Correlated with Systemic Levels of Progesterone and Not 17 β -Estradiol During the Estrous Cycle1. *Biology of Reproduction*, 65(3), 680–688. <https://doi.org/10.1095/biolreprod65.3.680>
- Feng, Y., Manka, D., Wagner, K.-U., & Khan, S. A. (2007). Estrogen receptor- α expression in the mammary epithelium is required for ductal and alveolar morphogenesis in mice. *Proceedings of the National Academy of Sciences*, 104(37), 14718–14723. <https://doi.org/10.1073/pnas.0706933104>
- Flint, D. J., Travers, M. T., Barber, M. C., Binart, N., & Kelly, P. A. (2005). Diet-induced obesity impairs mammary development and lactogenesis in murine mammary gland. *American Journal of Physiology-Endocrinology and Metabolism*, 288(6), E1179–E1187. <https://doi.org/10.1152/ajpendo.00433.2004>
- Forster, N., Saladi, S. V., van Bragt, M., Sfondouris, M. E., Jones, F. E., Li, Z., & Ellisen, L. W. (2014). Basal Cell Signaling by p63 Controls Luminal Progenitor Function and Lactation via NRG1. *Developmental Cell*, 28(2), 147–160. <https://doi.org/10.1016/j.devcel.2013.11.019>
- Frey, W. D., Chaudhry, A., Slepicka, P. F., Ouellette, A. M., Kirberger, S. E., Pomerantz, W. C. K., Hannon, G. J., & Dos Santos, C. O. (2017). BPTF Maintains Chromatin Accessibility and the Self-Renewal Capacity of Mammary Gland Stem Cells. *Stem Cell Reports*, 9(1), 23–31. <https://doi.org/10.1016/j.stemcr.2017.04.031>
- Fu, N. Y., Pal, B., Chen, Y., Jackling, F. C., Milevskiy, M., Vaillant, F., Capaldo, B. D., Guo, F., Liu, K. H., Rios, A. C., Lim, N., Kueh, A. J., Virshup, D. M., Herold, M. J., Tucker, H. O., Smyth, G. K., Lindeman, G. J., & Visvader, J. E. (2018). Foxp1 Is Indispensable for Ductal Morphogenesis and Controls the Exit of Mammary Stem Cells from Quiescence. *Developmental Cell*, 47(5), 629–643. <https://doi.org/10.1016/j.devcel.2018.04.018>

644.e8. <https://doi.org/10.1016/j.devcel.2018.10.001>

- Fu, R., Han, C.-F., Ni, T., Di, L., Liu, L.-J., Lv, W.-C., Bi, Y.-R., Jiang, N., He, Y., Li, H.-M., Wang, S., Xie, H., Chen, B.-A., Wang, X.-S., Weiss, S. J., Lu, T., Guo, Q.-L., & Wu, Z.-Q. (2019). A ZEB1/p53 signaling axis in stromal fibroblasts promotes mammary epithelial tumours. *Nature Communications*, 10(1), 3210. <https://doi.org/10.1038/s41467-019-11278-7>
- Fuster, G., Almendro, V., Fontes-Oliveira, C. C., Toledo, M., Costelli, P., Busquets, S., López-Soriano, F. J., & Argilés, J. M. (2011). Interleukin-15 Affects Differentiation and Apoptosis in Adipocytes: Implications in Obesity. *Lipids*, 46(11), 1033–1042. <https://doi.org/10.1007/s11745-011-3594-5>
- Gallego, M. I., Binart, N., Robinson, G. W., Okagaki, R., Coschigano, K. T., Perry, J., Kopchick, J. J., Oka, T., Kelly, P. A., & Hennighausen, L. (2001). Prolactin, Growth Hormone, and Epidermal Growth Factor Activate Stat5 in Different Compartments of Mammary Tissue and Exert Different and Overlapping Developmental Effects. *Developmental Biology*, 229(1), 163–175. <https://doi.org/10.1006/dbio.2000.9961>
- Gao, B., Qu, Y., Han, B., Nagaoka, Y., Katsumata, M., Deng, N., Bose, S., Jin, L., Giuliano, A. E., & Cui, X. (2017). Inhibition of lobuloalveolar development by FOXC1 overexpression in the mouse mammary gland. *Scientific Reports*, 7(1), 14017. <https://doi.org/10.1038/s41598-017-14342-8>
- García Solá, M. E., Stedile, M., Beckerman, I., & Kordon, E. C. (2021). An Integrative Single-cell Transcriptomic Atlas of the Post-natal Mouse Mammary Gland Allows Discovery of New Developmental Trajectories in the Luminal Compartment. *Journal of Mammary Gland Biology and Neoplasia*, 26(1), 29–42. <https://doi.org/10.1007/s10911-021-09488-1>
- Giraddi, R. R., Chung, C.-Y., Heinz, R. E., Balcioglu, O., Novotny, M., Trejo, C. L., Dravis, C., Hagos, B. M., Mehrabad, E. M., Rodewald, L. W., Hwang, J. Y., Fan, C., Lasken, R., Varley, K. E., Perou, C. M., Wahl, G. M., & Spike, B. T.

- (2018). Single-Cell Transcriptomes Distinguish Stem Cell State Changes and Lineage Specification Programs in Early Mammary Gland Development. *Cell Reports*, 24(6), 1653-1666.e7. <https://doi.org/10.1016/j.celrep.2018.07.025>
- Gouon-Evans, V., & Pollard, J. W. (2002). Unexpected Deposition of Brown Fat in Mammary Gland During Postnatal Development. *Molecular Endocrinology*, 16(11), 2618–2627. <https://doi.org/10.1210/me.2001-0337>
- Graesser, D., Solowiej, A., Bruckner, M., Osterweil, E., Juedes, A., Davis, S., Ruddle, N. H., Engelhardt, B., & Madri, J. A. (2002). Altered vascular permeability and early onset of experimental autoimmune encephalomyelitis in PECAM-1-deficient mice. *Journal of Clinical Investigation*, 109(3), 383–392. <https://doi.org/10.1172/JCI0213595>
- Gregor, M. F., Misch, E. S., Yang, L., Hummasti, S., Inouye, K. E., Lee, A.-H., Bierie, B., & Hotamisligil, G. S. (2013). The Role of Adipocyte XBP1 in Metabolic Regulation during Lactation. *Cell Reports*, 3(5), 1430–1439. <https://doi.org/10.1016/j.celrep.2013.03.042>
- Guo, W., Li, Z., Anagnostopoulos, G., Kong, W. T., Zhang, S., Chakarov, S., Shin, A., Qian, J., Zhu, Y., Bai, W., Cexus, O., Nie, B., Wang, J., Hu, X., Blériot, C., Liu, Z., Shen, B., Ventecler, N., Su, B., & Ginhoux, F. (2024). Notch signaling regulates macrophage-mediated inflammation in metabolic dysfunction-associated steatotic liver disease. *Immunity*, 57(10), 2310-2327.e6. <https://doi.org/10.1016/j.jimmuni.2024.08.016>
- Gurriarán-Rodríguez, U., Al-Massadi, O., Roca-Rivada, A., Crujeiras, A. B., Gallego, R., Pardo, M., Seoane, L. M., Pazos, Y., Casanueva, F. F., & Camiña, J. P. (2011). Obestatin as a regulator of adipocyte metabolism and adipogenesis. *Journal of Cellular and Molecular Medicine*, 15(9), 1927–1940. <https://doi.org/10.1111/j.1582-4934.2010.01192.x>
- Gustafson, B., & Smith, U. (2010). Activation of Canonical Wingless-type MMTV

- Integration Site Family (Wnt) Signaling in Mature Adipocytes Increases β -Catenin Levels and Leads to Cell Dedifferentiation and Insulin Resistance. *Journal of Biological Chemistry*, 285(18), 14031–14041. <https://doi.org/10.1074/jbc.M110.102855>
- Han, H., Tanigaki, K., Yamamoto, N., Kuroda, K., Yoshimoto, M., Nakahata, T., Ikuta, K., & Honjo, T. (2002). Inducible gene knockout of transcription factor recombination signal binding protein-J reveals its essential role in T versus B lineage decision. *International Immunology*, 14(6), 637–645. <https://doi.org/10.1093/intimm/dxf030>
- Han, Y., Watling, D., Rogers, N. C., & Stark, G. R. (1997). JAK2 and STAT5, but not JAK1 and STAT1, Are Required for Prolactin-Induced β -Lactoglobulin Transcription. *Molecular Endocrinology*, 11(8), 1180–1188. <https://doi.org/10.1210/mend.11.8.9952>
- Harris, J., Stanford, P. M., Sutherland, K., Oakes, S. R., Naylor, M. J., Robertson, F. G., Blazek, K. D., Kazlauskas, M., Hilton, H. N., Wittlin, S., Alexander, W. S., Lindeman, G. J., Visvader, J. E., & Ormandy, C. J. (2006). Socs2 and Elf5 Mediate Prolactin-Induced Mammary Gland Development. *Molecular Endocrinology*, 20(5), 1177–1187. <https://doi.org/10.1210/me.2005-0473>
- Hatzirodos, N., Hummitzsch, K., Irving-Rodgers, H. F., Breen, J., Perry, V. E. A., Anderson, R. A., & Rodgers, R. J. (2019). Transcript abundance of stromal and thecal cell related genes during bovine ovarian development. *PLOS ONE*, 14(3), e0213575. <https://doi.org/10.1371/journal.pone.0213575>
- Heeg, S., Das, K. K., Reichert, M., Bakir, B., Takano, S., Caspers, J., Aiello, N. M., Wu, K., Neesse, A., Maitra, A., Iacobuzio-Donahue, C. A., Hicks, P., & Rustgi, A. K. (2016). ETS-Transcription Factor ETV1 Regulates Stromal Expansion and Metastasis in Pancreatic Cancer. *Gastroenterology*, 151(3), 540–553.e14. <https://doi.org/10.1053/j.gastro.2016.06.005>
- Hennighausen, L. G., & Sippel, A. E. (1982). Characterization and Cloning of the

- mRNAs Specific for the Lactating Mouse Mammary Gland. *European Journal of Biochemistry*, 125(1), 131–141. <https://doi.org/10.1111/j.1432-1033.1982.tb06660.x>
- Hennighausen, L., & Robinson, G. W. (2005). Information networks in the mammary gland. *Nature Reviews Molecular Cell Biology*, 6(9), 715–725. <https://doi.org/10.1038/nrm1714>
- Hermiston, M. L., Xu, Z., & Weiss, A. (2003). CD45: A Critical Regulator of Signaling Thresholds in Immune Cells. *Annual Review of Immunology*, 21(1), 107–137. <https://doi.org/10.1146/annurev.immunol.21.120601.140946>
- Holmes, W. E., Sliwkowski, M. X., Akita, R. W., Henzel, W. J., Lee, J., Park, J. W., Yansura, D., Abadi, N., Raab, H., Lewis, G. D., Shepard, H. M., Kuang, W.-J., Wood, W. L., Goeddel, D. V., & Vandlen, R. L. (1992). Identification of Heregulin, a Specific Activator of p185^{erbB2}. *Science*, 256(5060), 1205–1210. <https://doi.org/10.1126/science.256.5060.1205>
- Horta, B. L., Loret De Mola, C., & Victora, C. G. (2015). Long-term consequences of breastfeeding on cholesterol, obesity, systolic blood pressure and type 2 diabetes: A systematic review and meta-analysis. *Acta Paediatrica*, 104(S467), 30–37. <https://doi.org/10.1111/apa.13133>
- Hovey, R. C., Trott, J. F., & Von der Haar, B. K. (2002). Establishing a Framework for the Functional Mammary Gland: From Endocrinology to Morphology. *Journal of Mammary Gland Biology and Neoplasia*, 7(1), 17–38. <https://doi.org/10.1023/A:1015766322258>
- Huang, Y., Simms, A. E., Mazur, A., Wang, S., León, N. R., Jones, B., Aziz, N., & Kelly, T. (2011). Fibroblast activation protein-α promotes tumor growth and invasion of breast cancer cells through non-enzymatic functions. *Clinical & Experimental Metastasis*, 28(6), 567–579. <https://doi.org/10.1007/s10585-011-9392-x>
- Inman, J. L., Robertson, C., Mott, J. D., & Bissell, M. J. (2015). Mammary gland

- development: Cell fate specification, stem cells and the microenvironment. *Development*, 142(6), 1028–1042. <https://doi.org/10.1242/dev.087643>
- Jerkic, M., & Letarte, M. (2015). Increased endothelial cell permeability in endoglin-deficient cells. *The FASEB Journal*, 29(9), 3678–3688. <https://doi.org/10.1096/fj.14-269258>
- Jin, Z., Du, Y., Schwaid, A. G., Asterholm, I. W., Scherer, P. E., Saghatelian, A., & Wan, Y. (2015). Maternal Adiponectin Controls Milk Composition to Prevent Neonatal Inflammation. *Endocrinology*, 156(4), 1504–1513. <https://doi.org/10.1210/en.2014-1738>
- Jones, F. E., Welte, T., Fu, X.-Y., & Stern, D. F. (1999). Erbb4 Signaling in the Mammary Gland Is Required for Lobuloalveolar Development and Stat5 Activation during Lactation. *The Journal of Cell Biology*, 147(1), 77–88. <https://doi.org/10.1083/jcb.147.1.77>
- Joshi, P. A., Waterhouse, P. D., Kasaian, K., Fang, H., Gulyaeva, O., Sul, H. S., Boutros, P. C., & Khokha, R. (2019). PDGFR α + stromal adipocyte progenitors transition into epithelial cells during lobulo-alveogenesis in the murine mammary gland. *Nature Communications*, 10(1), 1760. <https://doi.org/10.1038/s41467-019-09748-z>
- Kamikawa, A., Ichii, O., Yamaji, D., Imao, T., Suzuki, C., Okamatsu-Ogura, Y., Terao, A., Kon, Y., & Kimura, K. (2009). Diet-induced obesity disrupts ductal development in the mammary glands of nonpregnant mice. *Developmental Dynamics*, 238(5), 1092–1099. <https://doi.org/10.1002/dvdy.21947>
- Kanaya, N., Chang, G., Wu, X., Saeki, K., Bernal, L., Shim, H.-J., Wang, J., Warden, C., Yamamoto, T., Li, J., Park, J.-S., Synold, T., Vonderfecht, S., Rakoff, M., Neuhausen, S. L., & Chen, S. (2019). Single-cell RNA-sequencing analysis of estrogen- and endocrine-disrupting chemical-induced reorganization of mouse mammary gland. *Communications Biology*, 2(1), 406. <https://doi.org/10.1038/s42003-019-0618-9>

- Kim, Y.-J., Cho, S. Y., Yun, C. H., Moon, Y. S., Lee, T. R., & Kim, S. H. (2008). Transcriptional activation of Cidec by PPAR γ 2 in adipocyte. *Biochemical and Biophysical Research Communications*, 377(1), 297–302. <https://doi.org/10.1016/j.bbrc.2008.09.129>
- Kimura, T., Ito, Y., Einspanier, A., Tohya, K., Nobunaga, T., Tokugawa, Y., Takemura, M., Kubota, Y., Ivell, R., Matsuura, N., Saji, F., & Murata, Y. (1998). Expression and immunolocalization of the oxytocin receptor in human lactating and non-lactating mammary glands. *Human Reproduction*, 13(9), 2645–2653. <https://doi.org/10.1093/humrep/13.9.2645>
- Kitazawa, K., Hikichi, T., Nakamura, T., Nakamura, M., Sotozono, C., Masui, S., & Kinoshita, S. (2019). Direct Reprogramming Into Corneal Epithelial Cells Using a Transcriptional Network Comprising PAX6, OVOL2, and KLF4. *Cornea*, 38(1), S34–S41. <https://doi.org/10.1097/ICO.0000000000002074>
- Klopp, A., Vehling, L., Becker, A. B., Subbarao, P., Mandhane, P. J., Turvey, S. E., Lefebvre, D. L., Sears, M. R., Azad, M. B., Daley, D., Silverman, F., Hayglass, K., Kobor, M., Turvey, S., Kollmann, T., Brook, J., Ramsey, C., Macri, J., Sandford, A., ... Scott, J. (2017). Modes of Infant Feeding and the Risk of Childhood Asthma: A Prospective Birth Cohort Study. *The Journal of Pediatrics*, 190, 192-199.e2. <https://doi.org/10.1016/j.jpeds.2017.07.012>
- Kordon, E. C., & Smith, G. H. (1998). An entire functional mammary gland may comprise the progeny from a single cell. *Development*, 125(10), 1921–1930. <https://doi.org/10.1242/dev.125.10.1921>
- Korsunsky, I., Wei, K., Pohin, M., Kim, E. Y., Barone, F., Major, T., Taylor, E., Ravindran, R., Kemble, S., Watts, G. F. M., Jonsson, A. H., Jeong, Y., Athar, H., Windell, D., Kang, J. B., Friedrich, M., Turner, J., Nayar, S., Fisher, B. A., ... Raychaudhuri, S. (2022). Cross-tissue, single-cell stromal atlas identifies shared pathological fibroblast phenotypes in four chronic inflammatory diseases. *Med*, 3(7), 481-518.e14.

<https://doi.org/10.1016/j.medj.2022.05.002>

- Kotzbeck, P., Giordano, A., Mondini, E., Murano, I., Severi, I., Venema, W., Cecchini, M. P., Kershaw, E. E., Barbatelli, G., Haemmerle, G., Zechner, R., & Cinti, S. (2018). Brown adipose tissue whitening leads to brown adipocyte death and adipose tissue inflammation. *Journal of Lipid Research*, 59(5), 784–794. <https://doi.org/10.1194/jlr.M079665>
- Kouros-Mehr, H., Slorach, E. M., Sternlicht, M. D., & Werb, Z. (2006). GATA-3 Maintains the Differentiation of the Luminal Cell Fate in the Mammary Gland. *Cell*, 127(5), 1041–1055. <https://doi.org/10.1016/j.cell.2006.09.048>
- Krause, M., Sechi, A. S., Konradt, M., Monner, D., Gertler, F. B., & Wehland, J. (2000). Fyn-Binding Protein (Fyb)/Slp-76–Associated Protein (Slap), Ena/Vasodilator-Stimulated Phosphoprotein (Vasp) Proteins and the Arp2/3 Complex Link T Cell Receptor (Tcr) Signaling to the Actin Cytoskeleton. *The Journal of Cell Biology*, 149(1), 181–194. <https://doi.org/10.1083/jcb.149.1.181>
- Kugyelka, J. G., Rasmussen, K. M., & Frongillo, E. A. (2004). Maternal Obesity is Negatively Associated with Breastfeeding Success among Hispanic but Not Black Women. *The Journal of Nutrition*, 134(7), 1746–1753. <https://doi.org/10.1093/jn/134.7.1746>
- Kumar, T., Nee, K., Wei, R., He, S., Nguyen, Q. H., Bai, S., Blake, K., Pein, M., Gong, Y., Sei, E., Hu, M., Casasent, A. K., Thennavan, A., Li, J., Tran, T., Chen, K., Nilges, B., Kashikar, N., Braubach, O., ... Navin, N. (2023). A spatially resolved single-cell genomic atlas of the adult human breast. *Nature*, 620(7972), 181–191. <https://doi.org/10.1038/s41586-023-06252-9>
- LaMarca, H. L., Visbal, A. P., Creighton, C. J., Liu, H., Zhang, Y., Behbod, F., & Rosen, J. M. (2010). CCAAT/Enhancer Binding Protein Beta Regulates Stem Cell Activity and Specifies Luminal Cell Fate in the Mammary Gland. *Stem Cells*, 28(3), 535–544. <https://doi.org/10.1002/stem.297>

- Landskroner-Eiger, S., Park, J., Israel, D., Pollard, J. W., & Scherer, P. E. (2010). Morphogenesis of the developing mammary gland: Stage-dependent impact of adipocytes. *Developmental Biology*, 344(2), 968–978. <https://doi.org/10.1016/j.ydbio.2010.06.019>
- Lee, H. J., Gallego-Ortega, D., Ledger, A., Schramek, D., Joshi, P., Szwarc, M. M., Cho, C., Lydon, J. P., Khokha, R., Penninger, J. M., & Ormandy, C. J. (2013). Progesterone drives mammary secretory differentiation via RankL-mediated induction of Elf5 in luminal progenitor cells. *Development*, 140(7), 1397–1401. <https://doi.org/10.1242/dev.088948>
- Lee, H. J., Hinshelwood, R. A., Bouras, T., Gallego-Ortega, D., Valdés-Mora, F., Blazek, K., Visvader, J. E., Clark, S. J., & Ormandy, C. J. (2011). Lineage Specific Methylation of the *Elf5* Promoter in Mammary Epithelial Cells. *Stem Cells*, 29(10), 1611–1619. <https://doi.org/10.1002/stem.706>
- Lee, Y.-H., Petkova, A. P., Mottillo, E. P., & Granneman, J. G. (2012). In Vivo Identification of Bipotential Adipocyte Progenitors Recruited by β 3-Adrenoceptor Activation and High-Fat Feeding. *Cell Metabolism*, 15(4), 480–491. <https://doi.org/10.1016/j.cmet.2012.03.009>
- Li, C. M.-C., Shapiro, H., Tsibikas, C., Selfors, L. M., Chen, H., Rosenbluth, J., Moore, K., Gupta, K. P., Gray, G. K., Oren, Y., Steinbaugh, M. J., Guerrero, J. L., Pinello, L., Regev, A., & Brugge, J. S. (2020). Aging-Associated Alterations in Mammary Epithelia and Stroma Revealed by Single-Cell RNA Sequencing. *Cell Reports*, 33(13), 108566. <https://doi.org/10.1016/j.celrep.2020.108566>
- Li, H., Liu, P., Xu, S., Li, Y., Dekker, J. D., Li, B., Fan, Y., Zhang, Z., Hong, Y., Yang, G., Tang, T., Ren, Y., Tucker, H. O., Yao, Z., & Guo, X. (2017). FOXP1 controls mesenchymal stem cell commitment and senescence during skeletal aging. *Journal of Clinical Investigation*, 127(4), 1241–1253. <https://doi.org/10.1172/JCI89511>

- Li, L., Huang, J., & Liu, Y. (2024). The extracellular matrix glycoprotein fibrillin-1 in health and disease. *Frontiers in Cell and Developmental Biology*, 11, 1302285. <https://doi.org/10.3389/fcell.2023.1302285>
- Li, Y., Kang, H., Chu, Y., Jin, Y., Zhang, L., Yang, R., Zhang, Z., Zhao, S., & Zhou, L. (2018). Cidec differentially regulates lipid deposition and secretion through two tissue-specific isoforms. *Gene*, 641, 265–271. <https://doi.org/10.1016/j.gene.2017.10.069>
- Li, Y., Mao, A. S., Seo, B. R., Zhao, X., Gupta, S. K., Chen, M., Han, Y. L., Shih, T.-Y., Mooney, D. J., & Guo, M. (2020). Compression-induced dedifferentiation of adipocytes promotes tumor progression. *Science Advances*, 6(4), eaax5611. <https://doi.org/10.1126/sciadv.aax5611>
- Lin, Y., & Li, Q. (2007). Expression and function of leptin and its receptor in mouse mammary gland. *Science in China Series C: Life Sciences*, 50(5), 669–675. <https://doi.org/10.1007/s11427-007-0077-2>
- Liu, X., Ory, V., Chapman, S., Yuan, H., Albanese, C., Kallakury, B., Timofeeva, O. A., Nealon, C., Dakic, A., Simic, V., Haddad, B. R., Rhim, J. S., Dritschilo, A., Riegel, A., McBride, A., & Schlegel, R. (2012). ROCK Inhibitor and Feeder Cells Induce the Conditional Reprogramming of Epithelial Cells. *The American Journal of Pathology*, 180(2), 599–607. <https://doi.org/10.1016/j.ajpath.2011.10.036>
- Liu, X., Robinson, G. W., Wagner, K. U., Garrett, L., Wynshaw-Boris, A., & Hennighausen, L. (1997). Stat5a is mandatory for adult mammary gland development and lactogenesis. *Genes & Development*, 11(2), 179–186. <https://doi.org/10.1101/gad.11.2.179>
- Long, W., Wagner, K.-U., Lloyd, K. C. K., Binart, N., Shillingford, J. M., Hennighausen, L., & Jones, F. E. (2003). Impaired differentiation and lactational failure of *Erbb4*-deficient mammary glands identify ERBB4 as an obligate mediator of STAT5. *Development*, 130(21), 5257–5268.

<https://doi.org/10.1242/dev.00715>

- Lyons, K. E., Ryan, C. A., Dempsey, E. M., Ross, R. P., & Stanton, C. (2020). Breast Milk, a Source of Beneficial Microbes and Associated Benefits for Infant Health. *Nutrients*, 12(4), 1039. <https://doi.org/10.3390/nu12041039>
- Lyons, W. R. (1958). Hormonal synergism in mammary growth. *Proceedings of the Royal Society of London. Series B - Biological Sciences*, 149(936), 303–325. <https://doi.org/10.1098/rspb.1958.0071>
- Ma, Y., Gao, M., & Liu, D. (2016). Preventing High Fat Diet-induced Obesity and Improving Insulin Sensitivity through Neuregulin 4 Gene Transfer. *Scientific Reports*, 6(1), 26242. <https://doi.org/10.1038/srep26242>
- Ma, Z., Kang, S. W., Condie, B. G., & Manley, N. R. (2024). Mechanisms underlying the direct programming of mouse embryonic fibroblasts to thymic epithelial cells by FOXN1. *Development*, 151(14), dev202730. <https://doi.org/10.1242/dev.202730>
- Makarem, M., Kannan, N., Nguyen, L. V., Knapp, D. J. H. F., Balani, S., Prater, M. D., Stingl, J., Raouf, A., Nemirovsky, O., Eirew, P., & Eaves, C. J. (2013). Developmental Changes in the in Vitro Activated Regenerative Activity of Primitive Mammary Epithelial Cells. *PLoS Biology*, 11(8), e1001630. <https://doi.org/10.1371/journal.pbio.1001630>
- Mallepell, S., Krust, A., Chambon, P., & Brisken, C. (2006). Paracrine signaling through the epithelial estrogen receptor α is required for proliferation and morphogenesis in the mammary gland. *Proceedings of the National Academy of Sciences*, 103(7), 2196–2201. <https://doi.org/10.1073/pnas.0510974103>
- Mao, J., Molenaar, A., Wheeler, T., & Seyfert, H. (2002). STAT5 binding contributes to lactational stimulation of promoter III expressing the bovine acetyl-CoA carboxylase alpha-encoding gene in the mammary gland. *Journal of Molecular Endocrinology*, 29(1), 73–88.

<https://doi.org/10.1677/jme.0.0290073>

Matsunaga, K., Tsugami, Y., Kumai, A., Suzuki, T., Nishimura, T., & Kobayashi, K. (2018). IL-1 β directly inhibits milk lipid production in lactating mammary epithelial cells concurrently with enlargement of cytoplasmic lipid droplets. *Experimental Cell Research*, 370(2), 365–372.

<https://doi.org/10.1016/j.yexcr.2018.06.038>

Matsuo, J., Mon, N. N., Douchi, D., Yamamura, A., Kulkarni, M., Heng, D. L., Chen, S., Nuttonmanit, N., Li, Y., Yang, H., Lee, M. Y., Tam, W. L., Osato, M., Chuang, L. S. H., & Ito, Y. (2022). A Runx1-enhancer Element eR1 Identified Lineage Restricted Mammary Luminal Stem Cells. *Stem Cells*, 40(1), 112–122. <https://doi.org/10.1093/stmcls/sxab009>

Mauduit, O., Delcroix, V., Wong, A., Ivanova, A., Miles, L., Lee, H. S., & Makarenkova, H. (2024). A closer look into the cellular and molecular biology of myoepithelial cells across various exocrine glands. *The Ocular Surface*, 31, 63–80. <https://doi.org/10.1016/j.jtos.2023.12.003>

Mitani, T., Watanabe, S., Wada, K., Fujii, H., Nakamura, S., & Katayama, S. (2020). Intracellular cAMP contents regulate NAMPT expression via induction of C/EBP β in adipocytes. *Biochemical and Biophysical Research Communications*, 522(3), 770–775. <https://doi.org/10.1016/j.bbrc.2019.11.165>

Monks, J., Orlicky, D. J., Libby, A. E., Dzieciatkowska, M., Ladinsky, M. S., & McManaman, J. L. (2022). Perilipin-2 promotes lipid droplet-plasma membrane interactions that facilitate apocrine lipid secretion in secretory epithelial cells of the mouse mammary gland. *Frontiers in Cell and Developmental Biology*, 10, 958566. <https://doi.org/10.3389/fcell.2022.958566>

Morroni, M., Giordano, A., Zingaretti, M. C., Boiani, R., De Matteis, R., Kahn, B. B., Nisoli, E., Tonello, C., Pisoschi, C., Luchetti, M. M., Marelli, M., & Cinti, S.

- (2004). Reversible transdifferentiation of secretory epithelial cells into adipocytes in the mammary gland. *Proceedings of the National Academy of Sciences*, 101(48), 16801–16806.
<https://doi.org/10.1073/pnas.0407647101>
- Moynihan, A. T., Hehir, M. P., Glavey, S. V., Smith, T. J., & Morrison, J. J. (2006). Inhibitory effect of leptin on human uterine contractility in vitro. *American Journal of Obstetrics and Gynecology*, 195(2), 504–509.
<https://doi.org/10.1016/j.ajog.2006.01.106>
- Newman, A. M., Steen, C. B., Liu, C. L., Gentles, A. J., Chaudhuri, A. A., Scherer, F., Khodadoust, M. S., Esfahani, M. S., Luca, B. A., Steiner, D., Diehn, M., & Alizadeh, A. A. (2019). Determining cell type abundance and expression from bulk tissues with digital cytometry. *Nature Biotechnology*, 37(7), 773–782. <https://doi.org/10.1038/s41587-019-0114-2>
- Nguyen-Ngoc, K.-V., Shamir, E. R., Huebner, R. J., Beck, J. N., Cheung, K. J., & Ewald, A. J. (2015). 3D Culture Assays of Murine Mammary Branching Morphogenesis and Epithelial Invasion. In C. M. Nelson (Ed.), *Tissue Morphogenesis* (Vol. 1189, pp. 135–162). Springer New York.
https://doi.org/10.1007/978-1-4939-1164-6_10
- Niaudet, C., Hofmann, J. J., Mäe, M. A., Jung, B., Gaengel, K., Vanlandewijck, M., Ekvärn, E., Salvado, M. D., Mehlem, A., Al Sayegh, S., He, L., Lebouvier, T., Castro-Freire, M., Katayama, K., Hultenby, K., Moessinger, C., Tannenberg, P., Cunha, S., Pietras, K., ... Betsholtz, C. (2015). Gpr116 Receptor Regulates Distinctive Functions in Pneumocytes and Vascular Endothelium. *PLOS ONE*, 10(9), e0137949.
<https://doi.org/10.1371/journal.pone.0137949>
- Oakes, S. R., Naylor, M. J., Asselin-Labat, M.-L., Blazek, K. D., Gardiner-Garden, M., Hilton, H. N., Kazlauskas, M., Pritchard, M. A., Chodosh, L. A., Pfeffer, P. L., Lindeman, G. J., Visvader, J. E., & Ormandy, C. J. (2008). The Ets

- transcription factor Elf5 specifies mammary alveolar cell fate. *Genes & Development*, 22(5), 581–586. <https://doi.org/10.1101/gad.1614608>
- Ou-yang, Y., & Dai, M. (2023). Screening for genes, miRNAs and transcription factors of adipogenic differentiation and dedifferentiation of mesenchymal stem cells. *Journal of Orthopaedic Surgery and Research*, 18(1), 46. <https://doi.org/10.1186/s13018-023-03514-0>
- Park, J., Hu, R., Qian, Y., Xiong, S., El-Sabbagh, A. S., Ibrahim, M., Wang, J., Xu, Z., Chen, Z., Song, Q., Song, Z., Yan, G., Mahmoud, A. M., He, Y., Layden, B. T., Chen, J., Ong, S.-G., Xu, P., & Jiang, Y. (2024). Estrogen counteracts age-related decline in beige adipogenesis through the NAMPT-regulated ER stress response. *Nature Aging*, 4(6), 839–853. <https://doi.org/10.1038/s43587-024-00633-z>
- Patel, S., Sparman, N. Z. R., Arneson, D., Alvarsson, A., Santos, L. C., Duesman, S. J., Centonze, A., Hathaway, E., Ahn, I. S., Diamante, G., Cely, I., Cho, C. H., Talari, N. K., Rajbhandari, A. K., Goedeke, L., Wang, P., Butte, A. J., Blanpain, C., Chella Krishnan, K., ... Rajbhandari, P. (2023). Mammary duct luminal epithelium controls adipocyte thermogenic programme. *Nature*, 620(7972), 192–199. <https://doi.org/10.1038/s41586-023-06361-5>
- Pervolarakis, N., Nguyen, Q. H., Williams, J., Gong, Y., Gutierrez, G., Sun, P., Jhutty, D., Zheng, G. X. Y., Nemec, C. M., Dai, X., Watanabe, K., & Kessenbrock, K. (2020). Integrated Single-Cell Transcriptomics and Chromatin Accessibility Analysis Reveals Regulators of Mammary Epithelial Cell Identity. *Cell Reports*, 33(3), 108273. <https://doi.org/10.1016/j.celrep.2020.108273>
- Pezet, A., Buteau, H., Kelly, P. A., & Edery, M. (1997). The last proline of Box 1 is essential for association with JAK2 and functional activation of the prolactin receptor. *Molecular and Cellular Endocrinology*, 129(2), 199–208. [https://doi.org/10.1016/S0303-7207\(97\)00063-4](https://doi.org/10.1016/S0303-7207(97)00063-4)

- Plowman, G. D., Green, J. M., Culouscou, J.-M., Carlton, G. W., Rothwell, V. M., & Buckley, S. (1993). Heregulin induces tyrosine phosphorylation of HER4/p180erbB4. *Nature*, 366(6454), 473–475.
<https://doi.org/10.1038/366473a0>
- Prater, M. D., Petit, V., Alasdair Russell, I., Giraddi, R. R., Shehata, M., Menon, S., Schulte, R., Kalajzic, I., Rath, N., Olson, M. F., Metzger, D., Faraldo, M. M., Deugnier, M.-A., Glukhova, M. A., & Stingl, J. (2014). Mammary stem cells have myoepithelial cell properties. *Nature Cell Biology*, 16(10), 942–950.
<https://doi.org/10.1038/ncb3025>
- Prokesch, A., Smorlesi, A., Perugini, J., Manieri, M., Ciarmela, P., Mondini, E., Trajanoski, Z., Kristiansen, K., Giordano, A., Bogner-Strauss, J. G., & Cinti, S. (2014). Molecular Aspects of Adipoepithelial Transdifferentiation in Mouse Mammary Gland. *Stem Cells*, 32(10), 2756–2766.
<https://doi.org/10.1002/stem.1756>
- Queipo-Ortuño, M. I., Escoté, X., Ceperuelo-Mallafré, V., Garrido-Sánchez, L., Miranda, M., Clemente-Postigo, M., Pérez-Pérez, R., Peral, B., Cardona, F., Fernández-Real, J. M., Tinahones, F. J., & Vendrell, J. (2012). FABP4 Dynamics in Obesity: Discrepancies in Adipose Tissue and Liver Expression Regarding Circulating Plasma Levels. *PLoS ONE*, 7(11), e48605.
<https://doi.org/10.1371/journal.pone.0048605>
- Ramji, N., Challa, S., Murphy, P. A., Quinlan, J., & Crane, J. M. G. (2017). A comparison of breastfeeding rates by obesity class. *The Journal of Maternal-Fetal & Neonatal Medicine*, 31(22), 3021–3026.
<https://doi.org/10.1080/14767058.2017.1362552>
- Randall, K. L., Flesch, I. E. A., Mei, Y., Miosge, L. A., Aye, R., Yu, Z., Domaschenz, H., Hollett, N. A., Russell, T. A., Stefanovic, T., Wong, Y. C., Seneviratne, S., Ballard, F., Hernandez Gallardo, R., Croft, S. N., Goodnow, C. C., Bertram, E. M., Enders, A., & Tscharke, D. C. (2024). DOCK2 Deficiency Causes

- Defects in Antiviral T-Cell Responses and Impaired Control of Herpes Simplex Virus Infection. *The Journal of Infectious Diseases*, 230(3), e712–e721. <https://doi.org/10.1093/infdis/jiae077>
- Reed, A. D., Pensa, S., Steif, A., Stenning, J., Kunz, D. J., He, P., Twigger, A.-J., Kania, K., Barrow-McGee, R., Goulding, I., Gomm, J. J., Jones, L., Marioni, J. C., & Khaled, W. T. (2023). *A Human Breast Cell Atlas Mapping the Homeostatic Cellular Shifts in the Adult Breast*. *Cancer Biology*. <https://doi.org/10.1101/2023.04.21.537845>
- Regan, J. L., & Smalley, M. J. (2020). Integrating single-cell RNA-sequencing and functional assays to decipher mammary cell states and lineage hierarchies. *Npj Breast Cancer*, 6(1), 32. <https://doi.org/10.1038/s41523-020-00175-8>
- Reichenstein, M., Rauner, G., & Barash, I. (2011). Conditional repression of STAT5 expression during lactation reveals its exclusive roles in mammary gland morphology, milk-protein gene expression, and neonate growth. *Molecular Reproduction and Development*, 78(8), 585–596. <https://doi.org/10.1002/mrd.21345>
- Rios, A. C., Fu, N. Y., Lindeman, G. J., & Visvader, J. E. (2014). In situ identification of bipotent stem cells in the mammary gland. *Nature*, 506(7488), 322–327. <https://doi.org/10.1038/nature12948>
- Rodda, L. B., Lu, E., Bennett, M. L., Sokol, C. L., Wang, X., Luther, S. A., Barres, B. A., Luster, A. D., Ye, C. J., & Cyster, J. G. (2018). Single-Cell RNA Sequencing of Lymph Node Stromal Cells Reveals Niche-Associated Heterogeneity. *Immunity*, 48(5), 1014-1028.e6. <https://doi.org/10.1016/j.jimmuni.2018.04.006>
- Rosell, M., Kaforou, M., Frontini, A., Okolo, A., Chan, Y.-W., Nikolopoulou, E., Millership, S., Fenech, M. E., MacIntyre, D., Turner, J. O., Moore, J. D., Blackburn, E., Gullick, W. J., Cinti, S., Montana, G., Parker, M. G., & Christian, M. (2014). Brown and white adipose tissues: Intrinsic differences

- in gene expression and response to cold exposure in mice. *American Journal of Physiology-Endocrinology and Metabolism*, 306(8), E945–E964.
<https://doi.org/10.1152/ajpendo.00473.2013>
- Rosen, E. D. (2005). The transcriptional basis of adipocyte development. *Prostaglandins, Leukotrienes and Essential Fatty Acids*, 73(1), 31–34.
<https://doi.org/10.1016/j.plefa.2005.04.004>
- Rosen, E. D., & MacDougald, O. A. (2006). Adipocyte differentiation from the inside out. *Nature Reviews Molecular Cell Biology*, 7(12), 885–896.
<https://doi.org/10.1038/nrm2066>
- Rossi, E., Smadja, D. M., Boscolo, E., Langa, C., Arevalo, M. A., Pericacho, M., Gamella-Pozuelo, L., Kauskot, A., Botella, L. M., Gaussem, P., Bischoff, J., Lopez-Novoa, J. M., & Bernabeu, C. (2016). Endoglin regulates mural cell adhesion in the circulatory system. *Cellular and Molecular Life Sciences*, 73(8), 1715–1739. <https://doi.org/10.1007/s00018-015-2099-4>
- Ruiz, M., Devkota, R., Kaper, D., Ruhanen, H., Busayavalasa, K., Radović, U., Henricsson, M., Käkelä, R., Borén, J., & Pilon, M. (2023). AdipoR2 recruits protein interactors to promote fatty acid elongation and membrane fluidity. *Journal of Biological Chemistry*, 299(6), 104799.
<https://doi.org/10.1016/j.jbc.2023.104799>
- Russell, T. D., Palmer, C. A., Orlicky, D. J., Fischer, A., Rudolph, M. C., Neville, M. C., & McManaman, J. L. (2007). Cytoplasmic lipid droplet accumulation in developing mammary epithelial cells: Roles of adipophilin and lipid metabolism. *Journal of Lipid Research*, 48(7), 1463–1475.
<https://doi.org/10.1194/jlr.M600474-JLR200>
- Russell, T. D., Schaack, J., Orlicky, D. J., Palmer, C., Chang, B. H.-J., Chan, L., & McManaman, J. L. (2011). Adipophilin regulates maturation of cytoplasmic lipid droplets and alveolae in differentiating mammary glands. *Journal of Cell Science*, 124(19), 3247–3253. <https://doi.org/10.1242/jcs.082974>

- Saben, J. L., Bales, E. S., Jackman, M. R., Orlicky, D., MacLean, P. S., & McManaman, J. L. (2014). Maternal Obesity Reduces Milk Lipid Production in Lactating Mice by Inhibiting Acetyl-CoA Carboxylase and Impairing Fatty Acid Synthesis. *PLoS ONE*, 9(5), e98066. <https://doi.org/10.1371/journal.pone.0098066>
- Shackleton, M., Vaillant, F., Simpson, K. J., Stingl, J., Smyth, G. K., Asselin-Labat, M.-L., Wu, L., Lindeman, G. J., & Visvader, J. E. (2006). Generation of a functional mammary gland from a single stem cell. *Nature*, 439(7072), 84–88. <https://doi.org/10.1038/nature04372>
- Shan, D., Li, J., Wu, L., Li, D., Hurov, J., Tobin, J. F., Gimeno, R. E., & Cao, J. (2010). GPAT3 and GPAT4 are regulated by insulin-stimulated phosphorylation and play distinct roles in adipogenesis. *Journal of Lipid Research*, 51(7), 1971–1981. <https://doi.org/10.1194/jlr.M006304>
- Shehata, M., Teschendorff, A., Sharp, G., Novcic, N., Russell, I. A., Avril, S., Prater, M., Eirew, P., Caldas, C., Watson, C. J., & Stingl, J. (2012). Phenotypic and functional characterisation of the luminal cell hierarchy of the mammary gland. *Breast Cancer Research*, 14(5), R134. <https://doi.org/10.1186/bcr3334>
- Shepperd, L. A., Meadows, J. C., Sochaj, A. M., Lancaster, T. C., Zou, J., Buttrick, G. J., Rappaport, J., Hardwick, K. G., & Millar, J. B. A. (2012). Phosphodependent Recruitment of Bub1 and Bub3 to Spc7/KNL1 by Mph1 Kinase Maintains the Spindle Checkpoint. *Current Biology*, 22(10), 891–899. <https://doi.org/10.1016/j.cub.2012.03.051>
- Shi, H. B., Zhang, C. H., Zhao, W., Luo, J., & Loor, J. J. (2017). Peroxisome proliferator-activated receptor delta facilitates lipid secretion and catabolism of fatty acids in dairy goat mammary epithelial cells. *Journal of Dairy Science*, 100(1), 797–806. <https://doi.org/10.3168/jds.2016-11647>
- Shi, M., Li, Z., Miao, Z., Guo, Y., & Yi, L. (2019). Interleukin-15 inhibits adipogenic

differentiation of cattle bone marrow-derived mesenchymal stem cells via regulating the crosstalk between signal transducer and activator of transcription 5A and Akt signalling. *Biochemical and Biophysical Research Communications*, 517(2), 346–352.

<https://doi.org/10.1016/j.bbrc.2019.07.068>

Shin, H. Y., Willi, M., Yoo, K. H., Zeng, X., Wang, C., Metser, G., & Hennighausen, L. (2016). Hierarchy within the mammary STAT5-driven Wap super-enhancer. *Nature Genetics*, 48(8), 904–911.

<https://doi.org/10.1038/ng.3606>

Silberstein, G. B., & Daniel, C. W. (1982). Glycosaminoglycans in the basal lamina and extracellular matrix of the developing mouse mammary duct. *Developmental Biology*, 90(1), 215–222. [https://doi.org/10.1016/0012-1606\(82\)90228-7](https://doi.org/10.1016/0012-1606(82)90228-7)

Simian, M., Hirai, Y., Navre, M., Werb, Z., Lochter, A., & Bissell, M. J. (2001). The interplay of matrix metalloproteinases, morphogens and growth factors is necessary for branching of mammary epithelial cells. *Development*, 128(16), 3117–3131. <https://doi.org/10.1242/dev.128.16.3117>

Sizemore, G. M., Sizemore, S. T., Pal, B., Booth, C. N., Seachrist, D. D., Abdul-Karim, F. W., Kume, T., & Keri, R. A. (2013). FOXC1 Is Enriched in the Mammary Luminal Progenitor Population, but Is Not Necessary for Mouse Mammary Ductal Morphogenesis1. *Biology of Reproduction*, 89(1). <https://doi.org/10.1095/biolreprod.113.108001>

Smith, S. (1980). Mechanism of Chain Length Determination in Biosynthesis of Milk Fatty Acids. *Journal of Dairy Science*, 63(2), 337–352. [https://doi.org/10.3168/jds.S0022-0302\(80\)82935-3](https://doi.org/10.3168/jds.S0022-0302(80)82935-3)

Song, Y., Fioramonti, M., Bouvencourt, G., Dubois, C., Blanpain, C., & Van Keymeulen, A. (2023). Cell type and stage specific transcriptional, chromatin and cell-cell communication landscapes in the mammary gland.

Heliyon, 9(7), e17842. <https://doi.org/10.1016/j.heliyon.2023.e17842>

- Stingl, J., Eirew, P., Ricketson, I., Shackleton, M., Vaillant, F., Choi, D., Li, H. I., & Eaves, C. J. (2006). Purification and unique properties of mammary epithelial stem cells. *Nature*, 439(7079), 993–997. <https://doi.org/10.1038/nature04496>
- Student, A. K., Hsu, R. Y., & Lane, M. D. (1980). Induction of fatty acid synthetase synthesis in differentiating 3T3-L1 preadipocytes. *Journal of Biological Chemistry*, 255(10), 4745–4750. [https://doi.org/10.1016/S0021-9258\(19\)85559-X](https://doi.org/10.1016/S0021-9258(19)85559-X)
- Suburu, J., Shi, L., Wu, J., Wang, S., Samuel, M., Thomas, M. J., Kock, N. D., Yang, G., Kridel, S., & Chen, Y. Q. (2014). Fatty acid synthase is required for mammary gland development and milk production during lactation. *American Journal of Physiology-Endocrinology and Metabolism*, 306(10), E1132–E1143. <https://doi.org/10.1152/ajpendo.00514.2013>
- Sumbal, J., Chiche, A., Charifou, E., Koledova, Z., & Li, H. (2020). Primary Mammary Organoid Model of Lactation and Involution. *Frontiers in Cell and Developmental Biology*, 8, 68. <https://doi.org/10.3389/fcell.2020.00068>
- Sun, H., Miao, Z., Zhang, X., Chan, U. I., Su, S. M., Guo, S., Wong, C. K. H., Xu, X., & Deng, C.-X. (2018). Single-cell RNA-Seq reveals cell heterogeneity and hierarchy within mouse mammary epithelia. *Journal of Biological Chemistry*, 293(22), 8315–8329. <https://doi.org/10.1074/jbc.RA118.002297>
- Sun, Y., Luo, J., Zhu, J., Shi, H., Li, J., Qiu, S., Wang, P., & Loor, J. J. (2016). Effect of short-chain fatty acids on triacylglycerol accumulation, lipid droplet formation and lipogenic gene expression in goat mammary epithelial cells. *Animal Science Journal*, 87(2), 242–249. <https://doi.org/10.1111/asj.12420>
- Tansey, J. T., Sztalryd, C., Gruia-Gray, J., Roush, D. L., Zee, J. V., Gavrilova, O., Reitman, M. L., Deng, C.-X., Li, C., Kimmel, A. R., & Londos, C. (2001). Perilipin ablation results in a lean mouse with aberrant adipocyte lipolysis,

- enhanced leptin production, and resistance to diet-induced obesity. *Proceedings of the National Academy of Sciences*, 98(11), 6494–6499. <https://doi.org/10.1073/pnas.101042998>
- Tarulli, G. A., De Silva, D., Ho, V., Kunasegaran, K., Ghosh, K., Tan, B. C., Bulavin, D. V., & Pietersen, A. M. (2013). Hormone-sensing cells require Wip1 for paracrine stimulation in normal and premalignant mammary epithelium. *Breast Cancer Research*, 15(1), R10. <https://doi.org/10.1186/bcr3381>
- Teglund, S., McKay, C., Schuetz, E., Van Deursen, J. M., Stravopodis, D., Wang, D., Brown, M., Bodner, S., Grosveld, G., & Ihle, J. N. (1998). Stat5a and Stat5b Proteins Have Essential and Nonessential, or Redundant, Roles in Cytokine Responses. *Cell*, 93(5), 841–850. [https://doi.org/10.1016/S0092-8674\(00\)81444-0](https://doi.org/10.1016/S0092-8674(00)81444-0)
- Tidcombe, H., Jackson-Fisher, A., Mathers, K., Stern, D. F., Gassmann, M., & Golding, J. P. (2003). Neural and mammary gland defects in ErbB4 knockout mice genetically rescued from embryonic lethality. *Proceedings of the National Academy of Sciences*, 100(14), 8281–8286. <https://doi.org/10.1073/pnas.1436402100>
- Turksin, R., Bel, S., Galjaard, S., & Devlieger, R. (2014). Maternal obesity and breastfeeding intention, initiation, intensity and duration: A systematic review. *Maternal & Child Nutrition*, 10(2), 166–183. <https://doi.org/10.1111/j.1740-8709.2012.00439.x>
- Twigger, A.-J., Engelbrecht, L. K., Bach, K., Schultz-Pernice, I., Pensa, S., Stenning, J., Petricca, S., Scheel, C. H., & Khaled, W. T. (2022). Transcriptional changes in the mammary gland during lactation revealed by single cell sequencing of cells from human milk. *Nature Communications*, 13(1), 562. <https://doi.org/10.1038/s41467-021-27895-0>
- Ushijima, M., Uruno, T., Nishikimi, A., Sanematsu, F., Kamikaseda, Y., Kunimura, K., Sakata, D., Okada, T., & Fukui, Y. (2018). The Rac Activator DOCK2

- Mediates Plasma Cell Differentiation and IgG Antibody Production. *Frontiers in Immunology*, 9, 243. <https://doi.org/10.3389/fimmu.2018.00243>
- Vafaizadeh, V., Klemmt, P., Brendel, C., Weber, K., Doebele, C., Britt, K., Grez, M., Fehse, B., Desrivières, S., & Groner, B. (2010). Mammary Epithelial Reconstitution with Gene-Modified Stem Cells Assigns Roles to Stat5 in Luminal Alveolar Cell Fate Decisions, Differentiation, Involution, and Mammary Tumor Formation. *Stem Cells*, 28(5), 928–938. <https://doi.org/10.1002/stem.407>
- Valdés-Mora, F., Salomon, R., Gloss, B. S., Law, A. M. K., Venhuizen, J., Castillo, L., Murphy, K. J., Magenau, A., Papanicolaou, M., Rodriguez De La Fuente, L., Roden, D. L., Colino-Sanguino, Y., Kikhtyak, Z., Farbehi, N., Conway, J. R. W., Sikta, N., Oakes, S. R., Cox, T. R., O'Donoghue, S. I., ... Gallego-Ortega, D. (2021). Single-cell transcriptomics reveals involution mimicry during the specification of the basal breast cancer subtype. *Cell Reports*, 35(2), 108945. <https://doi.org/10.1016/j.celrep.2021.108945>
- Van Keymeulen, A., Rocha, A. S., Ousset, M., Beck, B., Bouvencourt, G., Rock, J., Sharma, N., Dekoninck, S., & Blanpain, C. (2011). Distinct stem cells contribute to mammary gland development and maintenance. *Nature*, 479(7372), 189–193. <https://doi.org/10.1038/nature10573>
- Vapola, M. H., Rokka, A., Sormunen, R. T., Alhonen, L., Schmitz, W., Conzelmann, E., Wäri, A., Grunau, S., Antonenkov, V. D., & Hiltunen, J. K. (2014). Peroxisomal membrane channel Pxmp2 in the mammary fat pad is essential for stromal lipid homeostasis and for development of mammary gland epithelium in mice. *Developmental Biology*, 391(1), 66–80. <https://doi.org/10.1016/j.ydbio.2014.03.022>
- Wakao, H., Gouilleux, F., & Groner, B. (1995). Mammary gland factor (MGF) is a novel member of the cytokine regulated transcription factor gene family and confers the prolactin response. *The EMBO Journal*, 14(4), 854–855.

<https://doi.org/10.1002/j.1460-2075.1995.tb07064.x>

Wang, C., Christin, J. R., Oktay, M. H., & Guo, W. (2017). Lineage-Biased Stem Cells Maintain Estrogen-Receptor-Positive and -Negative Mouse Mammary Luminal Lineages. *Cell Reports*, 18(12), 2825–2835.
<https://doi.org/10.1016/j.celrep.2017.02.071>

Wang, C., Xie, T., Li, X., Lu, X., Xiao, C., Liu, P., Xu, F., & Zhang, B. (2024). Effect of in vivo culture conditions on the proliferation and differentiation of rat adipose-derived stromal cells. *Mechanisms of Ageing and Development*, 219, 111935. <https://doi.org/10.1016/j.mad.2024.111935>

Wang, G.-X., Zhao, X.-Y., Meng, Z.-X., Kern, M., Dietrich, A., Chen, Z., Cozacov, Z., Zhou, D., Okunade, A. L., Su, X., Li, S., Blüher, M., & Lin, J. D. (2014). The brown fat-enriched secreted factor Nrg4 preserves metabolic homeostasis through attenuation of hepatic lipogenesis. *Nature Medicine*, 20(12), 1436–1443. <https://doi.org/10.1038/nm.3713>

Wang, L., Collins, C., Ratliff, M., Xie, B., & Wang, Y. (2017). Breastfeeding Reduces Childhood Obesity Risks. *Childhood Obesity*, 13(3), 197–204.
<https://doi.org/10.1089/chi.2016.0210>

Wang, Q. A., Song, A., Chen, W., Schwalie, P. C., Zhang, F., Vishvanath, L., Jiang, L., Ye, R., Shao, M., Tao, C., Gupta, R. K., Deplancke, B., & Scherer, P. E. (2018). Reversible De-differentiation of Mature White Adipocytes into Preadipocyte-like Precursors during Lactation. *Cell Metabolism*, 28(2), 282–288.e3. <https://doi.org/10.1016/j.cmet.2018.05.022>

Wang, S., Cao, S., Arhatte, M., Li, D., Shi, Y., Kurz, S., Hu, J., Wang, L., Shao, J., Atzberger, A., Wang, Z., Wang, C., Zang, W., Fleming, I., Wettschureck, N., Honoré, E., & Offermanns, S. (2020). Adipocyte Piezo1 mediates obesogenic adipogenesis through the FGF1/FGFR1 signaling pathway in mice. *Nature Communications*, 11(1), 2303. <https://doi.org/10.1038/s41467-020-16026-w>

- Wang, W., Cen, Y., Lu, Z., Xu, Y., Sun, T., Xiao, Y., Liu, W., Li, J. J., & Wang, C. (2024). scCDC: A computational method for gene-specific contamination detection and correction in single-cell and single-nucleus RNA-seq data. *Genome Biology*, 25(1), 136. <https://doi.org/10.1186/s13059-024-03284-w>
- Williams, J. M., & Daniel, C. W. (1983). Mammary ductal elongation: Differentiation of myoepithelium and basal lamina during branching morphogenesis. *Developmental Biology*, 97(2), 274–290. [https://doi.org/10.1016/0012-1606\(83\)90086-6](https://doi.org/10.1016/0012-1606(83)90086-6)
- Wiseman, B. S., & Werb, Z. (2002). Stromal Effects on Mammary Gland Development and Breast Cancer. *Science*, 296(5570), 1046–1049. <https://doi.org/10.1126/science.1067431>
- Wu, Y., Wu, C., Shi, T., Cai, Q., Wang, T., Xiong, Y., Zhang, Y., Jiang, W., Lu, M., Chen, Z., Chen, J., Wang, J., & He, R. (2023). FAP expression in adipose tissue macrophages promotes obesity and metabolic inflammation. *Proceedings of the National Academy of Sciences*, 120(51), e2303075120. <https://doi.org/10.1073/pnas.2303075120>
- Wu, Z., Bucher, N. L. R., & Farmer, S. R. (1996). Induction of Peroxisome Proliferator-Activated Receptor γ during the Conversion of 3T3 Fibroblasts into Adipocytes Is Mediated by C/EBP β , C/EBP δ , and Glucocorticoids. *Molecular and Cellular Biology*, 16(8), 4128–4136. <https://doi.org/10.1128/MCB.16.8.4128>
- Wuidart, A., Ousset, M., Rulands, S., Simons, B. D., Van Keymeulen, A., & Blanpain, C. (2016). Quantitative lineage tracing strategies to resolve multipotency in tissue-specific stem cells. *Genes & Development*, 30(11), 1261–1277. <https://doi.org/10.1101/gad.280057.116>
- Xu, D., Zhou, S., Liu, Y., Scott, A. L., Yang, J., & Wan, F. (2024). Complement in breast milk modifies offspring gut microbiota to promote infant health. *Cell*, 187(3), 750-763.e20. <https://doi.org/10.1016/j.cell.2023.12.019>

- Xu, L., Lochhead, P., Ko, Y., Claggett, B., Leong, R. W., & Ananthakrishnan, A. N. (2017). Systematic review with meta-analysis: Breastfeeding and the risk of Crohn's disease and ulcerative colitis. *Alimentary Pharmacology & Therapeutics*, 46(9), 780–789. <https://doi.org/10.1111/apt.14291>
- Yamagishi, Y., Yang, C.-H., Tanno, Y., & Watanabe, Y. (2012). MPS1/Mph1 phosphorylates the kinetochore protein KNL1/Spc7 to recruit SAC components. *Nature Cell Biology*, 14(7), 746–752. <https://doi.org/10.1038/ncb2515>
- Yamaji, D., Kang, K., Robinson, G. W., & Hennighausen, L. (2013). Sequential activation of genetic programs in mouse mammary epithelium during pregnancy depends on STAT5A/B concentration. *Nucleic Acids Research*, 41(3), 1622–1636. <https://doi.org/10.1093/nar/gks1310>
- Yamaji, D., Na, R., Feuermann, Y., Pechhold, S., Chen, W., Robinson, G. W., & Hennighausen, L. (2009). Development of mammary luminal progenitor cells is controlled by the transcription factor STAT5A. *Genes & Development*, 23(20), 2382–2387. <https://doi.org/10.1101/gad.1840109>
- Yoshitake, R., Chang, G., Saeki, K., Ha, D., Wu, X., Wang, J., & Chen, S. (2022). Single-Cell Transcriptomics Identifies Heterogeneity of Mouse Mammary Gland Fibroblasts With Distinct Functions, Estrogen Responses, Differentiation Processes, and Crosstalks With Epithelium. *Frontiers in Cell and Developmental Biology*, 10, 850568. <https://doi.org/10.3389/fcell.2022.850568>
- Zeng, G., Taylor, S. M., McColm, J. R., Kappas, N. C., Kearney, J. B., Williams, L. H., Hartnett, M. E., & Bautch, V. L. (2007). Orientation of endothelial cell division is regulated by VEGF signaling during blood vessel formation. *Blood*, 109(4), 1345–1352. <https://doi.org/10.1182/blood-2006-07-037952>
- Zeng, Y. A., & Nusse, R. (2010). Wnt Proteins Are Self-Renewal Factors for Mammary Stem Cells and Promote Their Long-Term Expansion in Culture.

- Cell Stem Cell*, 6(6), 568–577. <https://doi.org/10.1016/j.stem.2010.03.020>
- Zhang, Y., Zhao, Z., Huang, L. A., Liu, Y., Yao, J., Sun, C., Li, Y., Zhang, Z., Ye, Y., Yuan, F., Nguyen, T. K., Garlapati, N. R., Wu, A., Egranov, S. D., Caudle, A. S., Sahin, A. A., Lim, B., Beretta, L., Calin, G. A., ... Yang, L. (2023). Molecular mechanisms of snoRNA-IL-15 crosstalk in adipocyte lipolysis and NK cell rejuvenation. *Cell Metabolism*, 35(8), 1457-1473.e13. <https://doi.org/10.1016/j.cmet.2023.05.009>
- Zhang, Y., Zhu, Y., Wang, J., Jin, L., Guo, M., Chen, L., Zhang, L., Li, Y., Wan, B., Zhang, R., Jia, W., & Hu, C. (2023). Neuregulin4 Acts on Hypothalamic ErBb4 to Excite Oxytocin Neurons and Preserve Metabolic Homeostasis. *Advanced Science*, 10(16), 2204824. <https://doi.org/10.1002/advs.202204824>
- Zhu, Q., Zhu, Y., Hepler, C., Zhang, Q., Park, J., Gliniak, C., Henry, G. H., Crewe, C., Bu, D., Zhang, Z., Zhao, S., Morley, T., Li, N., Kim, D.-S., Strand, D., Deng, Y., Robino, J. J., Varlamov, O., Gordillo, R., ... Scherer, P. E. (2022). Adipocyte mesenchymal transition contributes to mammary tumor progression. *Cell Reports*, 40(11), 111362. <https://doi.org/10.1016/j.celrep.2022.111362>
- Zwick, R. K., Rudolph, M. C., Shook, B. A., Holtrup, B., Roth, E., Lei, V., Van Keymeulen, A., Seewaldt, V., Kwei, S., Wysolmerski, J., Rodeheffer, M. S., & Horsley, V. (2018). Adipocyte hypertrophy and lipid dynamics underlie mammary gland remodeling after lactation. *Nature Communications*, 9(1), 3592. <https://doi.org/10.1038/s41467-018-05911-0>